

# **ANALYSIS AND DESIGN OF MIMO ANTENNA FOR UWB APPLICATIONS**

Thesis Submitted For the Award of the Degree of

**DOCTOR OF PHILOSOPHY**

**in**

**(Electronics and Communication Engineering)**

**By**

**Pankaj Kumar Keshri**

**(41700098)**

**Supervised By**

**Dr. Sanjay Kumar Sahu**

**Co-Supervised by**

**Dr. Richa Chandel**



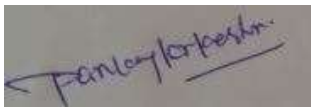
**LOVELY PROFESSIONAL UNIVERSITY  
PUNJAB  
2022**

# DECLARATION

I declare that the thesis entitled “**Analysis and Design of MIMO Antenna for UWB Applications**” has been prepared by me under the guidance of **Dr. Sanjay Kumar Sahu**, Associate Professor, School of **Electronics and Electrical Engineering** at Lovely Professional University, Punjab, India, and **Dr. Richa Chandel**, Assistant Professor, **University Institute of Technology, Himachal Pradesh University**, Shimla, India. No part of this thesis has been included in or has formed the basis for the award of any Degree or Diploma or Fellowship of any institution or university anywhere previously.

I further declare that there is no falsification or manipulation in terms of research materials, equipment or processes, experiments, methods, models, modeling, data, data analysis, results, or theoretical work.

I have checked the thesis using Turnitin for ensuring that there is no plagiarized material in my thesis and wherever any copyrighted material has been included, the same has been duly acknowledged.



**PANKAJ KUMAR KESHRI**

School of Electronics and Electrical Engineering

Lovely Professional University,

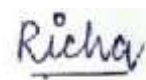
Phagwara, Punjab, India

We endorse the above declaration of Ph.D. student

Date-



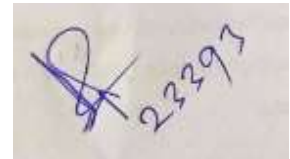
(Signature of the Ph.D. Supervisor)



(Signature of the Ph.D. Co-Supervisor)

# CERTIFICATE

We certify that **MR. PANKAJ KUMAR KESHRI** has prepared his thesis entitled “**Analysis and Design of MIMO Antenna for UWB Applications**”, for the award of the Ph.D. degree of the Lovely Professional University, under our guidance. He has carried out the work at the **School of Electronics and Electrical Engineering**, Lovely Professional University.



**DR.SANJAY KUMAR SAHU**

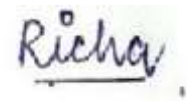
Associate Professor

School of Electronics and Communication Engineering

Lovely Faculty of Technology and Sciences

Lovely Professional University

Phagwara, Kapurthala-144411 (Punjab)



**DR. RICHA CHANDEL**

Assistant Professor

University Institute of Technology

Himachal Pradesh University

Shimla (Himachal Pradesh)

# ABSTRACT

Today, every wireless communication device is required to have a high data rate, high channel capacity, high bandwidth, good quality of service, and more reliability along with low power consumption. The demand can be fulfilled by the Multiple-Input Multiple-Output (MIMO) system along with the Ultra-Wideband Technology (UWB). To handle the multipath fading problem, it is necessary to involve multiple antennas on the receiver as well as transmitter side. Designing multiple antennas is not a big task but the real challenge lies with the proper positioning of the antennas in a limited space. Not only this but also implementation of fewer powerful techniques like polarization, space, or pattern diversity could be the possible solution to resolve the fading issue significantly. Though all these techniques play a vital role in the MIMO design is a concern but still there is some issue with the mutual coupling which arises by placing multiple antennas in a limited space. As a consequence of that, it affects the overall performance of the antenna.

The main focus of this research is to design and develop a miniature MIMO antenna with very good isolation. The initial design of this work witnesses two radiating elements placed on the upper side of the substrate whereas the other two identical radiators are housed just opposite it along with a decoupling structure to improve the isolation. In the very next step, the design has been modified where all four antennas are placed on the top side of the substrate in an orthogonal fashion which provides better isolation than the previous one without using any decoupling structure. The main objective of making an orthogonal arrangement is to improve polarization diversity. Later on, the above design is further modified where all four radiating elements are placed in a parallel fashion without orthogonality. In addition to that, we include an L-shaped stub and Complementary Split-Ring Resonator (CSRR) on the ground plane between antenna elements. By doing so, it is observed that the direction of surface current is diverted which leads to a reduction in the amount of mutual coupling.

In the final step, the CSRR structure on the ground plane is replaced by the modified Minkowski fractal geometry for better isolation. To get dual-band notch

characteristics, we have added one C- and L- shaped slot on the radiating element. For all individual designs, simulation has been carried out through the HFSS simulator. The simulation results helped in developing the required prototype with a suitable dimension. Finally, we have conducted the measurement process through a vector network analyzer (VNA) to make a comparison between the simulated and fabricated prototypes. From the comparison, it is estimated that there is not much deviation between simulated and measured ones. The radiation characteristics are also measured inside an anechoic chamber to get the complete performance of the proposed design. In conclusion, it can be stated that a good amount of matching is found to justify the work. Based on the result it can be expected that the design will be best suitable for the MIMO applications.

# Acknowledgement

First of all, I would like to express my gratitude to my supervisors, **Dr. Sanjay Kumar Sahu** and co-supervisor **Dr. Richa Chandel**. This research work would not have been possible without their support, supervision, and inspiration. Under their guidance, I successfully overcame many difficulties and learned a lot.

I am grateful to the members of the School of Research Degree Programme (RDP) for being in my entire research progress review panel and providing useful suggestions during the period. I am indeed thankful to all anonymous reviewers of my research papers submitted to the various international journal and international conferences, due to which I was able to improve upon the work contained herein.

I am indebted to the Honorable Chancellor, Worthy Pro-Chancellor, Vice-Chancellor, and successive Deans of Lovely Professional University for facilitating the administrative issue involved and encouraging me throughout my research work.

I express my gratitude to the Head of School, School of Electronics and Communication Engineering, faculty, and staff member for their co-operation and support. I am also thankful to IIT Roorkee, Uttarakhand for their help in the simulation, fabrication, and testing process of the work.

I would also like to say a heartfelt thanks to my parents and my wife **Pooja Keshri** for always believing in me and encouraging me to follow my dreams. I special thanks to my little champion “**Shivansh Keshri**”.

# Table of Contents

	<b>Title</b>	<b>Page No.</b>
	<b>Declaration</b>	<b>ii</b>
	<b>Certificate</b>	<b>iii</b>
	<b>Abstract</b>	<b>iv</b>
	<b>Acknowledgement</b>	<b>vi</b>
	<b>Table of Content</b>	<b>vii</b>
	<b>List of table</b>	<b>xi</b>
	<b>List of figure</b>	<b>xii</b>
	<b>List of abbreviations</b>	<b>xvi</b>
<b>Chapter 1</b>	<b>Introduction</b>	<b>1-22</b>
	1.1 Introduction	1
	1.2 Ultra Wide Band Technology	1
	1.3 Introduction to MIMO System	3
	1.4 MIMO Diversity Parameters	8
	1.5 Isolation Enhancement Techniques	13
	1.6 Miniaturization Techniques	17
	1.7 Research Motivation	20
	1.8 Objectives and outcomes	21
	1.9 Thesis Organization	21
	1.10 Summary	22
<b>Chapter 2</b>	<b>Literature Review</b>	<b>23-41</b>
	2.1 Introduction	23
	2.2 Literature Review on UWB and MIMO Antenna	23
	2.3 Research Gap	40
	2.4 Summary	41

<b>Chapter 3</b>	<b>Compact Multiple Input Multiple Output Antenna with High Isolation for UWB Applications</b>	<b>42-52</b>
3.1	Introduction	42
3.2	Two Port MIMO Antenna Design	43
3.3	Four Port MIMO Antenna Design	45
3.4	Results and Discussion	46
3.4.1	Return Loss and Isolation Parameter	47
3.4.2	Surface Current Distribution	48
3.4.3	Gain and Radiation Efficiency	49
3.4.4	Input Impedance	51
3.4.5	Envelope Correlation Coefficient and Diversity Gain	51
3.5	Summary	52
<b>Chapter 4</b>	<b>Compact Quad Port High Performance UWB MIMO Diversity Antenna With Slotted Ground Structure</b>	<b>53-74</b>
4.1	Introduction	53
4.2	Antenna Design Procedure	55
4.3	Evolution Steps of Single UWB Antenna	57
4.4	Evolution Steps of UWB MIMO Antenna	58
4.5	Effect of Ground Plane	61
4.6	Results and Discussion	62
4.7	MIMO Diversity Analysis	68
4.7.1	Envelope Correlation Coefficient	68
4.7.2	Diversity Gain	69
4.7.3	Total Active Reflection Coefficient	70
4.7.4	Mean Effective Gain	71
4.8	Effect of Device Housing	72
4.9	Summary	74
<b>Chapter 5</b>	<b>CSRR Loaded Compact Quad Port MIMO Diversity Antenna For UWB Applications</b>	<b>75-99</b>



5.1	Introduction	75
5.2	Antenna Design and Analysis	77
5.2.1	Evolution of Single UWB Antenna Element	77
5.2.2	Evolution of MIMO Antenna with Various Ground Structure	79
5.3	CSRR Structure and Equivalent Model	82
5.4	Equivalent Circuit Model for the Proposed MIMO Antenna	83
5.5	Results and Discussion	85
5.5.1	Return Loss and Isolation Parameter	87
5.5.2	Gain and Efficiency	88
5.5.3	Surface Current Distribution	89
5.5.4	Radiation Characteristics	92
5.6	MIMO Performance Analysis	93
5.6.1	Envelope Correlation Coefficient and Diversity Gain	94
5.6.2	Mean effective gain	95
5.6.3	Total active reflection coefficient	96
5.6.4	Channel capacity loss	97
5.7	Comparison of the Proposed Antenna with the Existing MIMO Antenna	97
5.8	Summary	99
<b>Chapter 6 High Isolation Miniature Antenna with Band Notch Characteristics For UWB MIMO Applications</b>		<b>100-116</b>
6.1	Introduction	100
6.2	Antenna Design and Analysis	102
6.2.1	Evolution Steps of Single Antenna Element	102
6.2.2	Effect of Ground Plane on UWB MIMO Antenna	104
6.3	Results and Discussion	106
6.3.1	Return Loss and Isolation Parameter	107
6.3.2	Gain and Radiation Efficiency	109

6.3.3 Surface Current Distribution	110
6.3.4 Radiation Characteristics	112
6.4 Diversity Performance	114
6.4.1 ECC and DG	114
6.4.2 TARC and CCL	115
6.5 Comparison of the Proposed Model with the Previous Work	116
6.6 Summary	117
<b>Chapter 7 Conclusion and Future Scope</b>	<b>119-120</b>
7.1 Summary	119
7.2 Future Scope	120
<b>List of Publications</b>	<b>121</b>
<b>Bibliography</b>	<b>122</b>

## List of Tables

<b>Table No.</b>	<b>Title</b>	<b>Page No.</b>
<b>TABLE 3.1</b>	Design parameters of the antenna	46
<b>TABLE 4.1</b>	Performance Comparison the of prototype antenna with Existing Literature	54
<b>TABLE 4.2</b>	Optimized dimension of the proposed antenna	55
<b>TABLE 4.3</b>	Comparisons of S-parameter of all three designs	61
<b>TABLE 5.1</b>	Simulated and theoretical resonant frequency	78
<b>TABLE 5.2</b>	Various parameter values of the proposed model	80
<b>TABLE 5.3</b>	Lumped parameter values	83
<b>TABLE 5.4</b>	Performance comparison of the prototype proposed model with the existing work	98
<b>TABLE-6.1</b>	Optimized design parameter of the proposed antenna with dimension	102
<b>TABLE 6.2</b>	Comparison of various existing UWB MIMO antenna with the prototype antenna	117

# List of Figures

<b>Figure No.</b>	<b>Caption</b>	<b>Page No.</b>
1.1	Comparison of power spectral density of the UWB system with other radio System	2
1.2	General outline of multiple input multiple output system	3
1.3	Different types of antenna configuration	4
1.4	Comparison of channel capacity of MIMO vs SIMO/MISO	5
1.5	Spatial Diversity	6
1.6	Spatial Multiplexing	7
1.7	Adaptive Antenna System	8
1.8	Various shapes of DGS (a) H-shaped slots (b) arrow head slots (c) I-shaped Slot (d) Inverted L-shaped stub (e) pair of slits (f) tree Shape DGS	14
1.9	Various shapes of EBG structure (a) 1-D EBG (b) 2-D mushroom shaped EBG (c) S-shape EBG (d) fork shape EBG (e) Split ring slot (SRS)- EBG	15
1.10	(a) Thin neutralization line between two monopole antennas (b) wideband neutralization line between two circular monopole	15
1.11	(a) Antenna arrangement without parasitic element (b) With parasitic element	16
1.12	Various shapes parasitic element (a) Metal Strip (b) T-shaped (c) Square shape (d) F-shaped (e) U-shape	17
1.13	Various shapes of metamaterial structure (a) meander type (b) CSRR (c) Circular SRR (d) metamaterial absorber	17
1.14	(a) Meander line dipole antenna (b) Koch fractal monopole	18
1.15	(a) Defects on the ground plane (b) Equivalent circuit model	19
1.16	Quarter wavelength MPA using shorting pin	20

3.1	Two-port MIMO antenna with different orientations	44
3.2	(a) Reflection coefficient (b) Isolation parameter	45
3.3	Two dimensional layouts of the proposed antenna	46
3.4	Reflection coefficient at various steps	47
3.5	$S_{12}/S_{13}/S_{14}$ at various steps	48
3.6	Two dimensional current distribution at operating frequency 4.3 GHz in (a), (b) and at 5.4 GHz in (c),(d)	49
3.7	Realized gain and radiation efficiency	49
3.8	Two dimensional radiation pattern (a) 4.3(b) 5.4 and (c) 10.4 GHz	50
3.9	Simulated impedance of the proposed antenna	51
3.10	Simulated ECC and DG of the proposed antenna	52
4.1	Structure of four-element MIMO antenna with dimension	56
4.2	Different evolution steps of single UWB antenna element	57
4.3	(a) Rectangular patch with the partial ground only (b) After etching a staircase shape structure at the corner of the patch (c) Introducing slot on the ground and etched arc shape structure on the radiator	59
4.4	Comparison of S-parameter of all the three designs (a) return loss (b) isolation parameters	60
4.5	Effect of a ground plane at various steps (a) $S_{11}$ (b) Isolation parameter	62
4.6	Fabricated prototype antenna (a) Front side (b) Back side	63
4.7	Simulated and measured $S_{11}$ parameter of the prototype MIMO antenna	63
4.8	Comparison of isolation parameter $S_{12}/S_{13}/S_{14}$	64
4.9	Radiation pattern at (a) 3.07 (b) 5.37 (c) 10.66 and (d) 15.14 GHz in xz and yz plane	65
4.10	3-D Radiation pattern at (a) 3.07 (b) 5.37 (c) 10.66 and (d) 15.14 GHz	66
4.11	Simulated and measured realized gain	66
4.12	Simulated and measured radiation efficiency	67
4.13	Surface current at (a) 3.07 GHz (b) 5.37 GHz (c) 10.66 GHz	

	(d) 15.14 GHz	68
4.14	Envelope correlation coefficient with frequency	69
4.15	Diversity gain with frequency	70
4.16	Simulate and measured TARC with frequency	71
4.17	Simulated and measured MEG with frequency	72
4.18	Comparison of S-parameter for different plastic materials with the proposed MIMO antenna (a) return loss (b) $S_{12}$ (c) $S_{13}$ (d) $S_{14}$	74
5.1	Structure of (a) the proposed antenna and (b) CSRR unit cell	77
5.2	Evolution steps of single UWB element	78
5.3	Return loss of a single antenna element at various steps	79
5.4	Evolution steps with different ground structures	80
5.5	Reflection coefficient of the MIMO antenna with different ground structure	81
5.6	Isolation parameter of the proposed antenna (a) only partial ground plane (b) partial ground with L-shape stub (c) partial ground and L-shape stub along with CSRR structure	82
5.7	(a) CSRR structure and (b) equivalent circuit	83
5.8	Equivalent circuit of the proposed MIMO antenna	84
5.9	EM and circuit simulator result	85
5.10	Fabricated prototype antenna (a) Front and (b) Backside	85
5.11	Antenna measurement setup (a), (b) with VNA and (c), (d) inside anechoic Chamber	86
5.12	Measured and simulated return loss	87
5.13	Measured and simulated isolation parameter	88
5.14	Peak gain and radiation efficiency of the proposed antenna	89
5.15	Current distribution at (a) 4 GHz (b) 8 GHz (c) 10.8 GHz	92
5.16	Two dimensional radiation pattern at (a) 4 (b) 8 (c) 10.8 GHz	93
5.17	ECC and DG for the prototype antenna	94
5.18	Mean effective gain at different ports	96

5.19	Measured and simulated TARC	96
5.20	Measured and simulated CCL	97
6.1	(a) Structure of the proposed MIMO antenna (b) Modified minkowski fractal Structure	101
6.2	Evolution steps (a) Rectangular patch (b) With C-slot (c) With C-slot and U-slot	103
6.3	Reflection coefficient of single antenna element at various steps	104
6.4	(a) Only partial ground (b) partial ground with L – shaped stub (c) partial ground, L-shape stub along with modified minkowski fractal Structure	105
6.5	Isolation parameter with different ground structure	106
6.6	Fabricated prototype (a) Top View (b) Bottom View	106
6.7	Measurement setup with VNA (a), (b) and inside an anechoic chamber (c) front view (d) back view	107
6.8	Simulated and measured (a) reflection coefficient and (b) isolation parameter	108
6.9	Gain and radiation efficiency of the proposed model	109
6.10	Surface current distribution with various ground structures at (a) 4.2 GHz (b) 6.4 GHz (c) 8.4 GHz	112
6.11	E-plane and H-plane radiation characteristics at (a) 4.2 (b) 6.4 and (C) 8.4 GHz	113
6.12	ECC and DG of the proposed design	115
6.13	TARC and CCL of the proposed design	116

## List of Abbreviations

<b>AAS</b>	Adaptive Antenna System
<b>ACS</b>	Asymmetric Coplanar Strip
<b>CCL</b>	Channel Capacity Loss
<b>CPS</b>	Coplanar Strip
<b>CPW</b>	Coplanar Wave Guide
<b>CSRR</b>	Complementary Split Ring Resonator
<b>DG</b>	Diversity Gain
<b>DGS</b>	Defected Ground Structure
<b>EBG</b>	Electromagnetic Bandgap Structure
<b>ECC</b>	Envelope Correlation Coefficient
<b>EIRP</b>	Effective Isotropic Radiated Power
<b>FCC</b>	Federal Communication Commission
<b>GPS</b>	Global Positioning System
<b>HDTV</b>	High Definition Television
<b>HFSS</b>	High Frequency Structure Simulator
<b>LOS</b>	Line of Sight
<b>LTE</b>	Long Term Evolution
<b>MEG</b>	Mean Effective Gain
<b>MIMO</b>	Multiple Input Multiple Outputs
<b>MISO</b>	Multiple Input Single Output
<b>PICA</b>	Planar Inverted Cone Antenna
<b>QSCA</b>	Quasi-Self-Complementary Antenna
<b>RFID</b>	Radio-Frequency Identification
<b>SIMO</b>	Single Input Multiple Outputs
<b>SIR</b>	Stepped Impedance Resonator
<b>SISO</b>	Single Input Single Output
<b>SNR</b>	Single to Noise Ratio
<b>TARC</b>	Total Active Reflection Coefficient



<b>TCM</b>	Theory of Characteristic Mode
<b>UMTS</b>	Universal Mobile Telecommunication Service
<b>UWB</b>	Ultra-Wideband
<b>Wi-Fi</b>	Wireless Fidelity
<b>Wi-Max</b>	Worldwide Interoperability for Microwave Access
<b>WLAN</b>	Wireless Local Area Network
<b>XPR</b>	Cross Polarization Coupling

# Chapter 1

## Introduction

### 1.1 Introduction

There is a significant growth in the field of wireless communication technology in the last few decades which is directly reflected in our daily life. The antenna is the backbone for this and without it, wireless technology never reached this stage. The standard definition of an antenna as per IEEE standard is “a means for radiating or receiving radio waves” [1]. It acts like a transducer that converts electrical energy to electromagnetic waves or vice versa. Nowadays, wireless communication has numerous applications like Wireless Fidelity (Wi-Fi), Worldwide Interoperability for Microwave Access (WiMAX), Bluetooth, Global Positioning System (GPS), remote sensing, mobile communication, wireless power transfer, satellite communication, security system, Wireless Local Area Network (WLAN), and High Definition Television (HDTV), etc. All these devices have a requirement of light weight, low cost, high data rates, high channel capacity, less interference, and compact size.

### 1.2 Ultra Wide Band Technology

The Ultra-Wideband Technology (UWB) fulfilled the demand for high data rates and is quite suitable for short-distance communication. Early days, people used to call it ‘pulse radio’. In the year 2002, Federal Communication Commission (FCC) allocated the unlicensed frequency band for the UWB system as 3.1- 10.6 GHz [2]. Today’s demand for this technology has mostly revolutionized wireless communication systems. There are several advantages of the UWB system like very large bandwidth because it transmitted a narrow pulse in the time domain, low power spectrum, and very high data rates (> 100 Mbps). According to the Shannon Hartley theorem, the channel capacity of a single antenna system directly depends on the signal-to-noise ratio and channel bandwidth [3].

$$C = B \log_2\left(1 + \frac{S}{N}\right) \quad (1.1)$$

Where ‘B’ denotes the bandwidth of the channel in Hz, ‘S’ indicates the signal power in watts, ‘N’ illustrates noise power in watts and ‘C’ defines the term called channel capacity in bits/s/Hz. The channel capacity of the single antenna system directly depends upon the bandwidth of the channel which leads to an increase in the transmitted power and thereby increases the SNR. On the other hand, it cannot exceed a certain limit which tends to increase the noise. The Effective Isotropic Radiated Power (EIRP) is another important parameter for the UWB system and it is defined as the maximum amount of power released from the antenna. As per FCC regulation, for the effective performance of the UWB system, the maximum value of EIRP is limited to  $-41.3 \text{ dBm / MHz}$ . Figure 1.1, shows the comparison of the power spectral density of the UWB system with all other radio communication systems. The data rate of the UWB system has high for short-distance communication preferably for indoor applications but low for mid-range frequency.

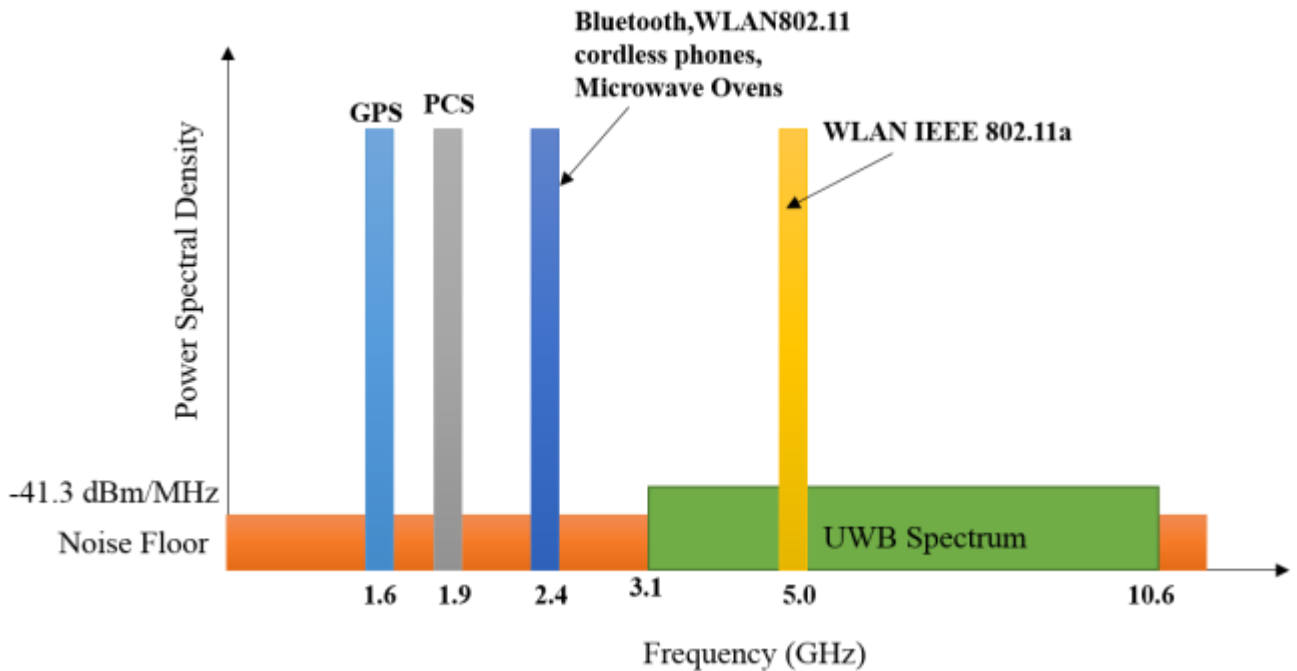


**Figure 1.1** Comparison of power spectral density of UWB system with other radio systems [2]

### 1.3 Introduction to MIMO System

In a single antenna system, multipath fading and co-channel interference are common issues. This can be reduced by associating MIMO technology, because of placing multiple numbers of antenna elements on the transmitter and receiver sides as depicted in Figure 1.2. The data rates, channel capacity, and coverage area are very well enhanced, just by adding the MIMO system. The good thing about MIMO is that it can provide all said points without any additional increment in power and frequency spectrum. Depending upon the arrangement of an antenna on the transmitter and receiver side, usually, there are four types of configuration possible as illustrated in Figure 1.3. In the conventional radio communication system, a single antenna is present on both transmitter and receiver sides which is commonly known as the Single Input Single Output (SISO) configuration. This configuration is very simple and does not require any additional processing. But SISO system has more chances of receiving interference and fading with the limited amount of bandwidth. In MISO configuration, multiple antennas are placed on the transmitter side and a single antenna on the receiver side. In this configuration, the same data is transmitted from multiple antennas and the receiver will receive the optimum signal thereafter it would extract the required data.

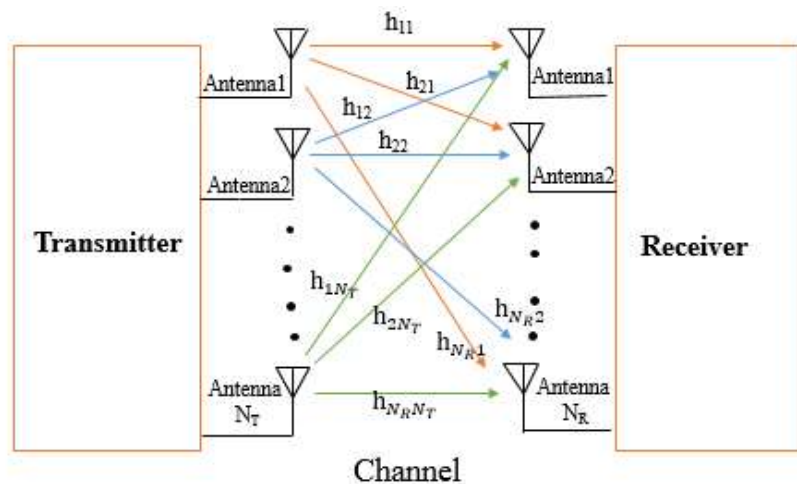


**Figure 1.2** General outline of the multiple input multiple output system[4]

In the MISO system, redundancy coding or processing is done on the transmitter side instead of the receiver side. As in the case of cellphone users, the lesser amount of processing on the receiver side is noticed which decreases the size and cost, and no additional circuitry is required for redundancy coding. Apart from that, the battery life is also improved due to low power consumption. There are single transmitting antennas and multiple receiving antennas present in the SIMO type antenna configuration. This configuration is also called receiver diversity which means, it will receive the signal from different sources and combat the effect of fading. This configuration is relatively easy to use in many applications but more processing is required on the receiver side which degraded the performance of battery life in the case of a mobile user. The MIMO antenna is the combination of all three configurations.

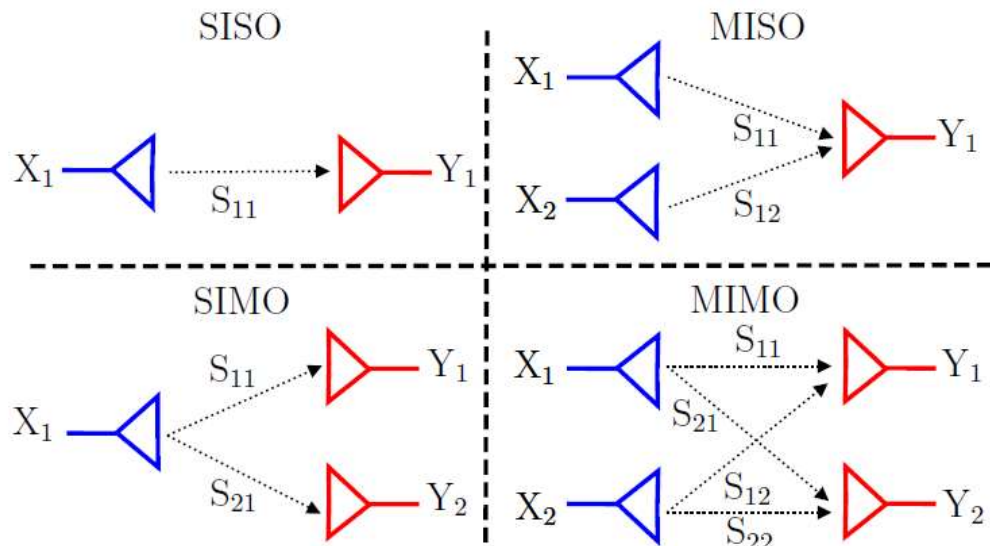


**Figure 1.3** Different types of antenna configuration [5]

The channel response for the MIMO system can be evaluated by equation 1.2 with  $N_T$  number of a transmitter antenna and  $N_R$  the number of receiver antennas.

$$Y = HX + n \quad (1.2)$$

Where the received and the transmitted signal vector are represented by  $Y$  and  $X$  respectively,  $n$  denotes the Additive White Gaussian Noise (AWGN) vector and  $H$  illustrates the channel matrix representing the coefficient between  $i^{\text{th}}$  transmitting antenna  $j^{\text{th}}$  receiving antenna. The received signal can be expressed in terms of vector as:

$$\begin{bmatrix} y_1 \\ y_2 \\ \vdots \\ y_{N_R} \end{bmatrix} = \begin{bmatrix} h_{11} & h_{12} & \dots & h_{1N_T} \\ h_{21} & h_{22} & \dots & h_{2N_T} \\ \vdots & \vdots & \dots & \vdots \\ h_{N_R1} & h_{N_R2} & \dots & h_{N_RN_T} \end{bmatrix} \begin{bmatrix} x_1 \\ x_2 \\ \vdots \\ x_{N_T} \end{bmatrix} + \begin{bmatrix} n_1 \\ n_2 \\ \vdots \\ n_{N_R} \end{bmatrix} \quad (1.3)$$

The theoretical channel capacity for the MIMO system can be evaluated from equation 1.2. It can be seen that channel capacity is linearly dependent upon the number of antenna elements and bandwidth.

$$C = N_T N_R B \log_2 \left[ \det \left( I_{N_R} + \frac{P}{N_T \sigma_n^2} H \cdot H^H \right) \right] \quad (1.4)$$

Where  $H$  represents the channel matrix,  $H^H$  denotes the hermitian transpose of the channel matrix,  $I_{N_R}$  indicates identity matrix,  $P$  denoted total transmitted power in watts,  $\sigma_n^2$  represents noise power in watts,  $N_T$  and  $N_R$  represent transmitting and receiving antenna respectively.

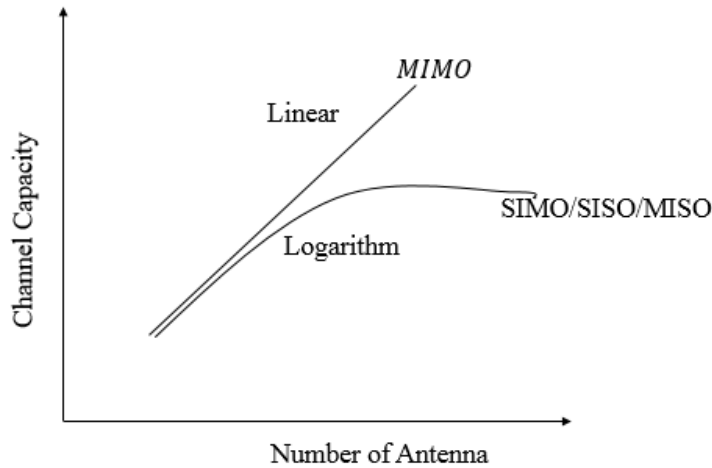


**Figure 1.4** Comparison of channel capacity of MIMO vs SIMO/MISO[6]

Figure 1.4 represents the comparison of the channel capacity of the SISO/ SIMO/ MISO and MIMO systems. It can be seen that in SISO / SIMO/ MISO system channel capacity is logarithmically dependent on SNR but in the MIMO system, it is linearly dependent on the number of antenna elements on the transmitter and receiver side. Numerous techniques have been implemented in multiple antenna systems for improving the performance of wireless links either reducing multipath by forming diversity or using spatial multiplexing.

### 1.3.1 Spatial Diversity

In the spatial diversity technique, multiple antennas are used for improving reliability and quality of service. It is very difficult for getting a LOS (Line of Sight) path in a densely populated area. The basic principle of this technique is if some signal gets faded still some signals have a LOS path and receive a clear signal because of several antennas placed on the transmitter and receiver side as depicted in Figure 1.5. In this technique, reliability has improved by sending multiple copies of data from the transmitting antenna and making full use of various received versions of data.

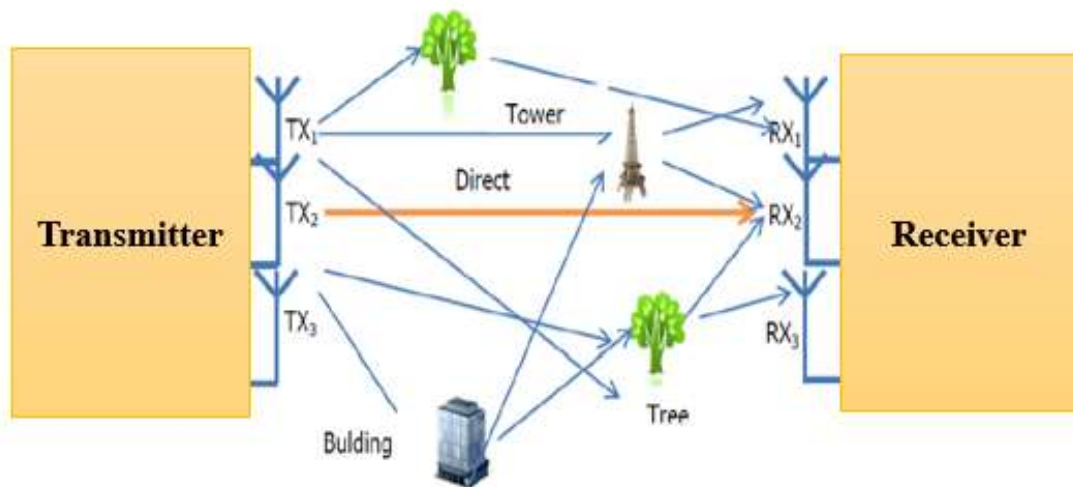


**Figure 1.5** Spatial Diversity [7]

### 1.3.2 Spatial Multiplexing

In this technique, the entire data stream is divided or demultiplexed into several data segments and transmitted independently through different multiple antennas as depicted in Figure 1.6. This technique uses multiple antennas which increases data rates without increasing bandwidth and transmission power. On the receiver side, each antenna receives a combination of all individual data segments, and after that data are separated by an interference cancellation algorithm.

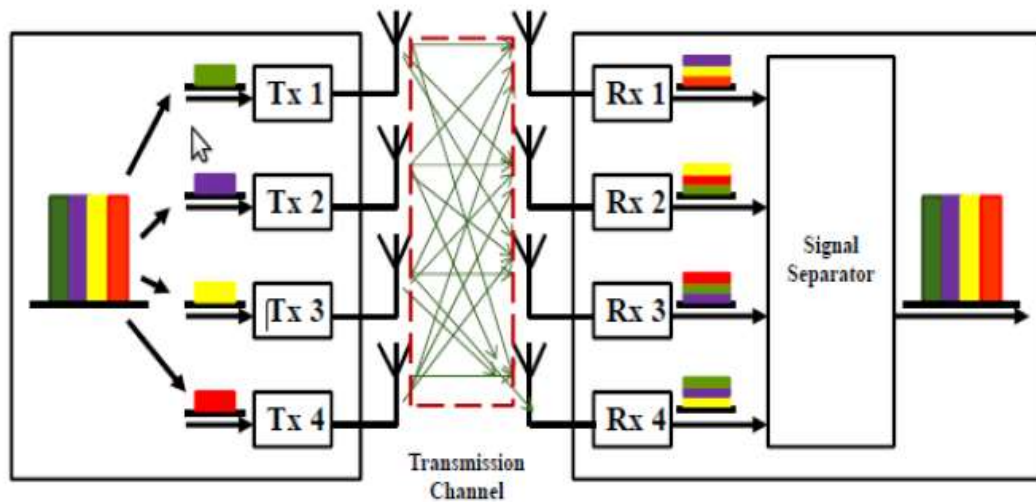


Figure 1.6 Spatial Multiplexing [4]

### 1.3.3 Adaptive Antenna Systems

In this technique, multiple antennas are placed on both the transmitter and receiver sides for better transmission over the channel. The beamforming technique is used in an Adaptive Antenna System (AAS) as illustrated in Figure 1.7. It mainly focuses on the specific device at the receiver rather than on all other devices and it increases the coverage area for the transmitter by reducing interference. Because of this technique system becomes faster, more reliable, and delivers a high-quality signal to the receiver without any increase in broadcast power. The main objective of this technique is to improve SNR by mixing the energy from each transmitter and directing it to the receiver without any increment in data



rate. If the position of the transmitter antenna is known then the receiver antenna increases the level of signal power by forming a directional pattern in the direction of the transmitter.

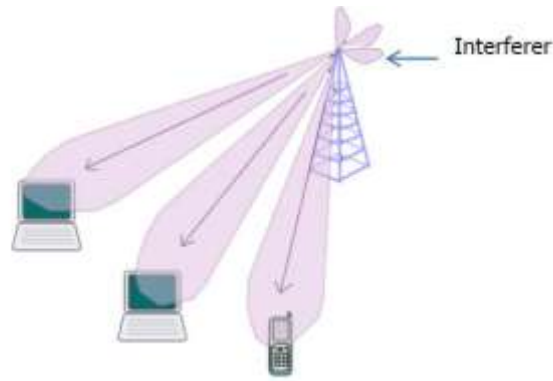


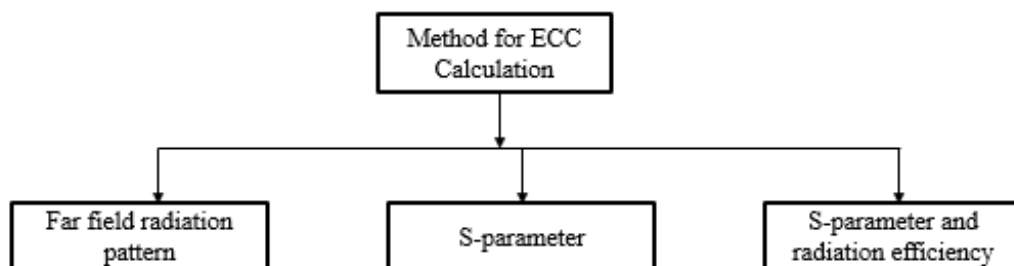
**Figure 1.7** Adaptive Antenna System [6]

## 1.4 MIMO Diversity Parameters

In this section, describes the various diversity parameter that decides the effective performance of the MIMO antenna.

### 1.4.1 Envelope Correlation Coefficient (ECC)

In the MIMO system, the capacity in a multipath environment depends upon the number of the antenna element. If we try to fix more antennas in close proximity then there is every possibility to increase the coupling which may degrade the antenna efficiency as well as channel capacity. If more antennas are placed in closed proximity then very high chances of coupling occur between antenna elements which will decrease the capacity of the MIMO antenna system and antenna efficiency. There are three ways to calculate the ECC parameter [8].



### Method-1: From far-field radiation pattern

The ECC value can be evaluated using far-field [9]. During the measurement of ECC, one port of the antenna is excited, and remaining all other ports are terminated with a load impedance of 50 ohms. This method uses both the elevation and azimuthal radiation field pattern for calculating the ECC value between  $i^{th}$  and  $j^{th}$  elements.

$$\rho_e(i, j) = \frac{|\iint_{4\pi}^0 [E_i(\theta, \phi, f) E_j(\theta, \phi, f)] d\Omega|^2}{\left[ \iint_{4\pi}^0 |E_i(\theta, \phi, f)|^2 d\Omega \right] \left[ \iint_{4\pi}^0 |E_j(\theta, \phi, f)|^2 d\Omega \right]} \quad (1.5)$$

Where  $E_i$  and  $E_j$  denote the magnitude of the electric radiated field of  $i^{th}$  and  $j^{th}$  antenna,  $\Omega$  represents the solid angle,  $\phi$  and  $\theta$  illustrate the azimuthal and the elevation angle for the spherical coordinate respectively. The ECC calculation from this method is very tedious in terms of calculation, measurement, time-consuming, and more expensive but this method is more accurate and exact. In this method, an anechoic chamber is used to extract the parameters.

### Method-2: From the scattering parameter

There is another simplest, easy and fast way to evaluate ECC value directly from the S-parameter value. The scattering parameters are extracted from each port with the help of VNA. The envelope correlation coefficient between the  $i^{th}$  and  $j^{th}$  element for the N number of the antenna element is evaluated as follows [10].

$$\rho_e(i, j, N) = \frac{|\sum_{n=1}^N S_{i,j}^* S_{n,j}|^2}{\prod_{k=i,j} [1 - \sum_{n=1}^N S_{k,n}^* S_{n,k}]} \quad (1.6)$$

### Method-3: S- parameter and radiation efficiency

This method is suitable for the correct measurement of a lossy antenna system. It is a very complex method and not suitable for pattern shape and tilt beam for ECC calculation. This method for ECC calculation requires the radiation efficiency of each radiating element and

is reliable for high efficiency. The ECC value for the N-port MIMO antenna is calculated as follows [11],

$$\rho_e(i, j, N) = \frac{\sum_{n=1}^N S_{ni}^* S_{nj}}{\sqrt{(1 - \sum_{n=1}^N |S_{ni}|^2)(1 - \sum_{n=1}^N |S_{nj}|^2)} \eta_{rad,i} \eta_{rad,j} + \sqrt{(\frac{1}{\eta_{rad,i}} - 1)(\frac{1}{\eta_{rad,i}} - 1)}} \quad (1.7)$$

Where  $\eta_{rad,i}$  and  $\eta_{rad,j}$  are radiation efficiency for  $i^{\text{th}}$  and  $j^{\text{th}}$  elements.

### 1.4.2 Diversity Gain

The diversity of the whole communication system is decided by the diversity gained. This is achieved when the transmitter and the receiver, transmit or receive multiple signals simultaneously in a multiple channel path. The ideal theoretical value for an uncorrelated antenna is  $-10$  dB. The higher is the value of diversity gain better is the performance of the MIMO system. The gain enhancement for the MIMO system in a combined signal over time average SNR is described by this parameter. The diversity gain is evaluated as follows [12].

$$DG = 10 \sqrt{1 - |\rho_e|^2} \quad (1.8)$$

### 1.4.3 Mean Effective Gain

This is a relative term that is compared by an isotropic antenna. In actual practice, this term explains the ratio of the amount of power received by the test antenna with reference to an isotropic antenna put in the same environment [13].

$$G_e = \frac{P_r}{P_{ref}} \quad (1.9)$$

For the MIMO system, MEG can be evaluated as follows [14],

$$MEG = \int_0^{2\pi} \int_0^\pi \left\{ \frac{XPR}{1+XPR} G_\theta(\theta, \phi) P_\theta(\theta, \phi) + \frac{1}{1+XPR} G_\phi(\theta, \phi) P_\phi(\theta, \phi) \right\} \sin \theta d\theta d\phi \quad (1.10)$$

Where  $G_\theta(\theta, \phi)$  represents the  $\theta$  component of antenna power gain,  $G_\phi(\theta, \phi)$  indicates the  $\phi$  component of antenna power gain,  $P_\theta(\theta, \phi)$  represents the  $\theta$  component of an angular density function,  $P_\phi(\theta, \phi)$  illustrates the  $\phi$  component of the angular density function and XPR denotes the cross-polarization coupling.

$$\text{XPR (cross – polarization coupling)} = \frac{P_1}{P_2} \quad (1.11)$$

Where  $P_1$  and  $P_2$  are the mean received power of vertically and horizontally polarized isotropic antenna respectively. There is another easier way to evaluate the parameter MEG that is by the knowledge of the scattering parameter [15].

$$\text{MEG}_i = 0.5[1 - \sum_{j=1}^N |S_{ij}|^2] \quad (1.12)$$

For effective performance of MIMO antenna, the mean effective gain for each antenna element should be less than  $-3$  dB and the magnitude of the difference of mean effective gain between two elements should be less than 3 dB.

#### 1.4.4 Channel Capacity Loss (CCL)

The maximum reliable data transmission over the transmission channel can be estimated by this parameter. For effective performance of the MIMO antenna, the practical accepted limit should be lower than 0.4 bits/s/Hz through the entire frequency band. It can be evaluated as follows [16].

$$C_{Loss} = -\log_2 \det(\psi^R) \quad (1.13)$$

Where  $\psi^R$  represents the correlation matrix for receiving antenna. For the N port MIMO system, it can be computed as follows.

$$\psi^R = \begin{bmatrix} \psi_{11} & \psi_{12} & \cdot & \cdot & \psi_{1N} \\ \psi_{21} & \psi_{22} & \cdot & \cdot & \psi_{2N} \\ \psi_{31} & \psi_{32} & \cdot & \cdot & \cdot \\ \psi_{41} & \psi_{42} & \cdot & \cdot & \cdot \\ \psi_{N1} & \psi_{N2} & \cdot & \cdot & \psi_{NN} \end{bmatrix} \quad (1.14)$$

$$\psi_{nn} = 1 - \sum_{m=1}^4 |S_{nm}|^2 \quad (1.15)$$

$$\psi_{nm} = -(S_{nn}^* S_{nm} + S_{mn}^* S_{nm}) \quad (1.16)$$

### 1.4.5 Total Active Reflection Coefficient (TARC)

For a single antenna element, the reflection coefficient ( $|S_{11}|$ ) is sufficient to analyze the performance of the antenna. But for the MIMO system, TARC is a very essential parameter to measure radiation characteristics and bandwidth for different polarization operations. It can be calculated as [17].

$$\Gamma_a^t = \sqrt{\frac{\text{available power} - \text{radiated power}}{\text{available power}}} = \sqrt{\frac{P_a - P_r}{P_a}} \quad (1.17)$$

TARC is a real number and its value normally ranges between zero and one. If all the delivered power is radiated by the antenna element then it will be zero and one, if completely reflected. TARC is generally expressed on a decibel scale. The practical accepted value for effective performance is less than  $-10$  dB through the entire operating band. For the N-port MIMO system, if the  $i^{\text{th}}$  port of the antenna is excited and the remaining ports are at matched loads, then TARC can be directly calculated from the scattering matrix by equation 1.18.

$$\Gamma_{ai}^t = \sqrt{1 - P_{ri}} = \sqrt{\sum_{j=1}^N |S_{ij}|^2} \quad i=1, 2, \dots, N \quad (1.18)$$

In another way, it can be expressed as [17].

$$\Gamma_a^t = \frac{\sqrt{\sum_{i=1}^N |b_i|^2}}{\sqrt{\sum_{i=1}^N |a_i|^2}} \quad (1.19)$$

Where  $b_i$  indicates the reflected power and  $a_i$  denotes the incident power. The scattering matrix for the  $N \times N$  MIMO antenna can be as follows.

$$\begin{bmatrix} b_1 \\ b_2 \\ \cdot \\ \cdot \\ b_N \end{bmatrix} = \begin{bmatrix} S_{11} & S_{12} & \cdot & \cdot & S_{1N} \\ S_{21} & S_{22} & \cdot & \cdot & S_{2N} \\ \cdot & \cdot & \cdot & \cdot & \cdot \\ \cdot & \cdot & \cdot & \cdot & \cdot \\ S_{N1} & S_{N2} & \cdot & \cdot & S_{NN} \end{bmatrix} \begin{bmatrix} a_1 \\ a_2 \\ \cdot \\ \cdot \\ a_N \end{bmatrix} \quad (1.20)$$

If the magnitude of the reflected signal is assumed to be unity but the phase is varying at a different angle. The TARC for the N-port MIMO antenna can be evaluated at different phase angles by [18],

$$\Gamma_a^t = \sqrt{\frac{|S_{11}+S_{12}e^{j\theta_1}+\dots+S_{1N}e^{j\theta_{N-1}}|^2 + |S_{21}+S_{22}e^{j\theta_1}+\dots+S_{2N}e^{j\theta_{N-1}}|^2 + |S_{N1}+S_{N2}e^{j\theta_1}+\dots+S_{NN}e^{j\theta_{N-1}}|^2}{\sqrt{N}}}$$
(1.21)

## 1.5 Isolation Enhancement Techniques

In the MMO system, multiple antennas are placed in a smaller area, so the chances of mutual coupling are very high. The overall antenna performance affects due to an increase in mutual coupling. In order to notify that there are several techniques used which lead to enhance the isolation like antenna orientation, defected ground structure, parasitic element, electromagnetic bandgap structure or material.

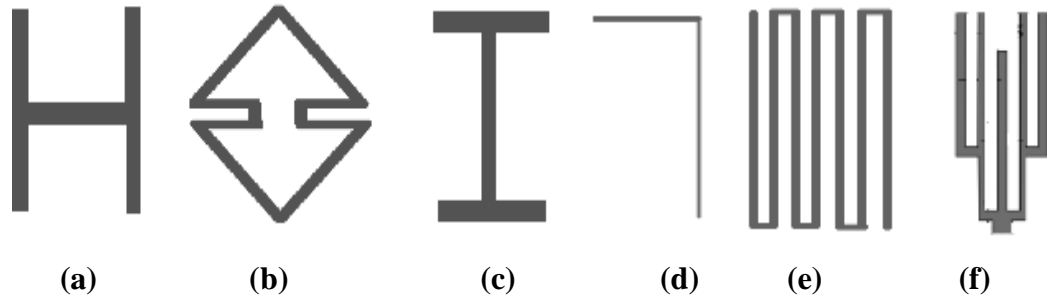
### 1.5.1 Antenna Placement and Orientation

The chances of mutual coupling are very high if the distance between antenna elements is less than  $\lambda/4$ . So placing multiple antennas in the proper position is very essential for designing the MIMO system. Mutual coupling can be reduced by placing antenna elements near the corner on the top surface or they can be placed on both sides of the substrate. It can also be enhanced by the positioning of multiple antennas orthogonal which increases the polarization diversity.

### 1.5.2 Defected Ground Structure (DGS)

This is another technique to reduce the mutual coupling by etching slots or stubs or creating defects on the ground plane. It stops the flow of current to other radiating elements and acts as a stop-band filter. There are several parameters of the MIMO system along with

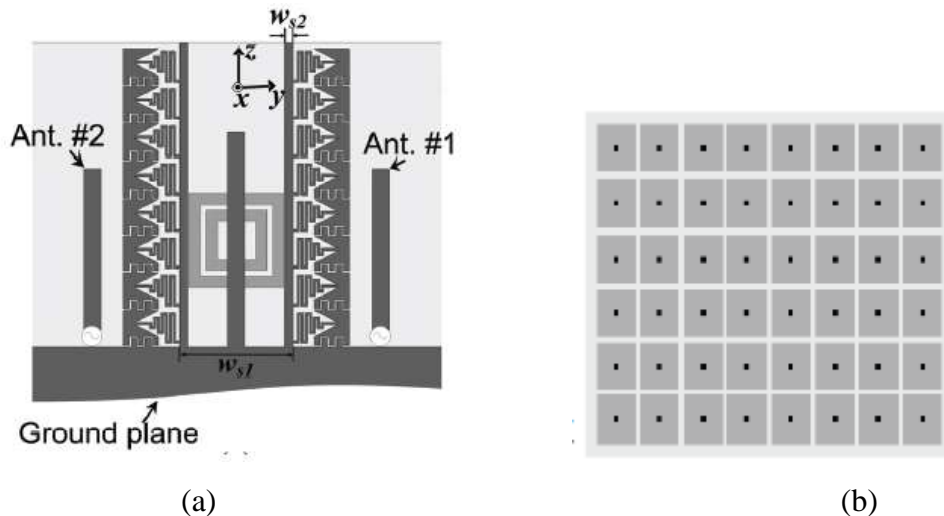
bandwidth, gain, and cross-polarization which are improved due to the DGS structure. Some of the DGS structures are listed in Figure 1.8.



**Figure 1.8** Various shapes of DGS (a) H-shaped slots (b) arrowhead slots (c) I-shaped slot (d) Inverted L-shaped stub (e) pair of slits (f) tree-shaped DGS

### 1.5.3 Electromagnetic Band Gap Structure (EBG)

It is a periodic or non-periodic artificial structure that is made up of various shapes such as mushroom, fork, S-shape, SRS shape or it may be 1-dimensional or 2-dimensional as illustrated below in Figure 1.9. The mutual coupling is improved by placing the EBG structure between the radiating elements. It acts like an LC filter to prevent the electromagnetic wave to travel from one element to another element. The capacitance is due to gap and inductance due to current flow along with adjacent cells. The EBG structure is also used for the miniaturization of the antenna.



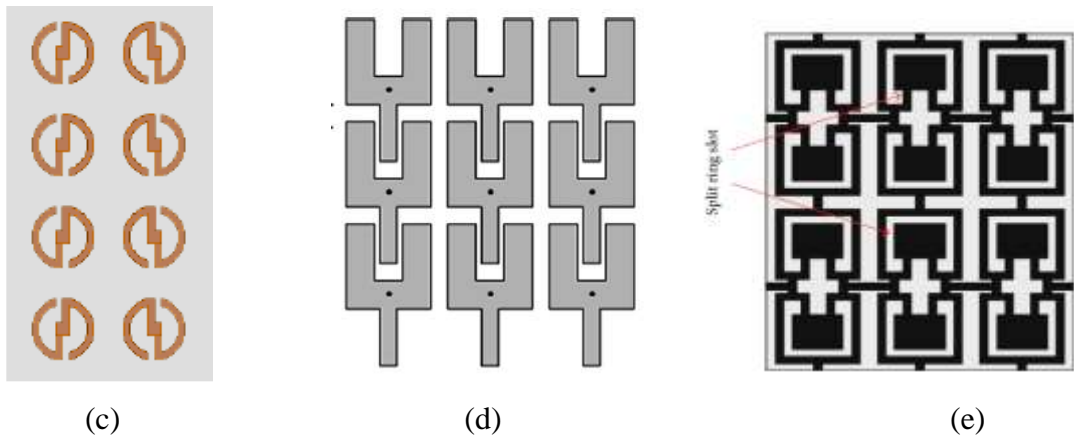


**Figure 1.9** various shapes of EBG structure (a) 1-D EBG [19], (b) 2-D mushroom shaped EBG [20], (c) S-shape EBG [21], (d) fork shape EBG [22], (e) Split ring slot (SRS)- EBG [23]

### 1.5.4 Neutralization Line

The isolation can also be enhanced by a neutralization line which is placed on the same side of the radiator between antenna elements.

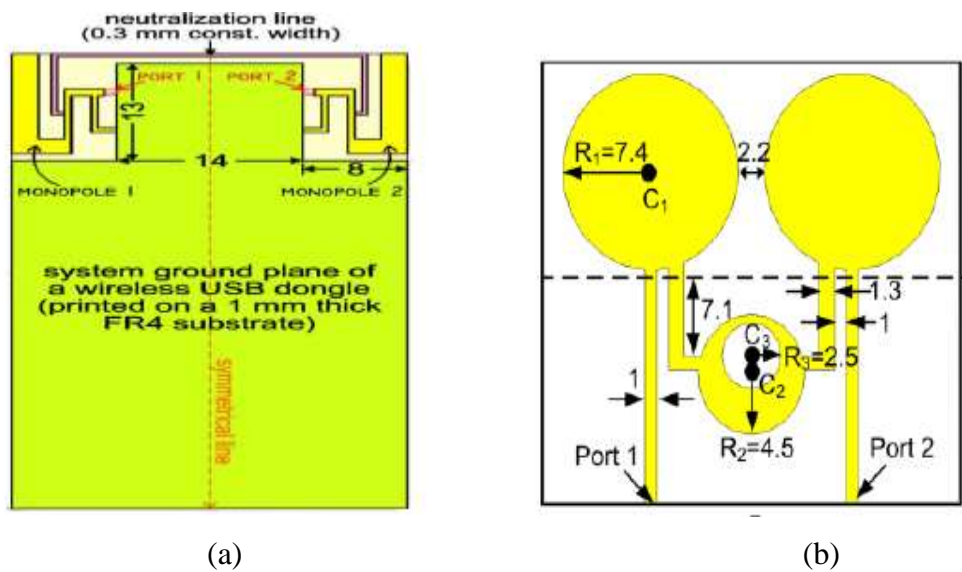


**Figure 1.10** (a) Thin neutralization line between two monopole antenna [24] (b) Wideband neutralization line between two circular monopole antenna [25].



The neutralization line takes the current from one antenna element then it is phase reversed by 180 degrees by selecting a proper length of the neutralization line. This reverse current is fed to the nearest antenna element and decreases the amount of coupling current. But in this technique, it is very difficult to find the exact location at which the current is being reversed. Figure 1.10, represents the example of a neutralization line structure.

### 1.5.5 Parasitic or slot Elements

In this technique, the parasitic element is not directly connected with the antenna element. It creates the opposite of coupled field and suppresses the mutual coupling current to other elements. Figure 1.11 (i) shows the two antenna element in which current  $I_0$  flow in the first antenna element and due to mutual coupling  $aI_0$  amount of current flow in the second antenna element. But after inserting the parasitic element between two antenna elements in Figure 1.11(ii), the additional mutual coupling current opposes the previous one due to the first element linked to the second antenna element. The overall effect of mutual coupling is reduced by inserting the parasitic element.

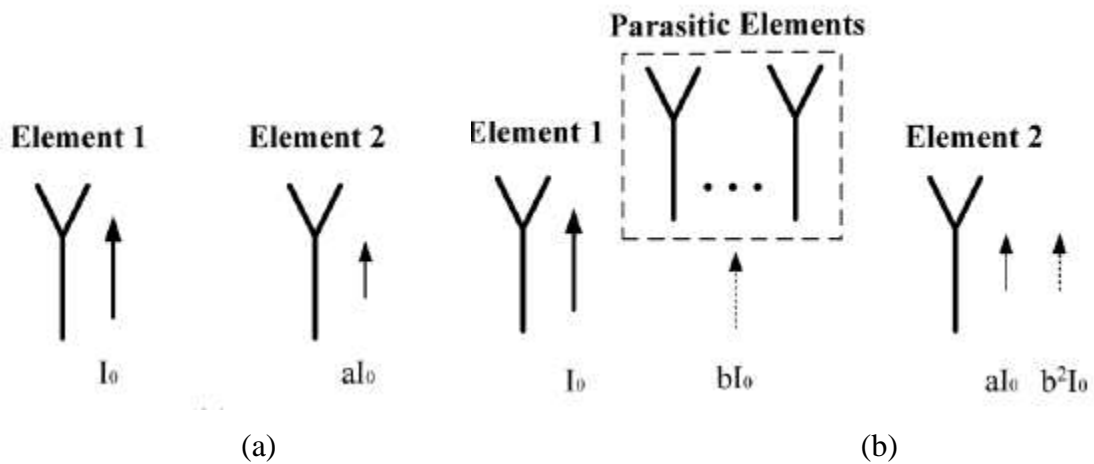


**Figure 1.11** (a) Antenna arrangement without parasitic element (b) With parasitic element [26]

There are various shapes used for a parasitic element that is presented in Figures 1.12.

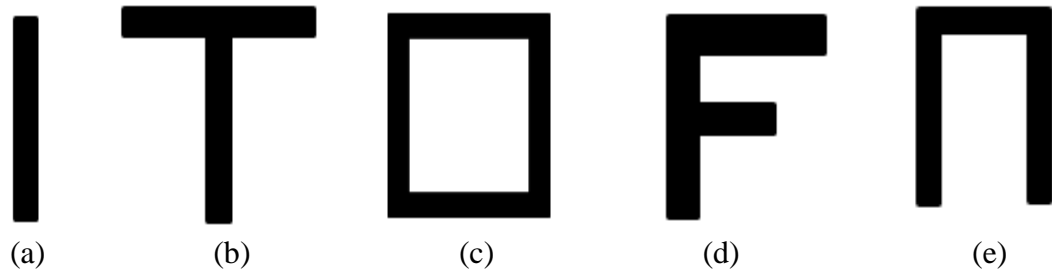


**Figure 1.12** various shapes parasitic element (a) Metal Strip (b) T-shaped (c) Square shape (d) F-shaped (e) U-shape

### 1.5.6 Metamaterial Structure

A metamaterial is an electrically small size artificial structure whose permittivity and permeability possess negative value. This structure blocks the current flowing from one element to another which enhances the isolation. There are various shapes of metamaterial structures available like meander-shaped, square, and circular split ring resonators or metamaterial absorbers as shown in Figure 1.13.

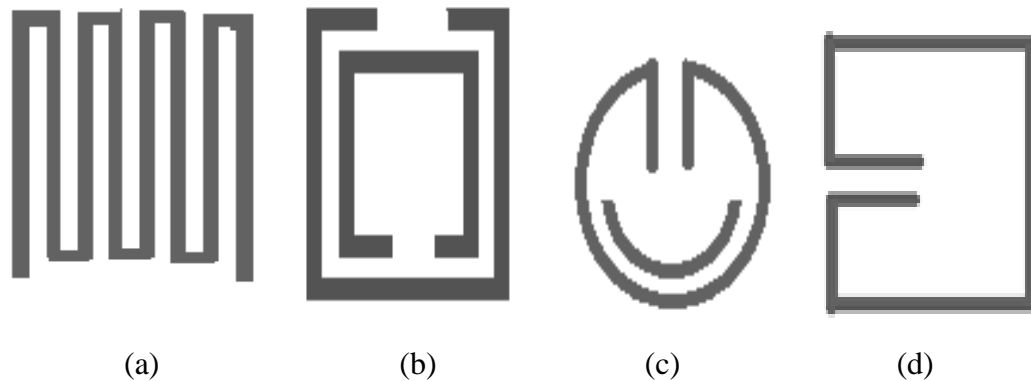


**Figure 1.13** various shapes of metamaterial structure (a) meander type (b) CSRR (c) Circular SRR (d) metamaterial absorber

### 1.6 Miniaturization Techniques

Miniaturization can be achieved either by placing multiple antennas very close to each other or reducing the size of radiating elements or sometimes antennas are placed in an orthogonal fashion. The miniaturization techniques change the physical and electrical properties of the antenna.

### 1.6.1 Antennas based on Space-Filling Curves

The basic idea to minimize the size of the antenna is either to increase the dimension or the space by inserting additional elements into the existing antenna element. There are two types of antenna incorporated in terms of meander antenna and fractal antenna. In the meander line antenna, folding a long straight line to a very small length is shown in Figure 1.14 (a). Due to the low cost and compactness of the meander line antenna, it is mostly preferred in Radio Frequency Identification Detection (RFID) applications. The antenna gain in the case of the meander line is not much high because of  $180^\circ$  phase difference in both sides' arms which cancels the far-field radiation in the respective arm. In fractal antenna, they provide radiation pattern and impedance same as a larger antenna with the very less occupied area. There are various shapes of structures like trees, snowflakes, coastlines, or ferns. The Koch dipole antenna is shown in Figure 1.14 (b) in which the start and the end position are the same as the ordinary dipole antenna which provides a larger length with a lower resonant frequency. It miniaturized the antenna size and was sensitive to both vertically and horizontally radio waves. This type of antenna is generally used inside radio telephone headsets.

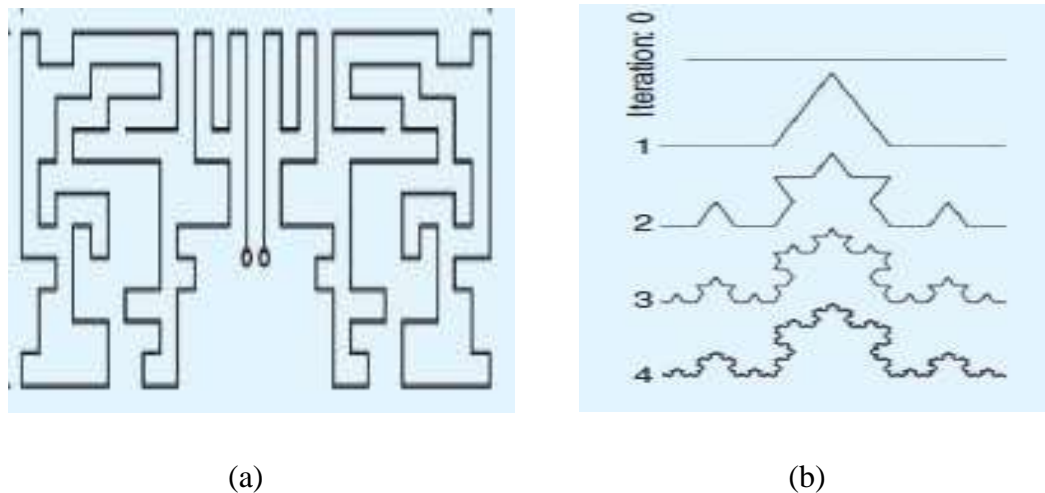


**Figure 1.14** (a) Meander line dipole antenna (b) Koch fractal monopole [27]

### 1.6.2 Material Loading

There is an inverse relationship between relative permittivity with the length and the width of the antenna element. The Higher is the value of permittivity, the smaller is the size of the antenna. In this technique by increasing the substrate value, surface wave excitation and dielectric loss within the substrate material increases which leads to a decrease in the bandwidth and radiation efficiency of the antenna. The various high value of dielectric constant like Rogers 3210 ( $\epsilon_r = 10.2$ ), ceramic alumina ( $\epsilon_r = 9.4$ ) and barium-titanate ( $\epsilon_r = 37$ ) etc. is used for miniaturization of antenna.

### 1.6.3 Antenna Reshaping and Introducing Slot on Radiator

The antenna size can be reduced either by etching the slot on a radiator or by changing the shape of the radiating element. It can be reduced by around 40-75 % by inserting a slot on radiating element. But by this technique, the low radiation efficiency is achieved. At the same time, it provides wider bandwidth using the slot.

### 1.6.4 Defects on Ground or Introducing Slots on Ground

The return current path changes due to adding slots whose size is comparable to  $\lambda$  on the ground plane. The portion of current converts into the displacement current due to introducing a slot on the ground plane and radiating current from one edge to another edge as shown in Figure 1.15 (a).

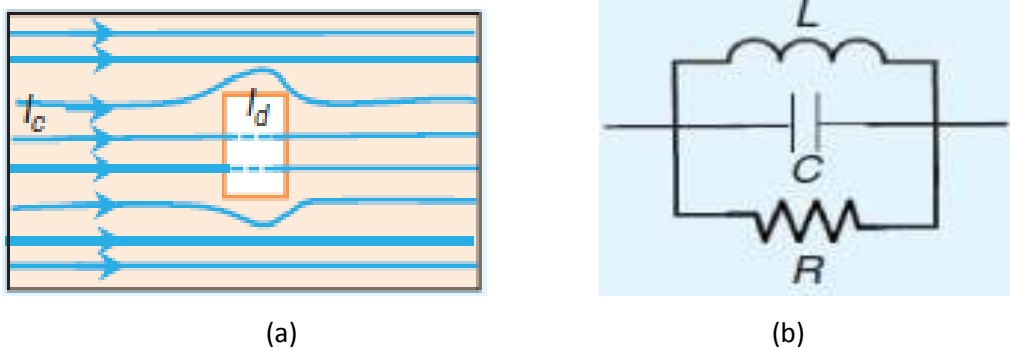


**Figure 1.15** (a) Defects on the ground plane (b) Equivalent circuit model [28]

The behavior of adding slots on the ground plane is modeled as a parallel combination of the R, L, and C components. The resistance, capacitance, and inductance are due to radiation, displaced current and extra path respectively. The main drawback of this technique is that signal generated from the slot on the ground plane is coupled with other elements. The phase of current changes due to combining these two phenomena which slow the flow of current.

### 1.6.5 Shorting and Folding

The size of the antenna can also be reduced by folding and connecting pins between the radiating patch and the ground plane because it makes the antenna electrically small. In the case of a half wavelength rectangular microstrip patch antenna, the electric field is maximum at the edge of the radiating patch and zero in the middle of the edge. After placing an electrical wall in the middle of the edge and removing other edges then it becomes a quarter-wave patch antenna that resonates at the same frequency as a half-wave patch antenna. It is very difficult for placing the conducting sheets between the radiating patch and the ground plane for practical implementation of quarter-wave. This can be resolved by adding an array of pins between the ground plane and radiating patch as illustrated in Figure 1.16.

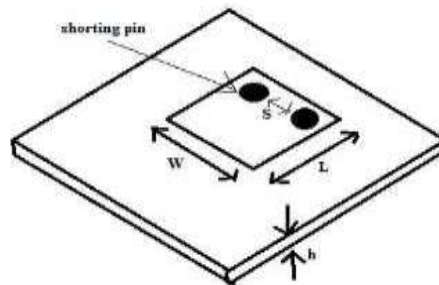


**Figure 1.16** Quarter wavelength MPA using shorting pin [29]

## 1.7 Research Motivation

Today everyone demands high data rates, large bandwidth, low cost with low power consumption, and the size of every wireless device becoming small, so the antenna placed inside these devices also needs to be compact. Over the last few years, UWB technology

has greatly enhanced the high frequency of operation and data rates with low power spectral density. But this technology is suitable for short-distance communication and has a very high chance of multipath fading occurring. So for achieving high diversity and high channel capacity UWB technology is employed with MIMO technology. However, there are certain challenges to placing multiple antennas in a small area because it will increase mutual coupling. The main target of this thesis is to design and developed a miniature MIMO antenna with wide bandwidth and high isolation for UWB applications.

## 1.8 Objectives and outcomes

The objectives of my research work are as follows.

1. To design and analyze of Ultra Wide Band antenna.
2. To design and performance analysis of novel and compact Ultra Wide Band Multiple-Input Multiple-Output antenna.
3. To fabricate the prototype MIMO antenna.
4. To measure the S-parameter using a vector network analyzer (VNA) and radiation pattern characteristics measured inside the anechoic chamber.

In our work, we have designed four different antennas by incorporating different techniques. In all cases, we have completed both the simulation and measurement process by developing the required prototypes. Though all the objectives are achieved in one or two designs, significant improvements in all aspects which are important for the MIMO system were not met. Therefore we tried to improve the required parameters step by step from design -1 to design-4.

## 1.9 Thesis Organization

The thesis report has organized into the following chapters.

**Chapter-1:** This chapter provides a brief introduction to UWB and MIMO technology, MIMO performance parameter, various techniques for isolation improvement and antenna miniaturization techniques, motivation of the research, and thesis organization presented.

**Chapter-2:** The detailed literature survey on the UWB monopole and the MIMO antenna for various applications is extensively discussed in this chapter.

**Chapter-3:** This chapter presents the MIMO antenna having two ports and four ports respectively with microstrip fed. The isolation has been improved due to the orthogonal arrangement of the antenna element and further for more isolation improvement, a decoupling structure has been incorporated between the partially slotted ground planes.

**Chapter-4:** A compact quad-port MIMO antenna that is orthogonally placed on the top surface of the substrate with a partial slotted ground plane is described in this chapter. The mutual coupling has been reduced by placing antenna elements orthogonally without any additional decoupling structure. At the end of this chapter, describes the effect of different housing materials on the return loss and the isolation parameter.

**Chapter-5:** In this chapter, a miniature MIMO antenna having four-port with CSRR structure placed on the ground is described. The isolation of the prototype antenna has been improved by etching 4 L-shape strips and two rectangular CSRR unit cells on the ground plane. This designed antenna is quite suitable for the various UWB portable devices.

**Chapter-6:** This chapter provides a dual notch band characteristics UWB MIMO antenna. The specialty of this design finds the compactness and very high isolation, which is achieved by etching the modified minkowski fractal structure and inverted L-shaped stub made available with the partial ground plane.

**Chapter-7:** This chapter presents the summary of the research work and future scope.

## **1.10 Summary**

This chapter provides a brief introduction to UWB technology and an introduction to the MIMO antenna along with various isolation enhancement and miniaturization techniques. It also gives the outlines of the motivation of research and thesis organization. In the next chapter, the literature review will be carried out.

# **Chapter-2**

## **Literature Review**

### **2.1 Introduction**

Heinrich Hertz is the first person who invented an antenna for transmitting and receiving a particular signal. But in elapse of time, there is continuous research made to improve the structure for different applications. Nowadays we are more focused on antenna size which leads to the development of 3-D antenna to planar antenna. Microstrip antenna is one of the exciting evolution in this area. This antenna possesses lightweight, low cost, easy integration with microwave monolithic integrated circuit, supports both linear and circular polarization, good radiation control, and is moreover easy to fabricate. It is available in a variety of shapes like rectangular, circular, square, and triangular. At the same time, narrow bandwidth, lower gain, and lower radiation efficiency along with poor power handling capability are the limitation of microstrip antenna. Over the last few years, many researchers have used UWB technology to improve the bandwidth and other parameters of microstrip antennas. But still, multipath fading and channel capacity are the big challenges for today's wireless communication devices. Further to resolve these issues the MIMO design combined with the UWB technology. There is a lot of research still going on on the MIMO antenna for the improvement of various diversity parameters.

### **2.2 Literature Review on UWB and MIMO Antenna**

In January 2008, Abbosh and bialkowski [30] proposed a UWB monopole antenna which was made of an intersection of either two circles or two ellipses. The designed model provided an impedance bandwidth from 3.1-10.6 GHz and achieved an efficiency of more than 90 %. This antenna possessed an omnidirectional radiation pattern. In March 2008, Wu et al.[31] designed a rectangular monopole antenna and the feeding structure which is made up of trident shaped combined with the tapered shaped structure. The proposed



prototype has a miniature size of 30 mm x 8 mm and offered a bandwidth from 2.75-16.2 GHz. The experimental results show that the gain increases linearly from 2 to 4 dB in the whole operating band. In the same year 2008, Cheng et al.[32], developed a UWB antenna which was based on the planar inverted cone antenna (PICA) concept and integrated with a two-layer PCB. The leaf-shaped metal structure radiator was used on the top and a larger leaf-shaped slot on the bottom of the substrate. The antenna size was 60 mm × 60 mm, which covered the impedance bandwidth from 2.2-30 GHz, and high radiation efficiency from 80-90% was achieved in the whole frequency range. In May 2008, Kim et al.[33] , reported a 45 mm × 40 mm MIMO antenna having two-port and the operating bandwidth lies between 2.3- 5.9 GHz. The proposed antenna consists of two identical elliptical shape radiators placed at 45<sup>0</sup> and -45<sup>0</sup> to generate the orthogonal current which leads to enhancing the isolation. Later on, in September 2008, Yang et al. [34], developed an SRR based UWB antenna and coupled it with the microstrip line structure. The proposed prototype provided a bandwidth from 3.6 to 14.6 GHz with a maximum gain of 9.8 dB. In October 2008, Dastranj et al.[35], designed the antenna with a dimension of 45 mm × 40 mm with a wide slot microstrip feed line. The impedance bandwidth was varied from 2.8-11.4 GHz. This designed antenna exhibits a stable far-field radiation pattern. The author enhanced the operating bandwidth and the radiation characteristics by implementing an E-shaped feedline. In the same year, Ahmed and Sebak [36], proposed a UWB antenna which is made up of a half-circular disc combined with a two-step rectangular patch and a circular shape slot etched on the radiator. The prototype model has dimension of 50 mm × 40 mm and measured an impedance bandwidth from 3-11.4 GHz. At the same time, antenna exhibits an omnidirectional pattern. Later on, in the same year 2008, Sze and Chang [37] reported a circularly polarized square slot antenna with CPW feed .The two inverted L-shaped ground strip was used for enhancing the impedance bandwidth. The antenna is achieved more than 52 % impedance bandwidth with 4 dB gain.

In January 2009, Yang et.al [38], developed an antenna that consists of multi resonant split ring loop. The different geometrical ground planes along with the dual concentric split ring loop were used. The antenna provided an operating bandwidth from 2

to 20 GHz. The taper transmission line was used by the author for improving the return loss. In May 2009, Raj Gopal and Sharma [39], reported a pentagon-shaped microstrip slot antenna for the ultra-wideband. The designed antenna has a bandwidth from 2.65-11.3 GHz with a dimension of 80 mm  $\times$  50 mm. In this design, both the straight line and tilted feed line has discussed with the different substrate materials. The measured results show that the antenna has a stable radiation pattern. In the same year in May 2009, Lin and Huang [40], proposed a Coplanar Waveguide (CPW) feed UWB antenna which consists of a rectangular patch radiator combined with an inverted L-shaped stub. The antenna has 32.4 mm  $\times$  24 mm in size and it covered an impedance bandwidth from 3.5 to 7.5 GHz. The measured gain increases from 2.5-6.4 dB. Further in June 2009, Guo et al. [41], reported an ultra-wideband antenna that consists of a half-circular disc radiator on the top and its complementary magnetic counterpart on another side. The antenna has a dimension of 16 mm  $\times$  25 mm and offered a bandwidth from 2.8-10.7 GHz. A triangular-shaped slot was used on the ground plane for impedance matching. In June 2009, See and Chen [42], investigated two ports triangular notch radiator with a dimension of 45 mm  $\times$  37 mm  $\times$  0.8 mm. A v-shaped slot was etched on the partial ground plane to reduce the mutual coupling. The measured results show that the antenna offered a bandwidth from 3.1-5 GHz, an average gain of more than 2 dB, and efficiency is more than 70% with isolation of less than -20 dB. In July 2009, Abbosh [43], investigated an antipodal tapered slot antenna for the ultra-wideband. The antenna offered 3.1-10.6 GHz impedance bandwidth with a dimension of 60 mm  $\times$  60 mm. This antenna was fabricated with the Rogers RT6010 substrate and the gain of the antenna varied between 2.7-8 dB. In November 2009, Toh et al.[44], reported a dual ports ultra wideband antenna with the differential feed strip on the radiator. The antenna finds an operating band of 3.1- 5.2 GHz and measured gain of 8.4-10.3 dB for the broadside mode and for the conical mode measured gain 3.2-5.1 dB with operating bandwidth 3.1 -4.9 GHz. The isolation between ports has more than 13.5 dB. Further in December 2009, Zhang et al. [45], proposed a UWB MIMO antenna having two ports and it consists of triangular patch radiator along with tree like structure etched on the ground plane for isolation improvement. The antenna was fabricated with Taconic ORCER RF-35

substrate with a dimension of 35 mm x 40 mm. The prototype model provided a bandwidth from 3.1-10.6 GHz with isolation of less than -16 dB.

In February 2010, Liu and Yang [46], developed an ultra-wideband antenna that consist of a hook-shaped radiator with a dimension of 10 mm x 10 mm and an overall dimension of 80 mm × 40 mm. The designed antenna operated between 3-10.7 GHz with an efficiency of more than 60 % and gain more than 1.2 dB. In March 2010, Sim et al.[47], proposed a UWB antenna in which a T-shaped open slot etched on the ground and microstrip feed was used for the excitation. The impedance matching at a lower frequency was achieved by introducing a small notch on the T-shaped open slot. Further impedance matching at the middle and higher frequencies has improved by extending a small section of the feed line. The designed antenna has a dimension of 28 mm × 14.5 mm and a maximum measured gain of 4.5 dB. This antenna offered bandwidth of 3.1- 11.45 GHz. In the same year in March 2010, Sonakki and Salonen [48], reported a two monopole antenna with a dimension of 120 mm × 70mm. The mutual coupling between antennas has been reduced by inserting two half-wavelength long narrow slits on the ground plane. The experimental results show that an impedance bandwidth significantly improved by 37.8 % at the resonance frequency. In May 2010, Zaker and Abdipour [49], reported a 16 mm × 11 mm dimension antenna which consists of a truncated shaped radiator that includes a partial ground structure. This prototype model has an operational bandwidth from 3.9-21.4 GHz. The measured results show that maximum gain of 5.85 dB with stable omnidirectional radiation pattern. Further, in 2010, Koohestani and Golpour [50], proposed an ultra-wideband antenna in which two parasitic stubs were used with a U-shaped patch. The antenna was fabricated with a 24 mm × 28 mm dimension of RT/ Duroid 5870 material. The antenna is operated between 2.76-12.8 GHz with peak gain varying from 1.6 -5.3 dB. Further Sheikhan et al.[51], proposed a 22 mm × 22 mm size rectangular shaped ultra-wideband antenna. The bandwidth of the antenna has been improved by implementing a ladder-shaped structure on the ground. This designed antenna offered a bandwidth from 2.7-20 GHz. The experimental results show that the antenna has a stable radiation pattern for the entire bandwidth and achieved a radiation efficiency of more than

80 %. Later on, in June 2010, Baek and Lim [52], developed a  $38 \text{ mm} \times 38 \text{ mm}$  dimension of a MIMO antenna that consists of an electric and a magnetic loop antenna which is orthogonally polarized. The measured results show that, the gain of an electric and magnetic loop antenna were found to be 1.36 dB and 0.48 dB respectively. This antenna also provided isolation less than  $-20 \text{ dB}$  in the entire operating frequency band.

In January 2011, Azim et al. [53], reported a double-sided printed antenna with a dimension of  $30 \text{ mm} \times 22 \text{ mm}$  that operates from 3.08-15.9 GHz. The antenna bandwidth has improved due to an etching of a saw tooth shape structure on the top of the partial ground plane. This designed antenna provided a maximum gain of 5.9 dB. In February 2011, Najam et al.[54], developed a model having two ports that consist of two circular monopole antennas with the partial ground plane. The mutual coupling between antennas has been reduced by etching an inverted Y-shaped stub on the ground. This designed antenna has a dimension of  $40 \text{ mm} \times 68 \text{ mm}$  and offered a bandwidth from 3.2-10.6 GHz. The experimental results show that radiation efficiency increases from 70 % to 85 % and the variation in gain are less than 2.5 dB. In May 2011, Ghosh [55] proposed an ultra-wideband antenna that consists of a crossed rectangular monopole antenna and is placed on the circular ground plane. This design provided an operating bandwidth from 3.1-10.6 GHz with a maximum gain of 6 dB. This prototype design enhanced the bandwidth by combining the effect of the crosses radiator and circular ground plane. In 2011, Koohestani et al. [56], presented a dome-topped bowl-shaped radiator for ultra-wide applications. The impedance of the antenna has improved by a truncated ground plane. The antenna has offered a wide band from 3.65-13 GHz and the overall size was found to be  $18 \text{ mm} \times 20 \text{ mm} \times 1.6 \text{ mm}$ . In June 2011, Ghaderi and Mohajeri [57], reported a UWB antenna that consists of an elliptical patch with a trapezoid shape and a hexagonal slot etched on the ground plane. The proposed prototype offered a bandwidth from 2.9-18 GHz. The measured results show that the designed antenna obtained an average gain of 3.7 dB with a variation of less than 0.8 dB. In the same years Mishra et al. [58], developed an antenna for Bluetooth and ultra-wideband applications. The antenna is made up of a U- shaped monopole for the ultra-wideband and a rectangular monopole for Bluetooth applications.

The antenna is operated between 2.4-2.484 GHz (Bluetooth) and between 3.1-10.6 GHz (UWB). The proposed antenna has more than 80% radiation efficiency with gain varied in the range of 2-5 dB. In May 2011, Chen et al. [59], investigated a super wideband antenna that has an egg-shaped monopole radiator. A semi-elliptical fractal complementary slot has developed on the asymmetrical ground for bandwidth improvement. This designed model provided a bandwidth from 1.44-18.8 GHz with an overall dimension of 35 mm  $\times$  77 mm. In September 2011, Sonkki et al.[60], proposed a wideband antenna which is achieved by the combined effect of an electric dipole and magnetic slot which was orthogonally placed. The experimental results show that ECC < 0.01, isolation less than -18 dB with DG > 8 dB.

In February 2012, Su et al. [24], proposed two elements multiple input and multiple outputs for the USB dongle application. A neutralization line technique had used for reducing the mutual coupling. The overall dimension of the antenna has 65 mm  $\times$  30 mm and isolation is less than -19 dB with a radiation efficiency of more than 70%. In the same year Li et al. [26], reported a MIMO antenna with a dimension of 95 mm  $\times$  60 mm, that consists of a symmetrical monopole antenna and slots introduce on the ground plane. A parasitic monopole element was placed between antenna elements for isolation improvement. This parasitic element creates a reverse coupling path and canceled the original coupling currents. The measured radiation efficiency of more than 80 % was achieved. Further in February 2012, Li and Chu [61], proposed a multiple input multiple output antenna that consists of two dual branch monopole radiators with two bent slits on the ground plane. These bent slits along with a triangular slot were created on the ground for isolation improvement. The proposed antenna has an overall dimension of 78 mm  $\times$  40 mm with operating impedance bandwidth from 2.4-6.55 GHz. The total efficiency of the antenna was more than 46 % with an ECC value of less than 0.01. In March 2012, Tsai and Yang et al. [62], reported an eye-shaped antenna with CPW feeding. It consists of an elliptic monopole radiator and coupling line. The antenna is operated between 1.2-4.5 GHz with a dimension of 60 mm  $\times$  30 mm. The gain and the efficiency of the antenna varied from 0.1-2.2 dB and 80-85% respectively. In March 2012, Gallo et al. [63], reported an annular slot

antenna that is etched from a square plane. The designed antenna has an overall dimension of  $80 \text{ mm} \times 80$  and is suitable for high diversity applications. The measurement shows that  $\text{ECC} < 0.11$ , diversity gain near to 10 dB, and provided a bandwidth from 3-12GHz. In May 2012, Kumar et al. [64], proposed a circular monopole antenna that inscribed the triangle to get a circular fractal structure and it is operated between 2.25-15 GHz. The antenna had used the CPW feeding technique and obtained a peak gain of less than 5 dB. The measured results show that as frequency increases, the radiation efficiency is decreased. In June 2012, Wu et al. [65], reported a UWB antenna, and two triangular notches were etched from the corner of the radiator for bandwidth improvement. Further, for more improvement, three slots were introduced on the notched radiator. This model provided a bandwidth from 2.86-13.38 GHz with an overall dimension of antenna  $37 \text{ mm} \times 15 \text{ mm}$ . The gain of the antenna is varied from 3-6.9 dB without any load and with a laptop as the load is decreased to 2.1- 6.4 dB due to the load effect. In July 2012, Tang et al. [66], presented an ultra-wideband that consists of two asymmetric U-shaped and staircase-shaped strips. For proper impedance matching, a CPW feeding technique was used. The antenna offered the bandwidth from 3-12.9 GHz and a dimension of  $23 \text{ mm} \times 25.5 \text{ mm}$ . The proposed antenna has almost constant gain in the whole operating band. In the same year, Lu and Yeh [67] reported an ultra-wideband antenna that consists of an arc-shaped radiator and a partially slotted ground plane. The multi resonant modes were excited by using rectangular parasitic elements on the top of the substrate. The impedance bandwidth of the antenna varied from 3.02-13.27 GHz with a size of  $30 \text{ mm} \times 30 \text{ mm}$ . The measured peak gain of the antenna lies in the range of 1.2-5.3 dB with 85-91% radiation efficiency. Further in July 2012, Fereidoony et al. [68] reported a circular monopole antenna which consist of a circular ground plane and fractal ground plane has used for the stable radiation. This antenna offered a bandwidth from 3.1-10.6 GHz for circular ground plane and 3.5-4 GHz, 5.5-6 GHz, 7-7.5 GHz for the fractal ground. In August 2012, Lin [69], developed a bow tie shaped UWB quasi-self-complementary antenna (QSCA). It consists of two radiating element, one a horn shaped radiator and other counter part of the horn shaped slot on the FR4 substrate material. This antenna has operating bandwidth from

3.1-10.6 GHz with dimension of 35 mm  $\times$  10 mm. A coplanar waveguide (CPW) feeding technique was used for the impedance matching. In August 2012, Li et al. [70], developed a two elements UWB MIMO antenna that consist of a basic rectangular monopole antenna with the partial ground plane. The rectangular and circular Stepped Impedance Resonator (SIR) created on the ground for isolation improvement. The designed antenna operated from 3.1-10 GHz and isolation  $< -23$  dB were measured. In October 2012, Wang et al. [71], presented a UWB antenna and it consist of reverse T- matched dipole and center feed dipole on the bottom layer, which has connected with the two shorting pin. The proposed antenna was fabricated with Wangling Teflon woven glass fabric and dimension of 23 mm  $\times$  32 mm. This antenna offered bandwidth from 2.89-6.50 GHz with stable radiation pattern.

In January 2013, Chang et al. [72], presented a UWB antenna which consists of a rectangular monopole antenna used as a radiator and modified the ground structure. In the ground plane, one semicircular slot and two stubs were introduced for bandwidth improvement. The author claimed a bandwidth from 2.1-2.6 GHz and 3.3-20 GHz with a maximum gain of 6.6 dB. The antenna has a dimension of 33.1 mm  $\times$  20 mm and is fabricated with Rogers RT/duroid 5880 substrate material. In March 2013, Bitchikh et al. [73], proposed an octagonal-shaped UWB antenna with a modified ground plane for bandwidth improvement. The operating bandwidth of the antenna varied from 2.3 to 14 GHz. The antenna was fabricated with an epoxy glass of dimension 45 mm  $\times$  45 mm and the measured gain was varied from 1-5.25 dB. In the same year, Mohammad et al. [74], reported a UWB MIMO antenna which consists of a U-shaped patch loaded with a T-shaped monopole antenna. For the bandwidth improvement, a pentagon-shaped structure was etched on the ground plane. The experimental results show that the prototype provided a bandwidth from 3.1-10.6 GHz and radiation efficiency increased from 85 % to 95 %. In March 2013, Chacko et al. [75], proposed an annular slot dual-polarized antenna for the UWB and the orthogonal feeding technique has been used for polarization diversity. A cross-shaped stub was used diagonally between two U-shaped stubs for the isolation improvement. The notch has also developed due to inserting an arc shape slot on the

radiator. The measured results provided a bandwidth from 2.8-11 GHz with  $ECC < 0.025$  through the entire operating band. In August 2013, Sefidi et al.[76], presented a  $22 \text{ mm} \times 26 \text{ mm}$  size ultra-wide antenna that operates from 2-11.2 GHz. The rectangular monopole antenna was modified by cutting two L-shapes and two triangular notches, which improves the impedance matching. The omnidirectional radiation patterns were obtained at all frequencies. In October 2013, Kim and Yun [77], proposed an ultra-wideband antenna that consists of a C-shaped radiator, and impedance bandwidth has improved due to an inverted L- shaped strip. This antenna offered the operating bandwidth from 2.3-10.8 GHz with a dimension of  $40 \text{ mm} \times 30 \text{ mm}$ . The gain of the antenna varied from 2.1-5.2 dB with a radiation efficiency of more than 70% over the entire operating range. In August 2013, Liu and Cheung [78], presented a  $26 \text{ mm} \times 40 \text{ mm}$  size, two ports MIMO antenna. It consists of a simple rectangular patch as a radiator and is placed perpendicular to each other for isolation improvement. Further, for more impedance matching and isolation improvement, two protruded ground stubs were used. The operating bandwidth from 3.1-10.6 GHz, isolation less than  $-15 \text{ dB}$  with measured gain varied from 0.9 dB to 6.5 dB were achieved. The simulated results were verified with the measured one. In August 2013, Sharawi et al. [79], developed a MIMO antenna having four ports and 76 % miniaturization had achieved by introducing a CSRR structure on the ground. The prototype was developed with a 0.8 mm thick FR4 substrate with a dimension of  $50 \text{ mm} \times 100 \text{ mm}$ . In November 2013, Gogosh et al. [80], designed a MIMO antenna having two ports that consist of elliptical radiators at some angle along with a circular slot in the middle position. The H-shaped structure was etched on the ground which suppresses the induced current that leads to improving the isolation. The author achieved an overall dimension of  $74 \text{ mm} \times 48 \text{ mm}$  and isolation of more than 25 dB. In the same year, Li et al.[81], reported a dual-port MIMO antenna which consists of a U-shaped radiator and metal strip attached to the radiator along. At the same time, two protruded ground parts were introduced for improving the impedance bandwidth and the isolation. This design offered an operating bandwidth from 3-11 GHz with dimension of  $27 \text{ mm} \times 30 \text{ mm}$ . The antenna has efficiency more than 65 % with mean effective gain less than 1.75 dB and envelope correlation coefficient less than 0.012.



In January 2014, Srivastava et al. [82], presented a UWB antenna made up of M shaped monopole-like slot and bandwidth has been enhanced by modifying the ground plane. The proposed antenna offered a bandwidth from 2.38-12.4 GHz with a dimension of 36 mm  $\times$  36 mm. In 2014, Liu et al.[83], reported a MIMO antenna that consists of two QSCA, both are the mirror image along with inverted T-shaped stubs on the ground. One half of a circular patch is placed on the top and the other half complement placed on the bottom of the substrate. The isolation between antenna elements has improved by etching two identical rectangular slots on the ground. Experimental results show that the proposed model provided a bandwidth from 3.4-12 GHz, an efficiency of more than 70 %, and a maximum gain of 4.3 dB. In the same year, Khan et al. [84], proposed a two-port UWB antenna, and for isolation improvement, the floating parasitic element was placed between antenna elements. The parasitic element is made up of a horizontal strip and vertical stub of unequal length. The antenna offered a bandwidth from 3.1-10.6 GHz with an antenna dimension of 33 mm  $\times$  45.5 mm. The proposed antenna has achieved radiation efficiency of more than 85 % and a peak gain of 5.3 dB with a low ECC value of less than 0.6 for the entire operating frequency band. In June 2014, Rawi et al. [85], proposed a four-port butterfly-shaped MIMO antenna, which consists of two self-grounded monopoles placed on one side and two monopoles placed on another side of the substrate material. The measured results show that the proposed antenna operated from 0.5-15 GHz. The antenna has an overall dimension of 250 mm  $\times$  250 mm. For the bandwidth improvement, they were implemented with a genetic algorithm. The isolation has been enhanced by the positioning of the antenna in an orthogonal fashion. In July 2014, Liu et al. [86], reported a MIMO antenna that consists of two semicircular patches, and its complementary structure is placed on either side of the substrate. This design prototype offered an impedance bandwidth from 2.19-11.07 GHz with an overall dimension of 30 mm  $\times$  41 mm. The proposed antenna provided a peak gain of 6.5 dB, radiation efficiency from 55 % to 88 %, isolation less than - 20 dB, and ECC < 0.25 over the entire operating frequency band. In August 2014, Ren et al. [87], reported a two-port MIMO antenna having a dimension of 32 mm  $\times$  32 mm and made up of a rectangular monopole radiator along with two open L-

shaped slots. The isolation was enhanced by placing the antenna elements orthogonally and narrow slits etched on the ground. Further added a T-stub on the radiator for bandwidth improvement. This antenna provided a bandwidth of 3.1-10.6 GHz and measured gain varied from 1.7 dB to 4.2 dB. In September 2014, Mao et al. [88], presented a dual polarized MIMO antenna having two and four ports. The compactness of the antenna has achieved due to sharing a single pentagon radiator by two port at the same time dual polarization was achieved due to a perpendicular feed structure. A T-shaped slots was etched on the radiator and extending a stub on the ground for isolation improvement. The designed model offered an operating bandwidth from 3-11 GHz with dimension of 48 mm  $\times$  48 mm. The obtained results show that more than 60 % radiation efficiency was achieved by the author. Further in the same year, Tang and Huang et al. [89], reported a 30 mm  $\times$  30 mm size of MIMO antenna having two ports. A strip was placed on the ground and it was connected to radiator via vias for isolation improvement. It provides an extra current path at the same time works as an impedance transformer. The proposed design provided an operating bandwidth from 3.1-10.6 GHz and ECC  $<$  0.05 in the entire frequency band.

In April 2015, Roshan et al. [90], presented a Coplanar Strip (CPS) line feed MIMO antenna having two ports and a radiator made up of a staircase-shaped radiator. The mutual coupling was reduced by using a metal strip that works as a reflector. The proposed antenna offered an operating frequency band from 3.1-10.6 GHz with a size of 25 mm  $\times$  30 mm. The proposed design provided a maximum efficiency of 90%, isolation  $<$  - 20dB with a peak gain of 5.2 dB. In May 2015, Liu et al. [91], reported a MIMO antenna that consists of a basic rectangular patch with tapered microstrip feed and modified the ground plane. A T- shaped stub was used on the ground for the reduction in mutual coupling. Further, for high isolation, a vertical slot is etched on the T- shaped stub. The notch band was produced due to two vertical strips placed on the ground plane. The antenna provided a bandwidth from 3.1-11 GHz. The measured isolation and ECC were less than - 15 dB and 0.1 respectively in the entire band. In August 2015, Zhang et al. [92], developed a 26 mm  $\times$  26 mm dimension of the Asymmetric Coplanar Strip (ACS)-fed two-port MIMO antenna that worked in the UWB range. It provided an operational bandwidth

from 3.1-10.6 GHz. The bandwidth and isolation were improved due to the etching of an I-slot on the radiator and cutting narrow slits on the ground plane. In December 2015, Srivastava and Mohan [93], reported a MIMO antenna having a crescent-shaped radiator on the top and a circular-shaped radiator on the bottom. These two antennas are placed orthogonal to each other and mutual coupling has been reduced by inserting a cross-shaped slot on the ground. For further isolation improvement sickle-shaped metallic strip is used on the top surface between antenna elements. The obtained results show that the ECC value is less than 0.02 and the channel capacity less than 0.4 bits/s/Hz over the entire frequency band. Further, in the same year, Alsath and Kanagasabai [94], proposed a two ports MIMO antenna and analyze the result by placing two antennas in a different position. The radiating patch consists of a half-circular and half rectangular ring. The bandwidth was enhanced by modifying a ground structure. This design offered a bandwidth from 3.1-10.9 GHz and is suitable for automotive communication. The experimental results show that the radiation efficiency has more than 75 %, the peak gain of 3.5 dB, isolation  $< -15$  dB, and  $ECC < 0.06$ . In 2015, Kang et al.[95], developed an offset microstrip feed antenna with a dimension of  $38.5 \text{ mm} \times 38.5 \text{ mm}$ . The high isolation and polarization diversity was achieved by placing antenna elements orthogonal. For Further improvement in isolation, a T- shaped parasitic element was inserted between the antenna elements. The author also achieved notch band characteristics by etching two L-shaped slits on the ground. The antenna provided a bandwidth from 3.08-11.8 GHz, isolation less than  $-15$  dB, and  $ECC < 0.02$ . In 2015, Luo et al. [96], proposed a defective ground structure-based two-port MIMO antenna. The isolation and impedance matching has improved due to the T-shaped slot etched on the ground plane which alters the surface current distribution. Further for better isolation, a 0.2 mm thin line slot etched on the ground produces an additional current that cancels the original coupling current. The antenna offered a bandwidth from 3.1-10.6 GHz, a radiation efficiency of around 90 %, and  $ECC < 0.5$ . In 2015, Sonkkki et al.[97], presented two Vivaldi antenna which is orthogonally placed cross-shaped. The antenna has fabricated with the Rogers 4003 RF-laminate and provided an operating bandwidth from 0.70-7.30 GHz. The designed antenna provided cross-polarization better than 19 dB and isolation  $<$

-30 dB. In 2015, Tripathi et al. [98], investigated four orthogonally placed octagonal-shaped Koch fractal antennas as a radiator and modified the ground plane. The antenna miniaturization and bandwidth have been enhanced due to Koch fractal geometry. Further isolation has been improved by a rectangular stub placed between antennas which works as a reflector. The band rejection was achieved by introducing a C-shaped slot on the radiating patch. The proposed antenna operated between 2-10.6 GHz with isolation better than 17 dB over the entire frequency band. In the same year, Zhang and Pedersen [25], proposed two closely spaced circular monopoles which provided operational bandwidth from 3.1-5 GHz. The neutralization line is made with a circular disc and two metal strips placed between antenna elements for isolation improvement. The decoupling current from the different paths is canceled by a circular disc. The overall dimension of the antenna has 35 mm x 33 mm with an isolation of more than 22 dB.

In 2016, Deng et al. [99], developed a MIMO antenna with a dimension of 30 mm × 40 mm and it consists of two meander monopoles. The bandwidth and impedance matching were improved by inserting two inverted L-shaped parasitic elements along with an L-shaped stub. The mutual coupling was reduced by cutting a slot on the ground. The designed antenna offered a bandwidth from 3.1-10.6 GHz and the performance of the antenna was measured in terms of ECC less than 0.15, radiation efficiency between 70-77.5 % in the entire frequency band. In April 2016, Huang and Xiao [100], proposed a two-element polygon-shaped MIMO antenna which is made by cutting a rectangular slot and triangular slot on the antenna element. The mutual coupling has been reduced by the stepped ground stub. Further rounded the corner of the partial ground plane for improving impedance matching. The designed model provided a bandwidth from 2.4-11 GHz. The measured results show that the proposed antenna has an efficiency of more than 70 %, ECC < 0.02, and isolation of less than -15 dB through the entire frequency band. In October 2016, Hakimi et al. [101], presented a two-port CPW feed MIMO antenna which was fabricated with the Rogers RT5880 substrate. The isolation between antenna elements has been enhanced due to the self-coupling patch which increases the current density. The antenna covered the bandwidth from 3.9-8.1 GHz and measured the mutual coupling as

less than  $-15$  dB in the entire operating band. In 2016, Srivastava et al. [102], proposed a four-port MIMO antenna in which each element is made up of a stepped slot with microstrip feed. The antenna provided operating bandwidth from 3.2-12 GHz with a dimension of  $42 \text{ mm} \times 25 \text{ mm}$ . The mutual coupling has reduced due to the directional radiation properties of a slot antenna and asymmetrical placement of the antenna element. The proposed antenna has achieved a constantly measured gain of 4 dB with a radiation efficiency of more than 80% and CCL  $< 0.4$  bits/s/Hz. In 2016, Zhu et al. [103], reported two ports quasi self-complementary MIMO antenna. It consists of fan shape radiator and its complement structure etched on the ground plane. These two elements were placed in orthogonal orientation which increases polarization diversity and reduced the mutual coupling. The proposed antenna produced notch band by etching bent shape slit on the radiating element. In the same paper four port MIMO antenna has also investigated. This antenna offered a bandwidth from 3-12 GHz and measured results show that isolation  $< -20$  dB with ECC  $< 0.5$  in the entire operating band.

In February 2017, Lin et al.[104], proposed a UWB MIMO antenna of size  $50 \text{ mm} \times 40 \text{ mm} \times 1.6 \text{ mm}$ . The designed model has an operational bandwidth from 2.5-11 GHz. The isolation between antenna elements has been improved by using carbon black films coated on the substrate. The carbon black film absorbs the interference between antenna elements. The designed antenna has an efficiency of 69.2% with a gain of more than 2.11dB. In February 2017, Totkas [105], presented a UWB MIMO antenna with a square element along with a G-shaped element for the mobile terminal. The T-shaped strip was used on the ground plane for reducing the mutual coupling between antenna elements. The designed antenna covered the bandwidth from 2.2-13.3 GHz with a low ECC value and more than 60 % efficiency was achieved. In March 2017, Liu and Tu [106], reported a  $44 \text{ mm} \times 44 \text{ mm}$  size UWB MIMO antenna that consists of a differential U-shaped microstrip feedline and stepped shaped slot. The isolation was improved by inserting four staged slots on the corner of the ground plane. It offered a bandwidth from 2.95-10.8 GHz with isolation of  $< -15.5$  dB in the entire band. In April 2017, Khan et al. [107], investigated a CSRR loaded UWB MIMO antenna. The proposed design consists of two

triangular monopole antennas with L-shaped stub inserted on the ground plane. Further CSRR structure was introduced on the ground between antenna elements to reduce the mutual coupling. The CSRR structure prevents the current from flowing to other elements. The antenna provided an operating frequency band from 3-12 GHz with the size of 23 mm  $\times$  29 mm. The measured gain varied from 1.2 dB to 5.9 dB and radiation efficiency of more than 82 %. In April 2017, Tao and Feng [108], presented a coplanar waveguide (CPW) fed elliptical shaped compact UWB MIMO antenna having size of 23 mm  $\times$  18 mm. The proposed antenna made up with two identical half slot antenna element and Y-shaped slot etched on the ground plane to improve isolation. The obtained results show that isolation less is than -15 dB for 3-4 GHz and less than -20 dB for 4 -12.4 GHz. This designed provided stable radiation pattern and low ECC value. In the same year, Bilal et al. [109], proposed a four port UWB MIMO antenna which was wrapped around a cuboidal polystyrene block. The isolation was improved by a series of Y-shaped slots embedded in an inverted L-shaped structure. A square spiral-shaped parasitic structure was introduced on the ground plane to improve impedance matching at the desired frequency. The overall dimension of the antenna was 32 mm  $\times$  36 mm and the measured ECC value was less than 0.0025. The obtained results show that CCL is less than 0.2 bits/s/Hz and radiation efficiency is more than 60 % through the entire operating band. In May 2017, Khan et al. [110], reported a UWB MIMO antenna which consists of a single radiator sharing the two perpendicular meander line feed and isolation was improved by cutting a slot on the radiator. The antenna offered an operating bandwidth from 3.1-10.6 GHz with a dimension of 22 mm  $\times$  24.3 mm. The size of the designed antenna was reduced due to the meander line because it brings the antenna closer. In June 2017, Rajkumar et al. [111], presented a swastika arm shaped MIMO antenna worked in hepta band (GSM 900/GSM 1800/LTE-A/UWB/Wi-Max/HIPERLAN). For proper utilization of the surface area, the radiator made up of quadric-Koch fractal geometry. The mutual coupling has been reduced without using any decoupling structure. The proposed model has dimension of 82 mm  $\times$  40 mm  $\times$  0.8 mm and it achieved stable radiation characteristics with low ECC value. In August 2017, Jehangir and Sharawi [112], investigated a Yagi like UWB MIMO antenna with size

of  $50 \text{ mm} \times 80 \text{ mm} \times 07.6 \text{ mm}$ . The antenna consists of half loop on the top of the substrate and another half loop on the bottom of the substrate. The designed antenna achieved more than 80% efficiency and 6 dB gain with maximum envelope correlation coefficient value 0.0568. In the same year, Sipal et al. [113], proposed a UWB MIMO antenna which was easily extendable to a larger size without using any decoupling circuit. The antenna placed on the orthogonal arrangement to reduce the coupling between antenna elements. The antenna exhibits an operating bandwidth from 3-15 GHz with size of  $38 \text{ mm} \times 38 \text{ mm}$ . The measured results show that peak gain of the antenna varied from 0.5-5 dB, ECC and channel capacity less than acceptable limit. In October 2017, Roshna et al. [114], proposed a UWB MIMO antenna with a compact CPS fed. The CPS fed techniques has advantages like good impedance matching and easily integrate with the various communication devices. The miniaturization of the antenna was achieved by three stairs case-shaped structures on the radiator. The overall size of the antenna has  $45 \text{ mm} \times 25 \text{ mm}$  with operating bandwidth from 3.1-11.5 GHz. Experimental results show that the ECC and  $MEG_i/MEG_j$  is less than 0.2 and 0.5 dB respectively. In December 2017, Ali et al.[115], investigated a four identical circular monopole UWB MIMO antenna with a dimension of  $40 \text{ mm} \times 40 \text{ mm}$ . The two-element placed on the top and others were placed on the ground. The mutual coupling was reduced by placing antenna elements orthogonal on both sides along with decoupling structure between partial ground planes. This design offered a bandwidth from 3.1-11 GHz and experimental results show that  $ECC < 0.004$  and channel capacity  $< 0.4 \text{ bits/s/Hz}$  in the entire frequency band.

In January 2018, Zhao et al. [116], presented two UWB antennas placed at the opposite edge of the ground plane. The designed antenna was based on the Theory of Characteristic Mode (TCM) in which one behaves like an electric source and the other behaves as a magnetic source at a lower frequency band. The antenna achieved high isolation without any decoupling structure and a measured efficiency of more than 70%. In January 2018, Morsy et al. [117], reported a two-element MIMO antenna for the Long-Term Evolution (LTE) band and Universal Mobile Telecommunication Service (UMTS) band. This antenna consists of a two-meander-type radiator which was separated by the

ground plane. A T-shaped slot is etched between the antenna elements for isolation improvement. The antenna has a dimension of 110 mm  $\times$  150 mm and the measured total efficiency varied from 59-71 % with  $ECC < 0.085$ . In April 2018, Chandel et al. [118], proposed a UWB MIMO antenna which consists of two circular monopole antennas in which an eye-shaped slot is etched on the radiator. The mutual coupling was enhanced by a T-shaped stub on the ground plane. The designed antenna provided an operating bandwidth from 2.8-20 GHz with a compact size of 18 mm  $\times$  36 mm. In April 2018, Jehangir et al. [119], reported a two ports MIMO antenna, and miniaturization was achieved due to a small loop meandered line-driven element. For improving the end-fire radiation pattern multiple slits were etched on the partial ground plane. The antenna worked in telemetry L-band and LTE band with an overall size of 120 mm  $\times$  50 mm. The experimental results show that gain is more than 5 dB, the total maximum radiation efficiency is 78 %,  $ECC < 0.0785$  with a diversity gain of 9.5 dB.

In June 2019, Prabhu and Malarvizhi [120], reported a double-sided UWB MIMO antenna that is composed of a polygon-shaped radiator on the bottom and top of the substrate. The mutual coupling was reduced by using the EBG structure on both sides of the substrate. The antenna provided impedance bandwidth from 3.1-11 GHz with a maximum peak gain of 6.8 dB. In 2019, Suriya and Anbazhagan [121], proposed a dual-band notch characteristics UWB MIMO antenna. It consists of an inverted A-shaped radiator which is orthogonally placed for isolation improvement. The designed antenna has a dimension of 38.5mm  $\times$  38.5 mm and provided a bandwidth from 3.1-10.6 GHz. The fractional bandwidth of 109.48 % was achieved with a low ECC value. In July 2019, Babu and Anuradha et al. [122], presented a two-port MIMO antenna for the UWB system with an overall size of 65 mm  $\times$  35 mm. This design consists of a rectangular patch and half circular-shaped etched from each corner of the radiator and a semi arc-shaped structure cut on the ground plane. The prototype antenna achieved a bandwidth from 3-10 GHz with an ECC value of less than 0.25. In August 2019, S.Chouhan et al. [123], reported a two-port MIMO antenna worked for a multiband (Wi-Fi / WiMAX /Bluetooth /C-band) application. The multiband has been achieved due to the multiple arms of a spider-shaped radiator. At



the same time due to fractal structure antenna get miniaturization. The overall dimension of the antenna has  $37 \text{ mm} \times 56 \text{ mm}$  and mutual coupling has been reduced by inserting Y-shaped stub on the ground plane. The measurement results show that antenna provided a gain and radiation efficiency more than 2 dB and 73 % respectively.

In May 2020, Pannu and Sharma [124], proposed a dual-band notch MIMO antenna having four ports. The designed antenna is made up of four identical elliptical-shaped radiators which are orthogonally placed. The bandwidth of the antenna has been enhanced due to defected ground structure. The overall size of the antenna has  $45 \text{ mm} \times 45 \text{ mm}$  and offered an impedance bandwidth from 2-16.8 GHz. The dual-band notch has been achieved due to H-shaped and C- shaped slots etched on the radiator. In 2020, Tang et al. [125], reported a UWB MIMO antenna composed of DGS, a u-shaped branch on the ground, and window shaped patch along with folded feed line. The proposed antenna has a dimension of  $80 \text{ mm} \times 35 \text{ mm}$  and provides bandwidth from 2.57-12.2 GHz. The experimental results show that the gain of the antenna varied from 3.06 to 4.669 dB, with isolation of less than  $-15 \text{ dB}$  without using any decoupling structure. In 2020, Roy et. Al [126], presented a MIMO antenna using a textile substrate. In this design, a meander-type structure was placed on the top and bottom surface of the substrate to improve the diversity performance of the antenna. The performance was measured in terms of  $\text{ECC} < 0.1$ ,  $\text{DG} > 9.8$ , and  $\text{MEG}$  lies between  $+ 3 \text{ dB}$  to  $-3 \text{ dB}$ . This prototype antenna was analyzed in the human body and found to be a low envelope correlation coefficient.

### **2.3 Research Gap**

After the extensive literature review, we found that over the last few years there are lots of work has been done in the designing of the UWB-MIMO antenna. But still, a few challenges need to be discussed here more precisely. Till now, all the available designs for the quad ports antenna have a size too large, high mutual coupling among antenna elements, and various other diversity parameters were also not that much effective. The main target of this thesis is to design and developed a miniature MIMO antenna with wide bandwidth, and high isolation (less than  $-20 \text{ dB}$ ). We have achieved miniaturization by

using DGS structure and isolation has been enhanced by inserting CSRR structure and fractal structures on the ground plane between antenna elements.

## **2.4 Summary**

In this chapter, several research articles on the UWB antenna with different shapes and bandwidth enhancement techniques have been presented. This chapter also presented various types of MIMO antenna, isolation enhancement techniques, and miniaturization techniques from previous literature. It has been observed that the problem of miniaturization and isolation enhancement along higher bandwidth is still required more attention. Therefore, I choose my research to design and fabricate a very compact UWB MIMO antenna, high bandwidth, and high isolation simultaneously for today's wireless communion devices. The next chapter presents the design and the analysis of a compact multiple input multiple output antenna with high isolation for the UWB applications.

## Chapter-3

# Compact Multiple Input Multiple Output Antenna with High Isolation for UWB Applications

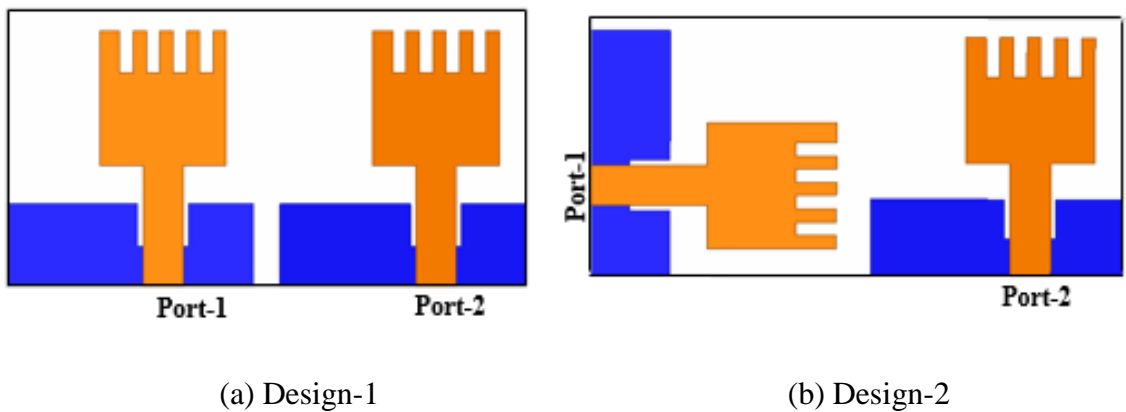
### 3.1 Introduction

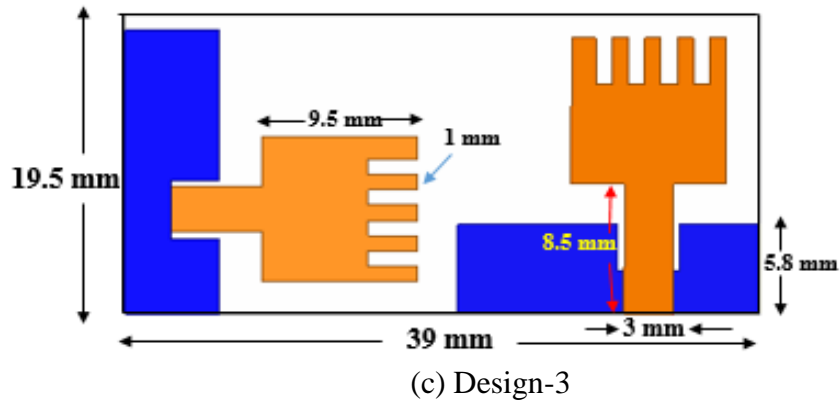
Nowadays, due to fast development in wireless communication, every wireless device requires a high data rate along with large bandwidth. The UWB technology holds the capability to full fill the above demand with low power spectral density, low cost, and low power consumption. The unlicensed frequency range of 3.1-10.6 GHz for the UWB was decided by FCC in the year 2002 [2]. This technology is quite suitable for short-distance communication, but there is an issue of multipath fading. This issue can be resolved by the suitable implementation of the MIMO antenna along with the UWB technology. The high polarization diversity is achieved in the MIMO system, because of placing multiple antennas on the transmitter and the receiver side. In MIMO, multiple signals are transmitted simultaneously and the receiver received the required signal correctly in the presence of any obstacle. On the contrary, as the MIMO system includes many antennas within a small space, there is a high chance of developing mutual coupling among those antenna elements. Due to mutual coupling, the performance of the MIMO antenna may be degraded. This coupling effect could be improved by placing the antenna at more distance or by reducing the size of the radiator. The other method of controlling is just by placing the antenna elements in an orthogonal fashion. In recent years, there are several techniques are used to reduce the mutual coupling such as defected ground structure [127], [128],[129],[102], adding tree-like structure [45], electromagnetic bandgap structure (EBG) which absorbs interference [130], [131], metamaterial structure [132], different type of structure such as F-shaped, T-shaped or inverted L-shaped stub [95],[12],[133]. The isolation can also be improved by using a complementary split-ring resonator on the ground [107], and a neutralization line between the feed line [134], [25].

In this chapter, two-port, and four-port miniature MIMO antennas are presented. The miniaturization and the bandwidth of the antenna are improved by introducing multiple slits on the radiator and etching a slot at an optimum position on the partial ground plane. The isolation is enhanced by placing the antenna orthogonally and high diversity is achieved by placing two antenna elements placed on the opposite side of the substrate. The polarization diversity and dual-polarization are achieved due to the positioning of the antenna elements in an orthogonal manner. Further, the isolation is improved by adding the decoupling structure on the ground plane and top surface between two partial slotted ground. It acts as a filter to restrict the flow of current from one antenna element to another. The impedance bandwidth of the designed antenna satisfies the UWB range decided by FCC. It is expected that the designed antenna is suitable for the recent wireless devices.

### 3.2 Two Port MIMO Antenna Design

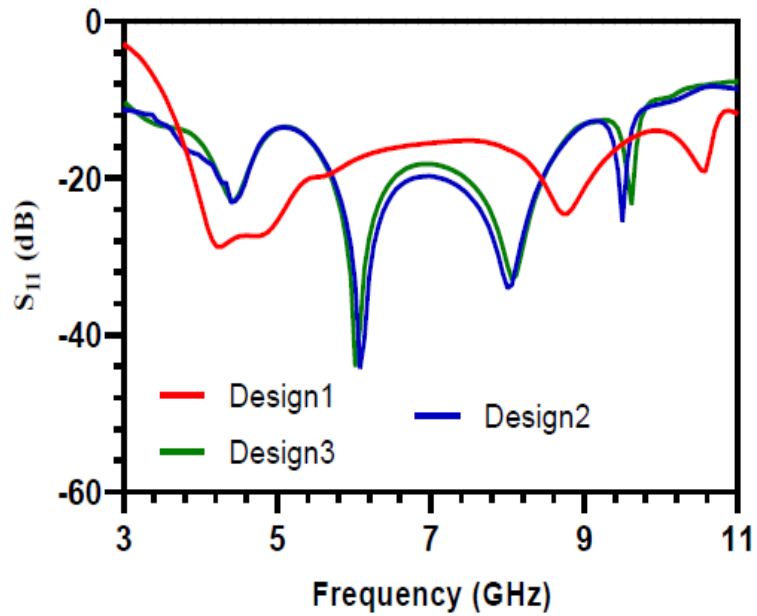
Two-port MIMO antenna with a different orientation is illustrated in Figure 3.1. In design1, two radiating elements are placed in parallel orientation. It can be seen that the return loss  $S_{11} < -10$  dB in the entire operating band but the isolation between radiators is very poor. Further, these radiators were placed orthogonally in the same plane. After that, both return loss and isolation are significantly improved due to the polarization diversity.

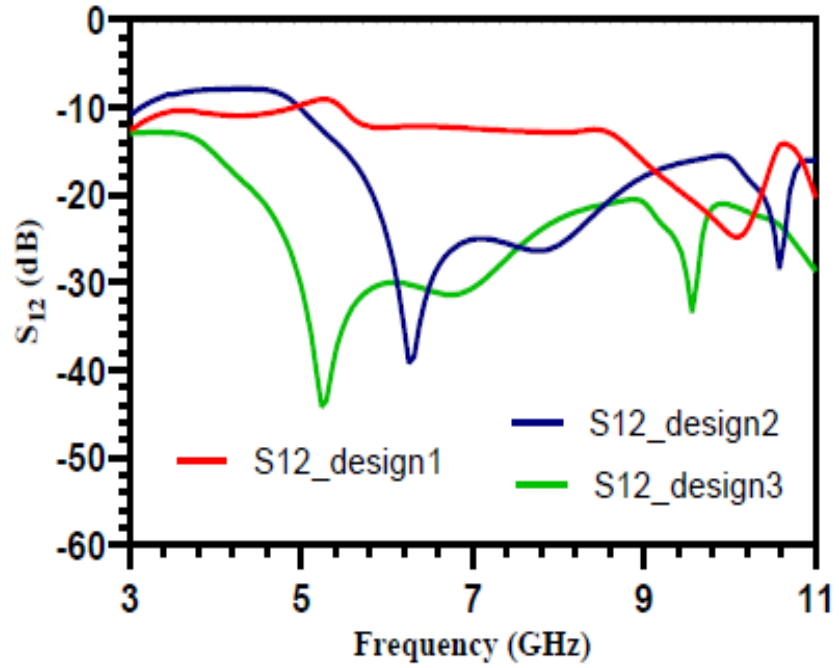




**Figure 3.1** Two-port MIMO antenna with different orientation

Finally, in design 3, one radiator is placed on the top side and the other on the bottom of the substrate material in an orthogonal fashion. It can be observed that return loss is almost identical to design 2, but it achieved high isolation of  $< -17$  dB in the entire frequency band as shown in Figure 3.2. The overall dimension of the antenna is very compact  $19.5 \text{ mm} \times 39 \text{ mm}$ .



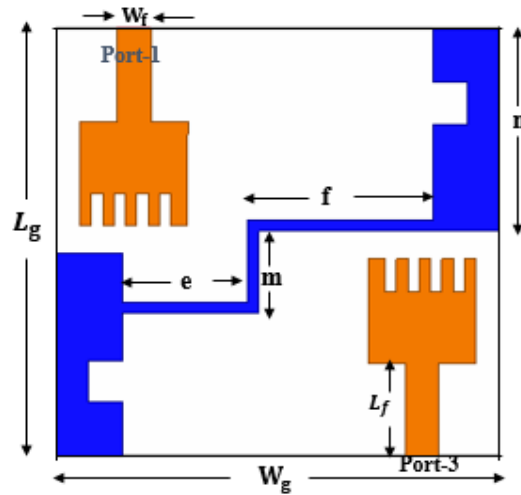


(b)

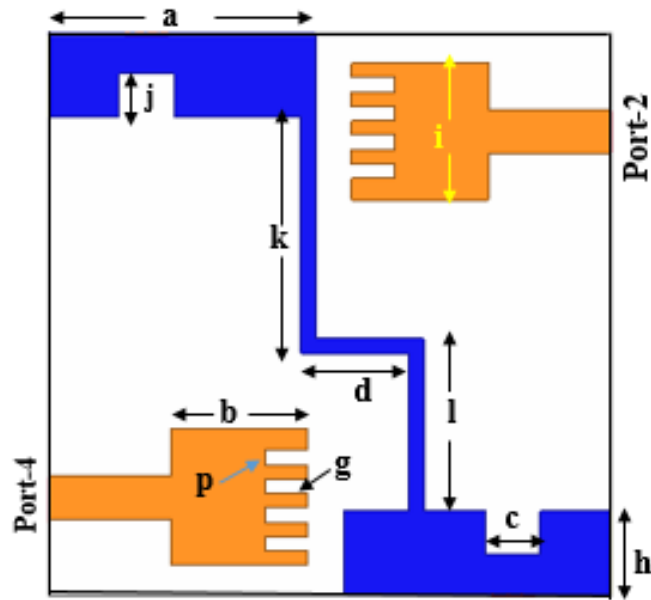
Figure 3.2 (a) Reflection coefficient (b) Isolation parameter

### 3.3 Four Port MIMO Antenna Design

The two-dimensional layout of the four-port MIMO antenna is presented in Figure 3.3. In this proposed design, four identical radiating elements are orthogonally placed. The overall dimension of the antenna is very compact  $39 \times 39 \text{ mm}^2$ .



(a) Top



(b) Bottom

**Figure 3.3** Two dimensional layouts of the proposed antenna

The antenna is optimized and designed using high-frequency structure simulator (HFSS) software. The substrate material FR4 (dielectric constant 4.4 and loss tangent 0.02) with 1.6 mm thick is used to design the antenna. The optimized dimension of various parameters labeled in the antenna structure is illustrated in Table 3.1.

**TABLE 3.1.** Design parameters of the antenna

Parameter	$W_g$	$W_f$	$a$	$b$	$c$	$d$	$e$	$f$	$g$	$p$
Dimension (mm)	39	3	18	9	3.8	7.5	11	16.4	3	1
Parameter	$L_g$	$L_f$	$h$	$i$	$j$	$k$	$l$	$m$	$n$	
Dimension (mm)	39	8.5	5.8	9	3	16.4	12	7.5	3	

### 3.4 Results and Discussion

The various antenna characteristics parameter and the diversity parameters are illustrated in this section.

### 3.4.1 Return Loss and Isolation Parameter

Figure 3.4, represents the return loss at various steps. In step1, all elements are placed orthogonally and they are resonating at 5.6, 7.6, and 10.6 GHz respectively. The isolation is very poor up to 8 GHz, but it is improved for high frequency and is accepted as it lies below  $-15$  dB. In step-2, the strip is placed on top of the substrate, which is adding one lower resonant frequency and also improves the isolation.

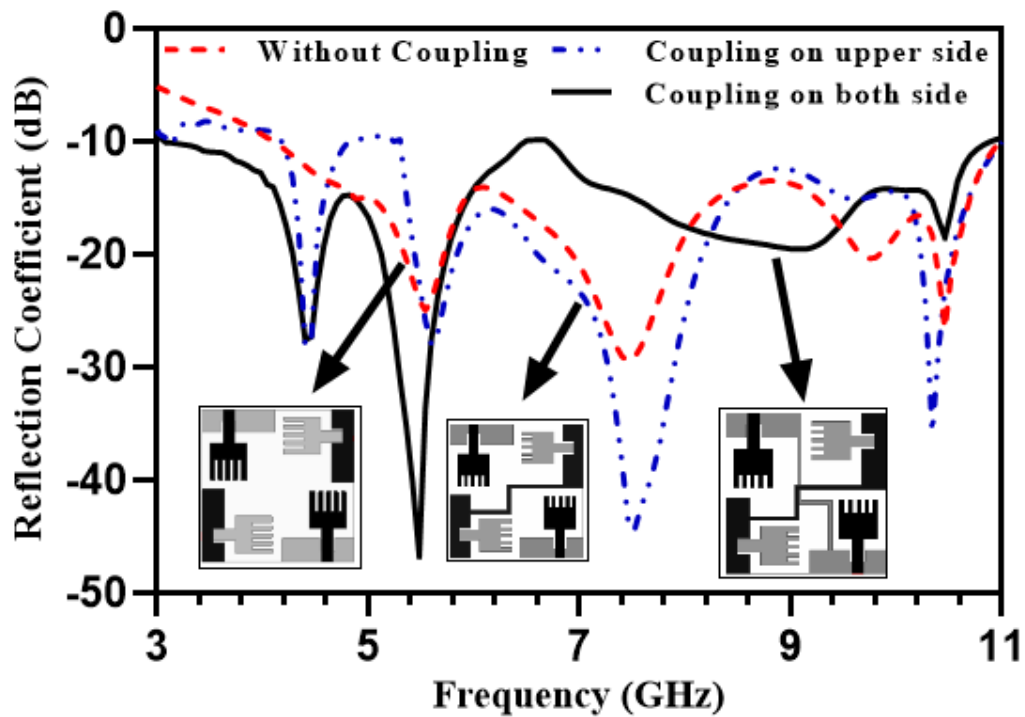


**Figure 3.4** Reflection coefficient at various steps

Further for more reduction of the mutual coupling, thin strips are added to the ground plane as well as on the top surface. It can be seen from Figure 3.5, that isolation is less than  $-20$  dB up to 7.8 GHz and at the higher frequency it is less than  $-16$  dB. The isolation parameters are measured when port-1 is excited and other ports remain deactivated.



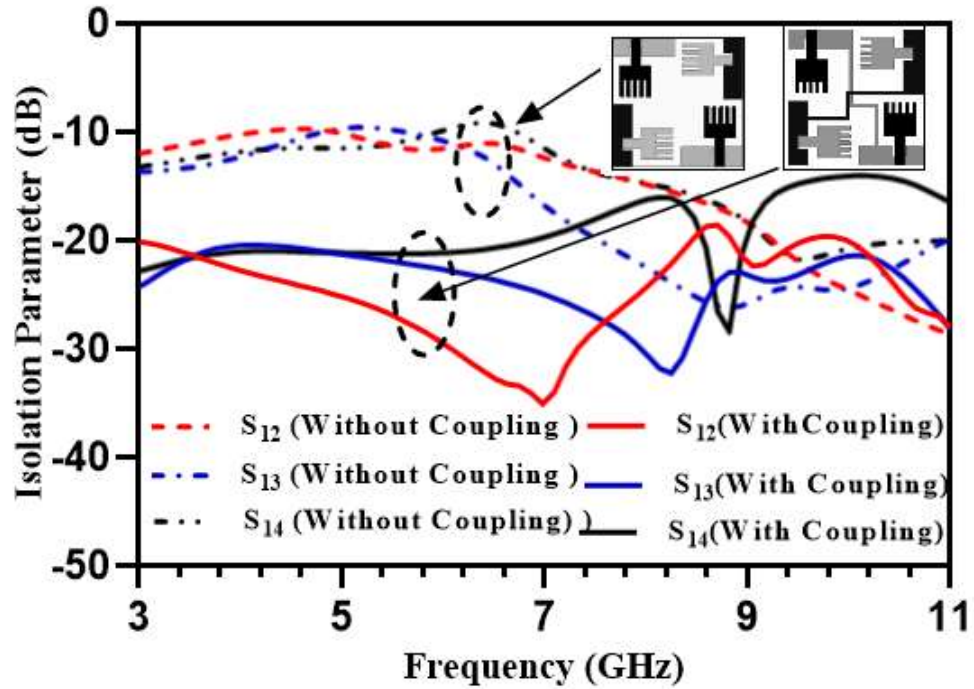
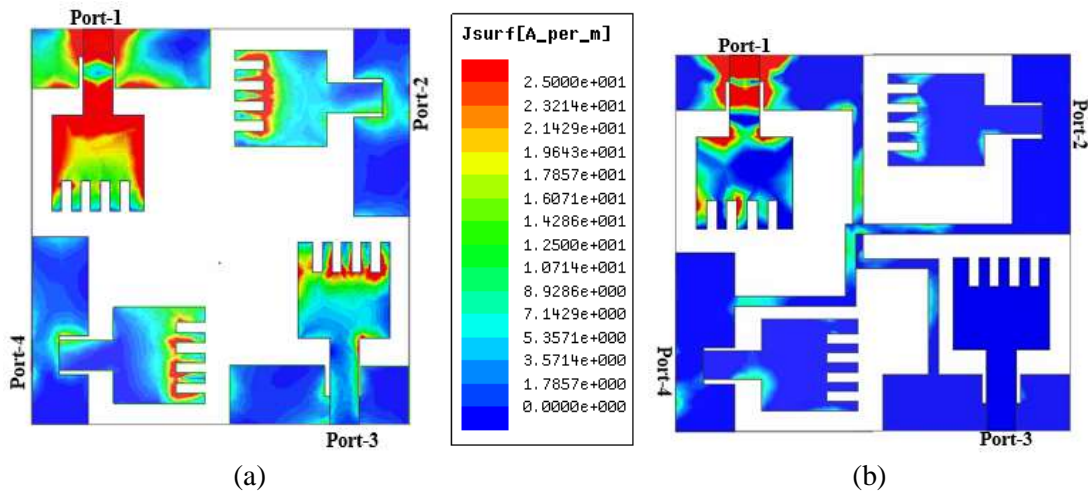
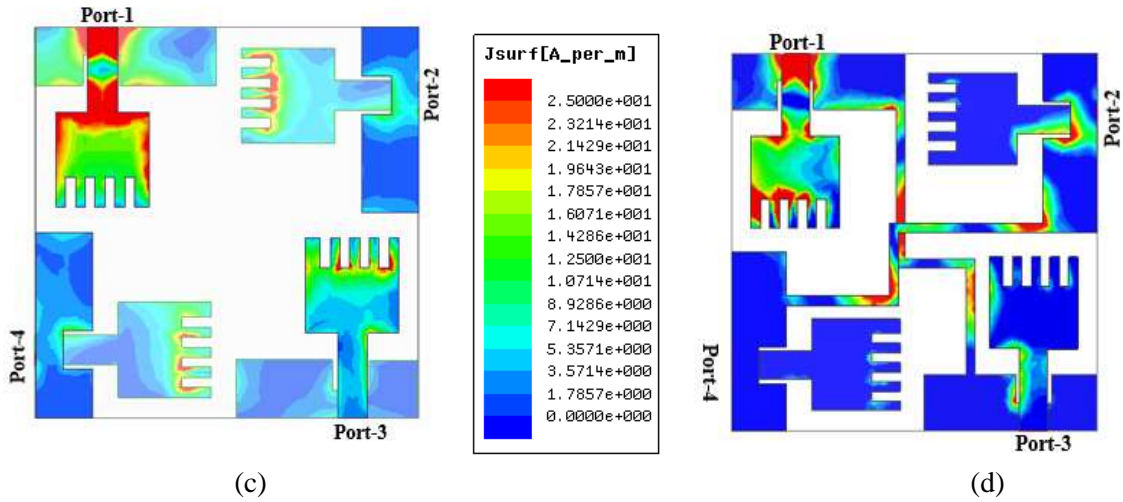


Figure 3.5  $S_{12}/S_{13}/S_{14}$  at various steps

### 3.4.2 Surface Current Distribution

The two-dimensional surface current distribution is depicted in Figure 3.6, from the diagram it is very clear that the current density is highly coupled in Figure 3.6 (a) and (c) without using any decoupling structure.





**Figure 3.6** Two dimensional current distribution at operating frequency 4.3 GHz in (a), (b), and at 5.4 GHz in (c),(d)

But when the decoupling structure is implemented, the amount of the mutual coupling current is significantly reduced. The function of the decoupling element is to restrict the flow of current to another element. It acts as a filter to reject the current and divert it in some other direction.

### 3.4.3 Gain and Radiation Efficiency

The gain of the antenna lies in the range of 1.1 to 5.3 dB. In addition, it is also observed that the radiation efficiency is varying from 28 % to 76 %.

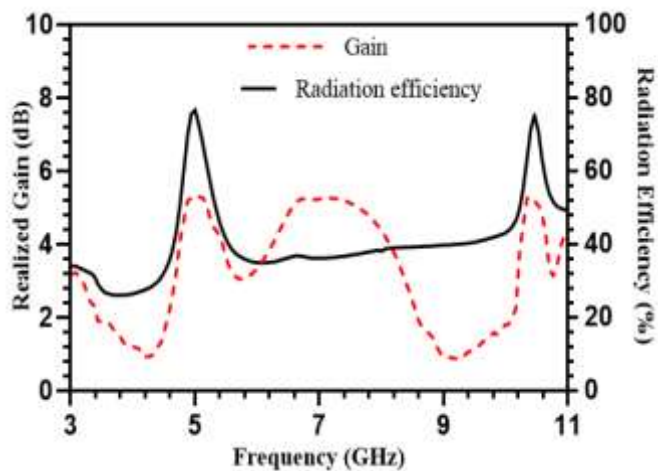


**Figure 3.7** Realized gain and radiation efficiency

The two-dimensional radiation pattern in the  $xz$  (E-plane) and  $yz$  (H-plane) direction at 4.3 and 5.4 GHz is presented in Figure 3.8. It can be noticed that the radiation pattern is unstable at 4.3 GHz and directional in E-plane and close to the omnidirectional in H-plane at 5.4 GHz. Further at higher frequency splitting the radiation lobe due to the higher-order mode.

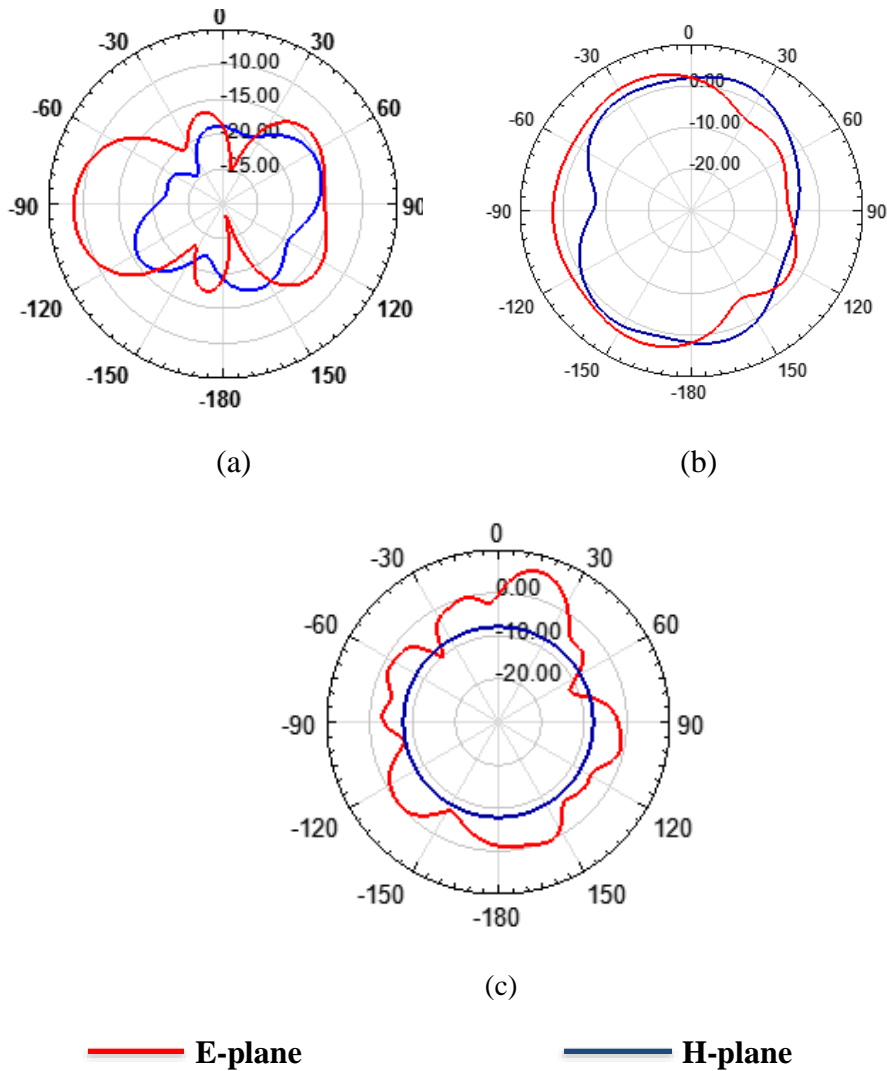


**Figure 3.8** Two dimensional radiation pattern (a) 4.3 GHz (b) 5.4 GHz and (c) 10.4 GHz

### 3.4.4 Input Impedance

The simulated impedance at port 1 is illustrated in Figure 3.9, in which the real part of the impedance at resonance frequency is very close to 50 ohms and the imaginary part is near to zero. This means that the antenna has good impedance matching at all the resonance frequencies 4.3 GHz, 5.4 GHz, and 10.4 GHz.

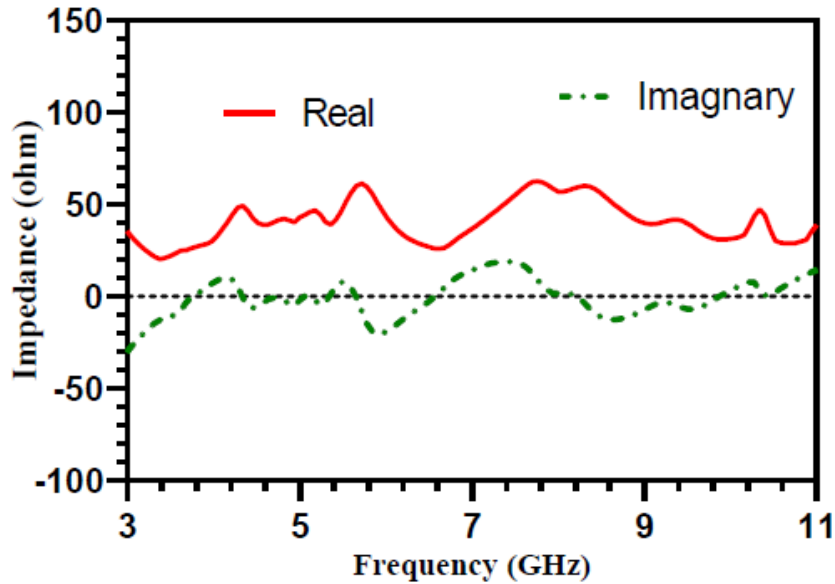
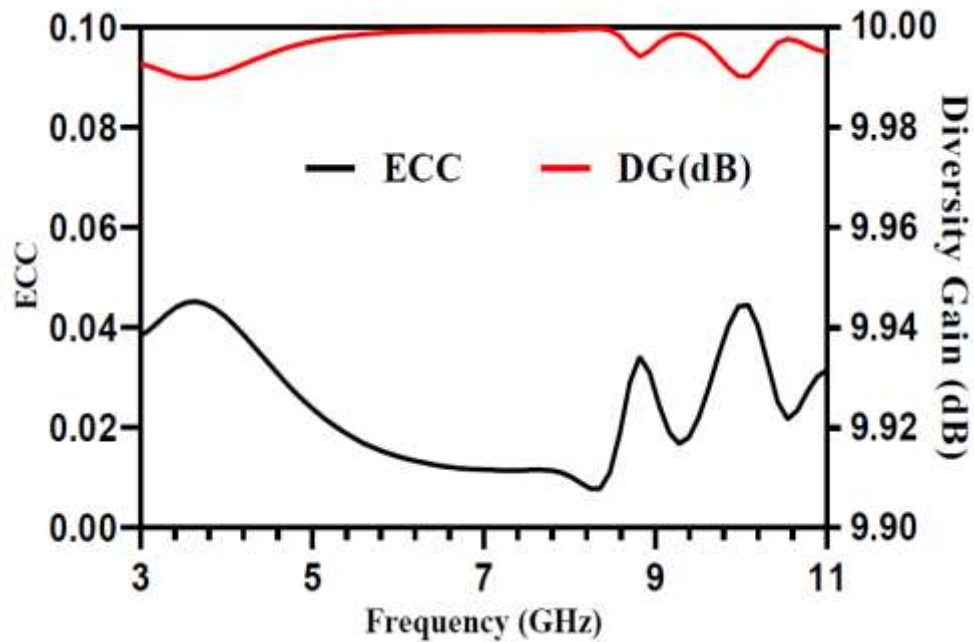


Figure- 3.9 Simulated impedance of the proposed antenna

### 3.4.5 Envelope Correlation and Diversity Gain

Envelope correlation and diversity gain are important parameters for deciding the MIMO performance. The ECC value decides the amount of correlation between antennas. The lower the value of ECC, the better will be the isolation among antenna elements. The ECC value for the four-port antenna can be computed from equation 1.6. The ECC value of the designed antenna is very low 0.047 as compared to the practical accepted value. It means the proposed antenna is quite suitable for wireless devices. The diversity gain of the antenna is directly calculated from equation 1.9. The value of DG is more than 9.9 dB for the whole UWB range. It is very close to the practical accepted value.



**Figure 3.10** Simulated ECC and DG of the proposed antenna

### 3.5 Summary

In this chapter, a two-port and four-port MIMO antenna are presented. The high bandwidth of 3.1-11 GHz is achieved due to the partial ground and the multiple slits on the radiator. The isolation is enhanced by adding strips on the ground and top surface along with the proper placement of antenna elements in orthogonal orientation. The antenna has achieved less than  $-20$  dB isolation in most of the band, lower ECC value, good efficiency, and suitable gain value. The results obtained in this work are sufficient to claim that, this antenna will be quite handy for the devices applicable to wireless communication. In the next chapter, the design and development of the UWB MIMO antenna without using any decoupling structure will be discussed.

## Chapter-4

### Compact Quad-Port High-Performance UWB MIMO Diversity Antenna with Slotted Ground Structure

#### 4.1 Introduction

A UWB technology is quite suitable for short-range wireless communications like personal area network applications. The high data rate, larger bandwidth, and low power spectral density are the advantages of UWB which is suitable for today's wireless communication portable devices. In spite of various advantages of UWB technology, it also has certain limitations observed like multipath fading and reliability. These problems are resolved by combining the UWB technology with the MIMO technology. In the MIMO system, multiplexing and diversity gain increase as multiple antennas are used at the both sender and the receiver sides, which in turn increases the transmission capacity. Since accommodating the multiple antennas into a small area leads to chances of coupling among the antenna elements. Therefore, it is a big challenge for the antenna designer to design a miniature MIMO antenna with low coupling between the antenna elements. In [108], Y-shaped slots are used in half slot CPW feed MIMO antenna to improve the isolation. In [107], isolation is improved by using a Complementary Split-Ring Resonator (CSRR) and an inverted L-stub on the ground plane. Two perpendicular meander feed lines on the single radiator and an open stub at the corner of the structure are used to improve the isolation parameter [110]. An array of slotted Y-shaped frequency selective surfaces along with an inverted L-structure provides isolation among the antenna elements[109], in which antenna elements are designed around a polystyrene block in a cuboidal geometry. Some other techniques are also being used for isolation improvement such as neutralization line between antenna elements [135], electromagnetic bandgap structure [136], [137], introducing various Defective Ground Structure (DGS) or stub and slots on antenna element [125],[138],[99],[93],[87],[45]. A carbon black film is also used for reducing

mutual coupling because it absorbs electromagnetic signals [104]. In [139],[132], a metamaterial, which is an artificial structure and magneto dielectric material is also used to decrease the mutual coupling by absorbing the mutual interference signal. A DGS and U-shaped stubs are inserted on the radiator [140], [125], whereas a decoupling structure is used on the top and bottom of the dielectric substrate to improve an isolation as well as bandwidth of the UWB MIMO antenna in [115]. Further, overall size of the antenna decreases by using ACS fed structure [141]. In [142], [143], [144], antenna elements are placed orthogonally to enhance the isolation. It is a big challenge to design a MIMO antenna in compact size with low mutual coupling. The performance of the prototype antenna compared with the existing literature in terms of antenna size, frequency band, isolation and ECC value are available in Table 4.1. It can be seen that, size of the proposed antenna is very compact in reference to all other antenna. In addition, it is also showing better performance in achieving high isolation, low ECC value and high gain which is favorable for the today wireless portable devices.

**TABLE 4.1:** Performance comparison of the prototype antenna with existing literature

Existing literature	Antenna size (mm <sup>2</sup> )	Frequency band (GHz)	No of port	Isolation (dB)	Gain (dBi)	ECC
[109]	32 × 36 = 1152	3-10	4	< -20	--	< 0.002
[135]	48 × 34 = 1632	3.52-10.08	4	< -23	0.95-2.91	< 0.039
[136]	27.2 × 46 = 1251	3.6-17.6	2	< -18	1.4-4	< 0.018
[137]	60 × 60 = 3600	3-16.2	4	< -17.5	8.4	< 0.300
[104]	50 × 40 = 2000	2.5-11	2	< -15	4.6	< 0.01
[140]	80 × 80 = 6400	3.18-11.5	4	< -15	6	< 0.005
[125]	80 × 35 = 2800	2.57-12.2	2	< -15	3.06-4.6	< 0.005
[115]	40 × 40 = 1600	3.1-11	4	< -20	3.28	< 0.002
[141]	36 × 36 = 1296	3.1-10.6	4	< -15	3.7	< 0.02
[142]	26 × 55 = 1430	3.1-12.3	4	< -20	4.2	< 0.10
[143]	50 × 39.8 = 1990	2.7-12	4	< -17	6	< 0.02
[144]	39 × 39 = 1521	2.3- 13.75	4	< -22	4.6	< 0.02
<b>Proposed Antenna</b>	<b>30 × 30 = 900</b>	<b>2.15-16.75</b>	<b>4</b>	<b>&lt; -22</b>	<b>1.2-4.8</b>	<b>&lt; 0.06</b>

In this chapter, very compact size of  $30 \times 30 \text{ mm}^2$  quad-port UWB MIMO diversity antenna without using any additional decoupling structure is proposed. The decoupling structure unnecessarily increases the complexity and size of the antenna. A great amount of isolation is achieved by placing four identical antenna elements orthogonally along with cutting arc-shaped structures on the radiator. This compensates for the amount of interference via polarization diversity. The bandwidth of the antenna is improved by modifying the ground plane and cutting a slot in the ground plane at an optimum position to alter the surface current distribution. The compactness is achieved due to the staircase-shaped structure cut at each bottom corner of the radiating patch. The prototype antenna has a very high bandwidth ranging from 2.15-16.75 GHz, high isolation, and very low ECC value which is suitable for modern communication devices, especially for portable UWB-MIMO devices.

## 4.2 Antenna Design Procedure

The structure of the  $30 \times 30 \times 1.6 \text{ mm}^3$  four-element MIMO antenna is presented in Figure 4.1. The design consists of four identical antenna elements which are orthogonally placed on the top surface of the substrate and the ground structure is modified by the cutting slot at a suitable position. The design and simulation work was carried out on the ANSYS HFSS full-wave electromagnetic simulator and the optimized dimensions are presented in Table 4.2.

**TABLE 4.2:** Optimized dimension of the proposed antenna

Parameter	L	$L_f$	$L_{g1}$	$L_{g2}$	$L_{g3}$	$L_1$	$L_2$	$L_3$
Dimensions (MM)	30	6.4	15	5.8	5.8	3.8	1	3.5
Parameter	W	$W_f$	$W_{g1}$	$W_s$	$W_1$	$W_2$	$W_3$	
Dimensions (MM)	30	3	5	3.4	10.8	0.5	6	



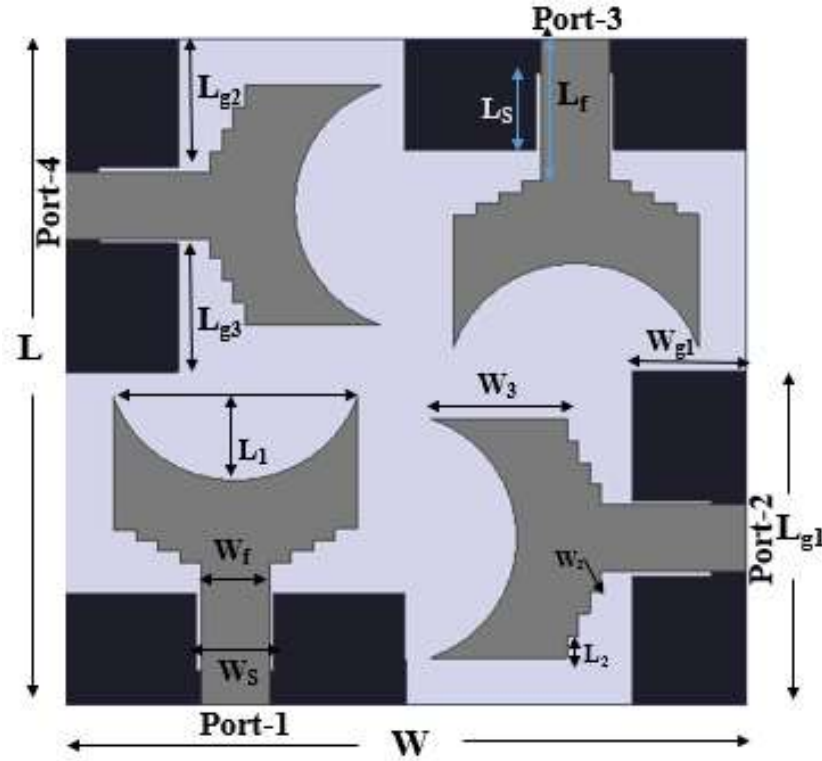


**Figure 4.1** Structure of four-element MIMO antenna with dimension

The proposed radiating element consists of a rectangular patch of length ( $L_p$ ) and width ( $W_p$ ) etched with an arc-shaped radiator on the top of the radiator to improve the bandwidth. Further truncated stair case-shaped slots are etched on the radiator to increase the path of current and hence reduced the size of the antenna. To obtain a lower cutoff frequency, the size of the antenna should be larger enough to provide the longest current path. In this chapter, to achieve lower frequency, rectangular-shaped slots of length and width of ( $L_s \times W_s$ ) are etched on the partial ground plane. The micro strip-line of length and width of  $L_f$  and  $W_f$  are connected at the lower middle edge of the radiator. The approximate lower resonant frequency for the designed antenna is evaluated by [145],

$$f_r = \frac{14.4}{l_1 + l_2 + g + \frac{A_1}{2\pi l_1 \sqrt{\epsilon_{re}}} + \frac{A_2}{2\pi l_2 \sqrt{\epsilon_{re}}}} \quad (4.1)$$

Where  $l_1$  and  $l_2$  denote the length of the ground plane and length of the patch,  $A_1$  and  $A_2$  define the area of the ground plane and radiating patch,  $g$  refers to the gap between the radiating patch and the ground plane, and  $\epsilon_{re} = (\epsilon_r + 1) / 2$  assumes the relative permittivity. The lower resonant frequency obtained from the above formula is 5.8 GHz by inserting the value  $l_1 = Lg_1$ ,  $l_2 = Lp$ ,  $g = L_f - Lg$ ,  $A_1 = Lg_1 Wg_2 - L_s W_s$ ,  $A_2 = Lp Wp + L_f W_f - 2 * \{(L_2 W_2) + (2 * L_2 W_2) + (3 * L_2 W_2)\} - 0.5 * \pi * r^2$ , which is very close to the simulated value 5.6 GHz as shown in Figure 4.4.

### 4.3 Evolution Steps of Single UWB Antenna

The various evolution steps of a single UWB antenna are presented in Figure 4.2. In step-1, the antenna design starts with the basic rectangular patch whose dimension is 7.5 mm x 10.8 mm and it is resonating around 4.4 GHz.

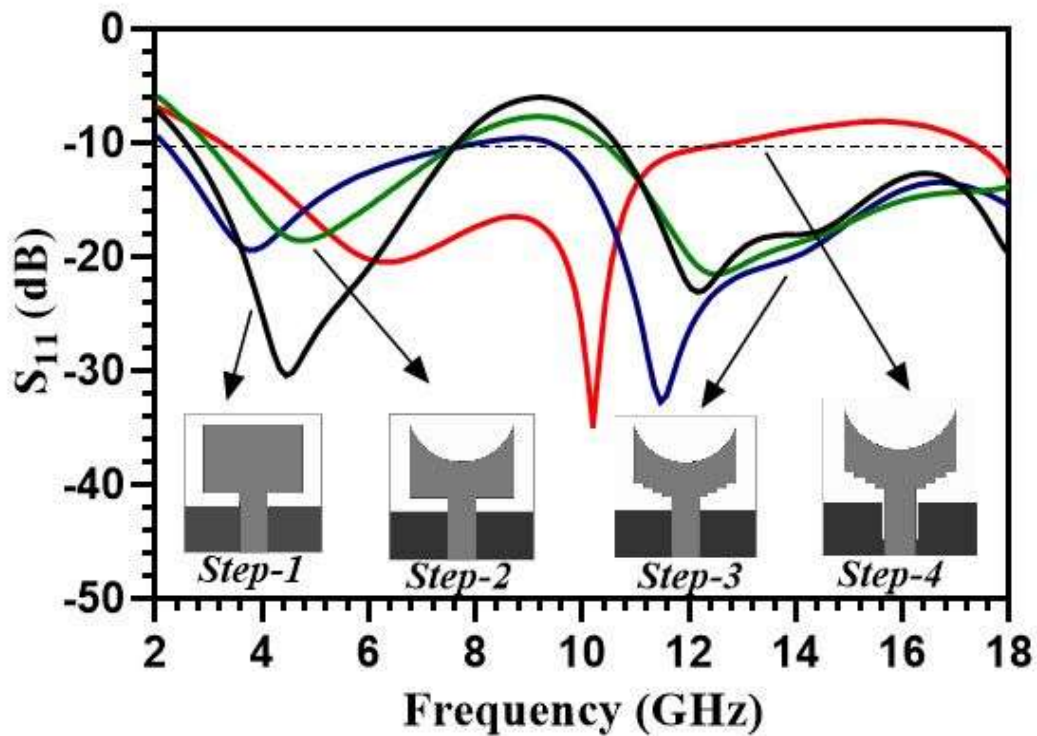
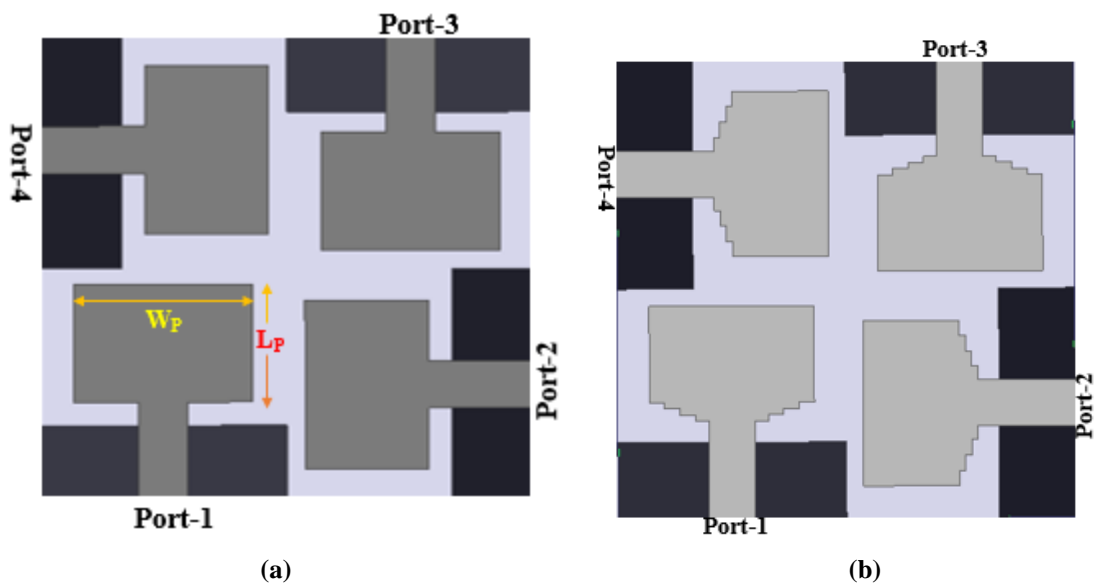


Figure 4.2 Different evolution steps of a single UWB antenna element

After removing an arc-shaped slot in step-2 and including the staircase structure in step-3, the resonating frequency shifted to 3.8 GHz approximately. This is due to the increase in the electrical length of current without disturbing the overall dimension of the radiator. In this approach, it has got an improvised result, by introducing a slot on the ground plane at an optimum place and we have achieved the ultra-wideband in step-4.

#### 4.4 Evolution Steps of UWB MIMO Antenna

Design -1, illustrated in Figure 4.3 (a) is designed with a basic rectangular patch along with a modified ground structure in which the reflection coefficient at all four ports is found to be lower than -10 dB from 2.26-11.70 GHz. The isolation parameters  $S_{12}$ ,  $S_{13}$  and  $S_{14}$  were seemed to be very poor in the whole UWB band. To improve the bandwidth and isolation further, we made necessary changes in design-1 by cutting the staircase shape at both the lower corner of radiators to get design-2. Further for more improvement of isolation and bandwidth, the design-3 shown in Figure 4.3 (c) is designed with optimum dimensions listed in Table 4.2. In this design, cutting of the rectangular slot on the ground plane at an optimum position leads to alter in the surface current distribution whereas cutting of the arc on the radiator, finds an improvement in the isolation without using any additional decoupling network.



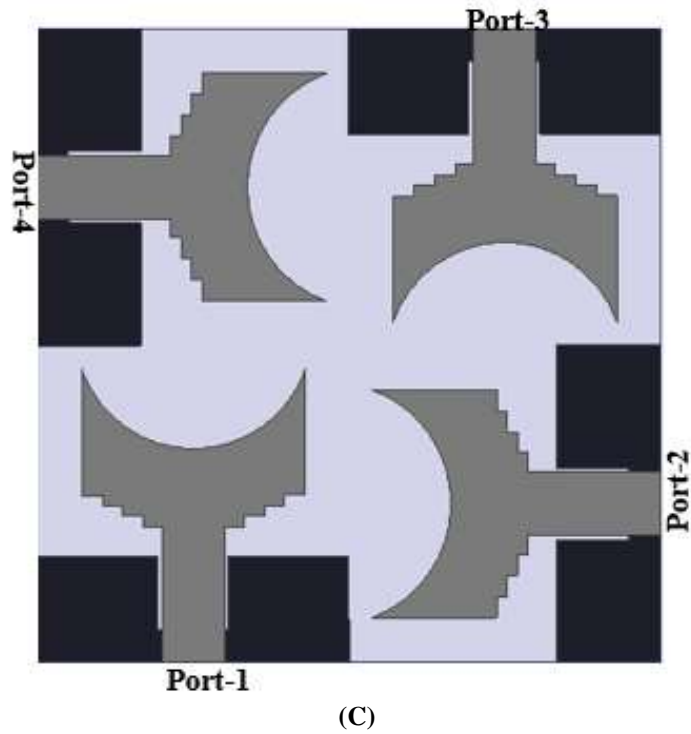
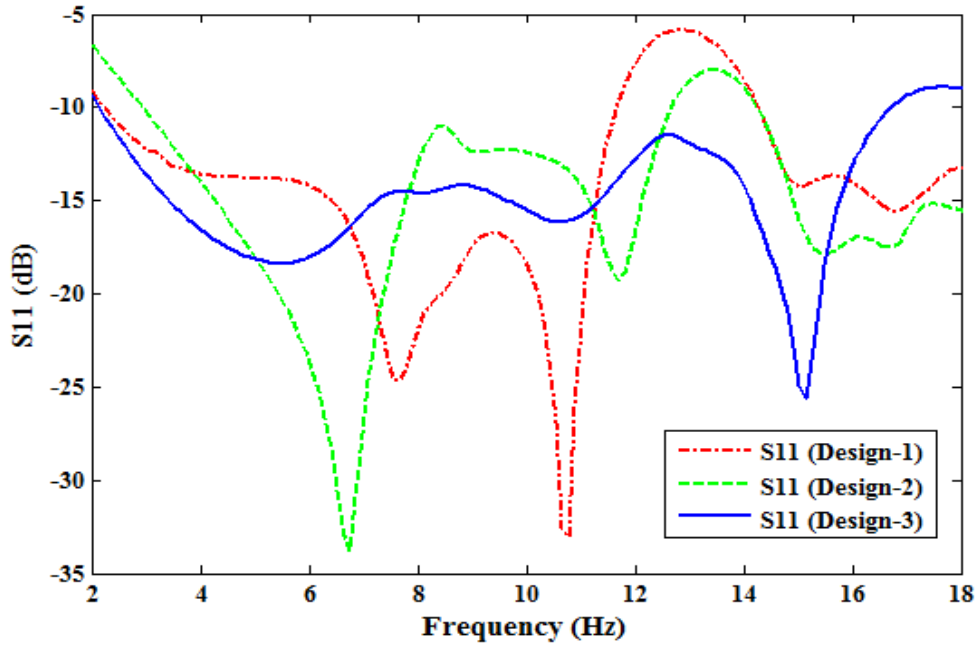
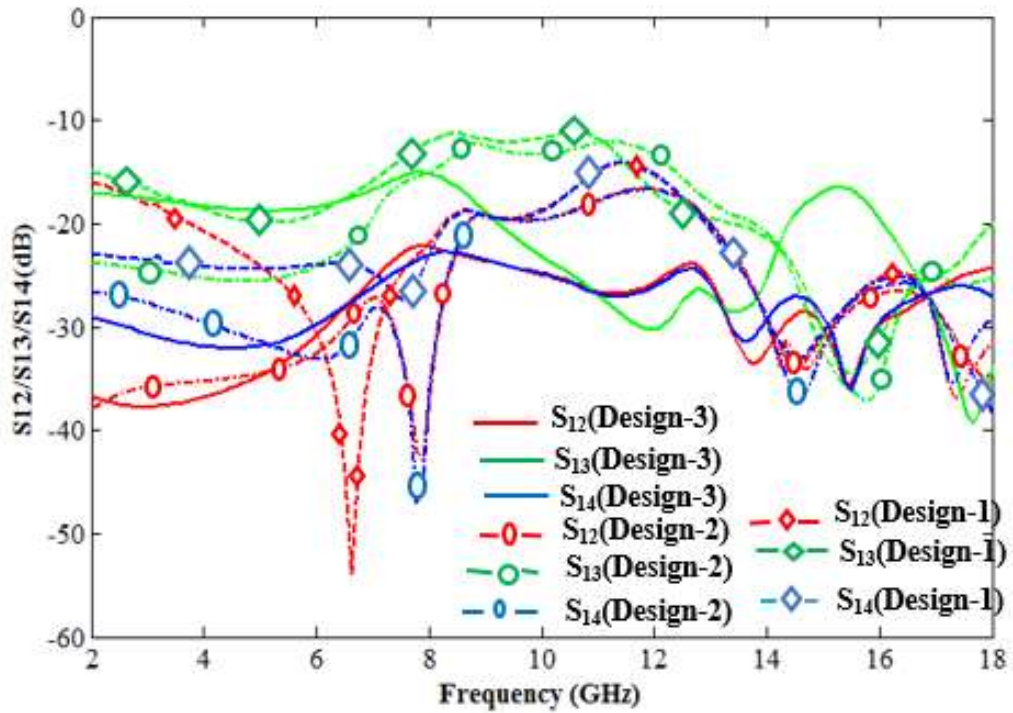


**Figure 4.3** (a) Rectangular patch with the partial ground only (b) After etching a staircase shape structure at the corner of the patch (c) Introducing slot on the ground and etched arc shape structure on the radiator

In all three designs, the antenna elements were placed orthogonally for the mutual coupling reduction. The simulated S-parameters of all three designs when port-1 is excited are presented in Figure 4.4. Table- 4.3, represents the range of operating frequency and value of isolation parameter of all three antennas. It is evident from the table that design-3 has a wider bandwidth (14.6 GHz) and maintains very good isolation among all three designs.



(a)



(b)

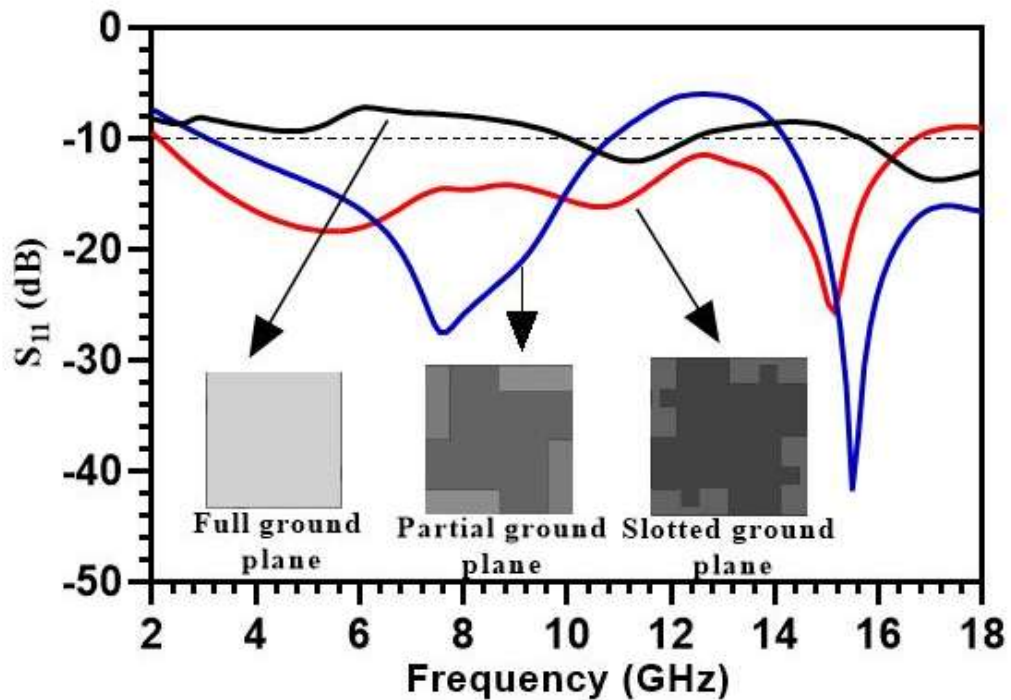
**Figure 4.4** Comparison of S-parameter of all the three designs (a) return loss (b) Isolation parameters

**TABLE 4.3:** Comparisons of S-parameter of all three design

Parameter	Design-1	Design-2	Design-3 (proposed antenna)
$S_{11}$	< -10 dB (2.26-11.70) GHz	< -10 dB (2.95-12.75) GHz	< -10 dB (2.15-16.75) GHz
$S_{12}$	< -14.2 dB	< -16.5 dB	< -22 dB
$S_{13}$	< -11 dB	< -12 dB	< -17 dB
$S_{14}$	< -14.11 dB	< -16.75 dB	< -23 dB

#### 4.5 Effect of Ground Plane

The use of a partial ground plane reduces the amount of energy stored in the substrate. As a consequence, the quality factor has been reduced and it is quite obvious that bandwidth naturally will increase as the quality factor is inversely proportional to bandwidth.



(a)

Due to the etching slot on the ground plane, it increases the electrical path length of the current which in turn increases the bandwidth. In addition, the antenna also gets miniaturized. The result of return loss and isolation parameters for different steps of the ground plane is illustrated in Figure 4.5. It is found that a MIMO antenna with a slotted ground plane provides high impedance bandwidth along with very good isolation.

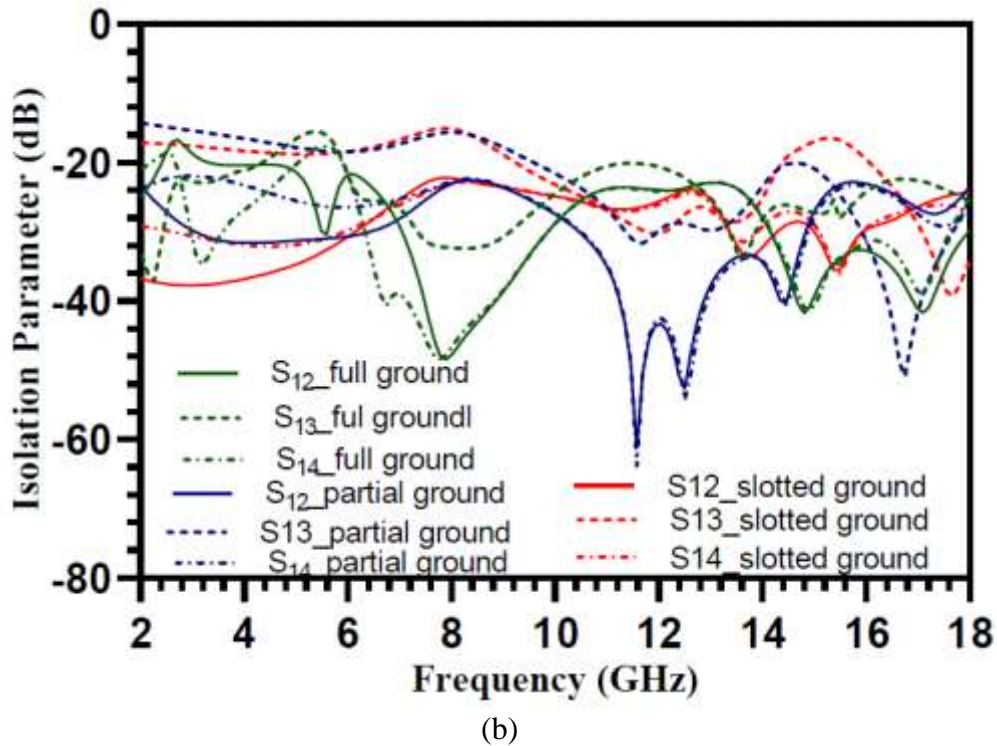
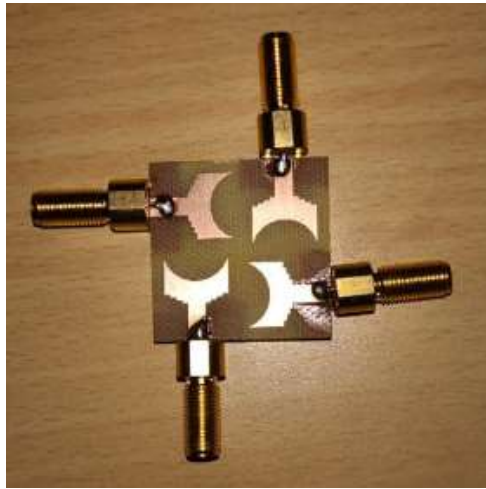


**Figure 4.5** Effect of the ground plane at various steps (a)  $S_{11}$  (b) Isolation parameter

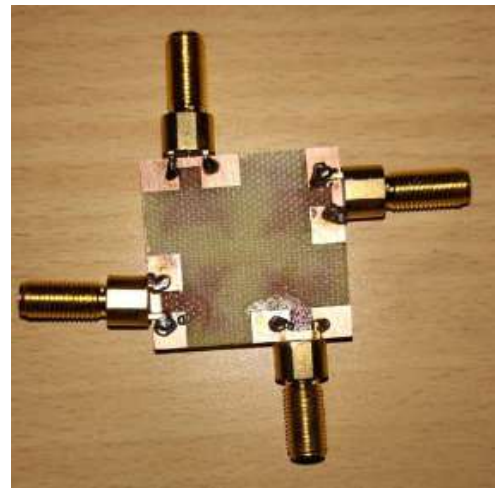
#### 4.6 Results and Discussion

The front and backside of the prototype four-port MIMO antenna are presented in Figures 4.6 (a) and 4.6 (b) respectively.





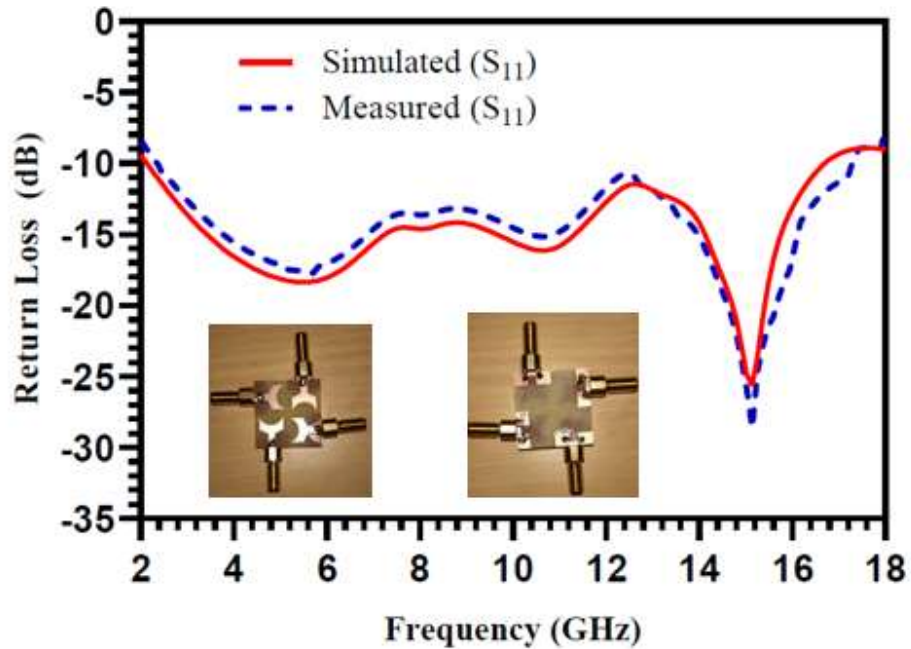
(a)



(b)

**Figure 4.6** Fabricated prototype antenna (a) Front side (b) Backside

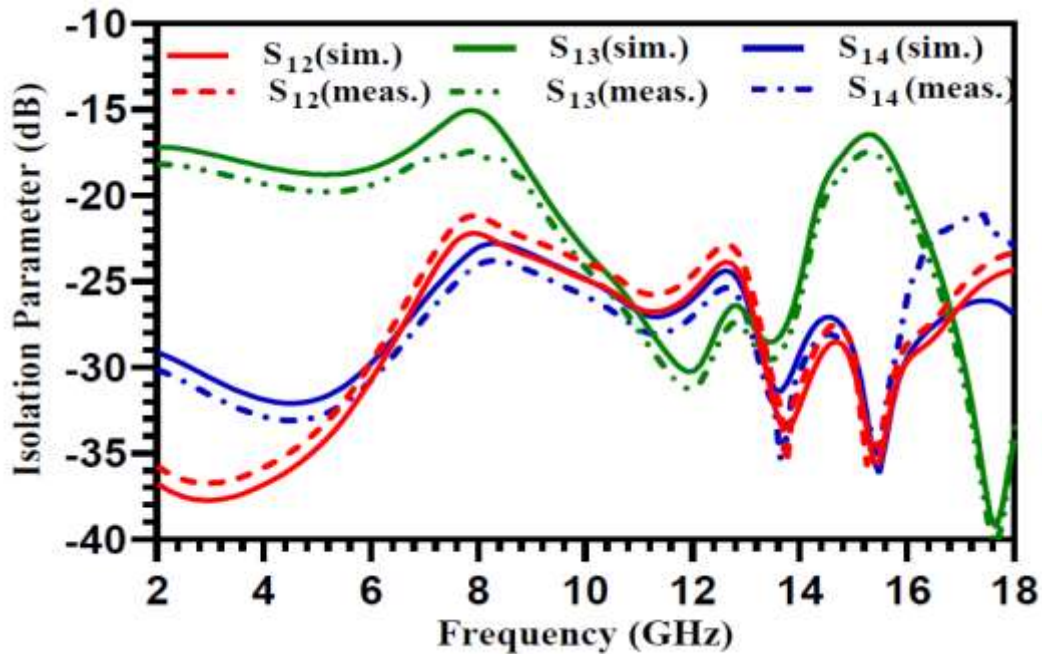
The antenna is fabricated on an FR4 substrate with a thickness of 1.6 mm. The measurement of antenna parameters was carried out on an Agilent N5230A vector network analyzer.



**Figure 4.7** Simulated and measured  $S_{11}$  parameter of the prototype MIMO antenna

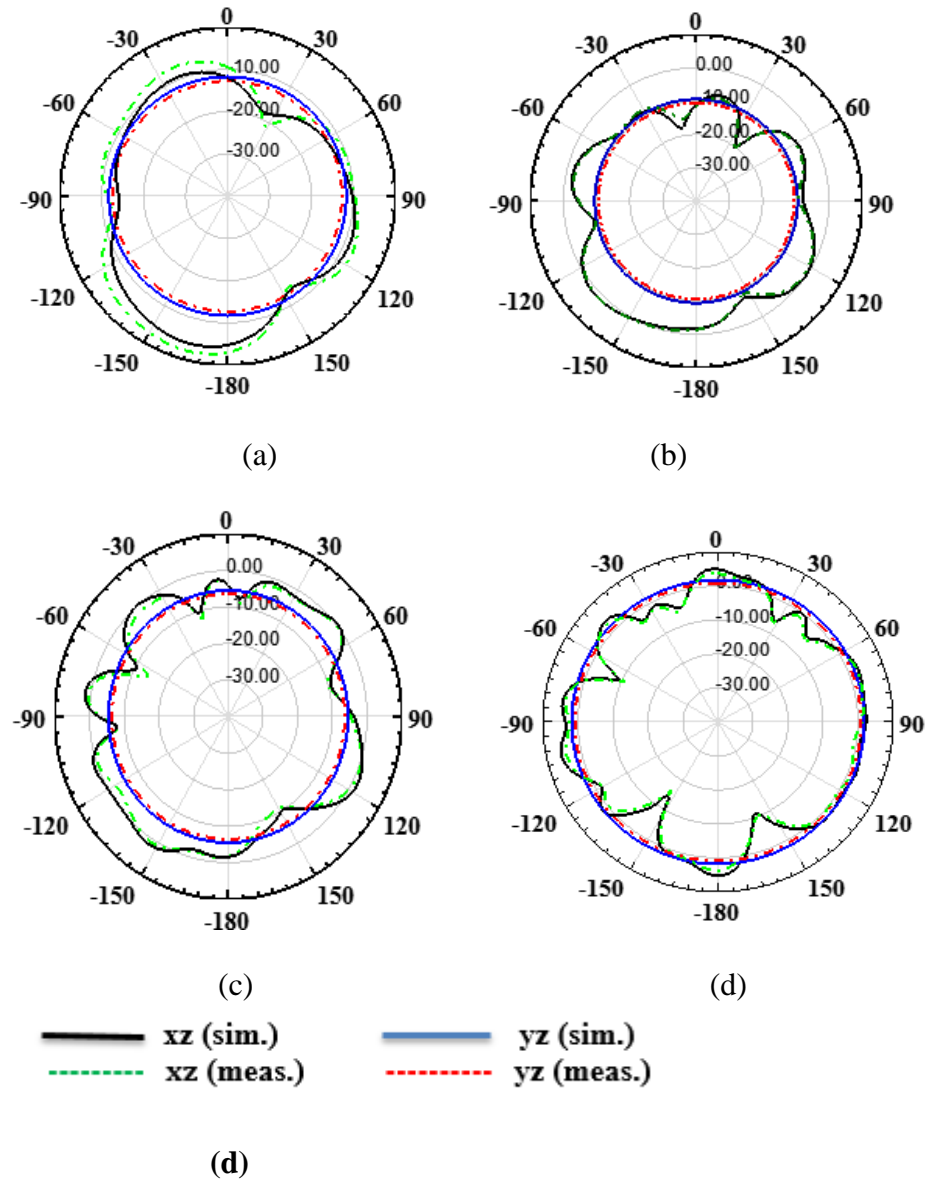


Figures 4.7 and 4.8, illustrated the comparison of measured and simulated S-parameters along with mutual coupling. It is found to be a good agreement between them. As per the FCC requirement for UWB (3.1-10.6 GHz), this prototype antenna finds a larger bandwidth (2.15- 16.75 GHz) than UWB. The high isolation is achieved between first and second, first and fourth which are found to be  $S_{12} < -22$  dB and  $S_{14} < -23$  dB respectively.



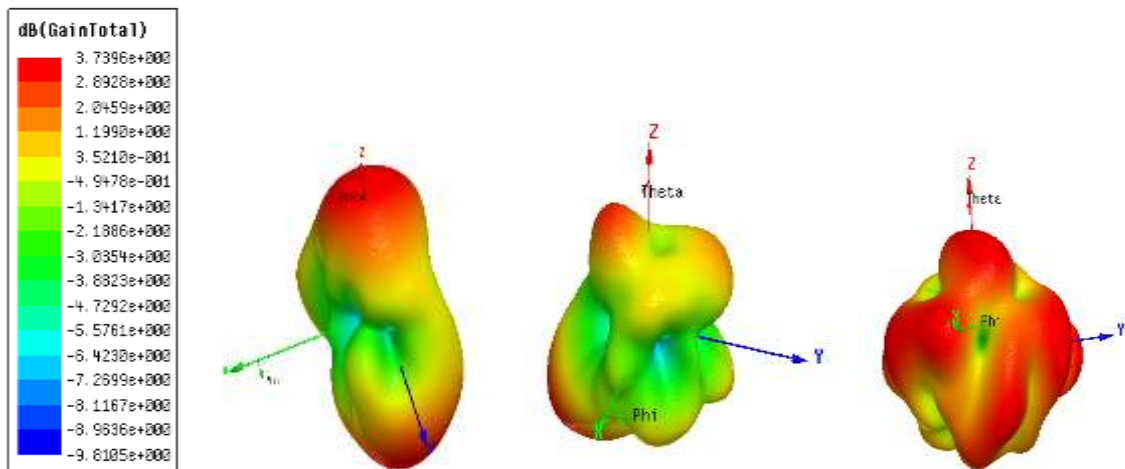
**Figure 4.8** Comparison of isolation parameter  $S_{12}/S_{13}/S_{14}$

Figure 4.9, represents the two-dimensional radiation pattern of the proposed MIMO antenna in E-plane and H-plane directions at 3.07, 5.37, 10.66, and 15.14 GHz. It is evident that for the entire range of frequency band, the radiation pattern follows an omnidirectional characteristic. Further at higher frequency splitting the radiation lobe due to higher-order mode. The 3-D radiation pattern of the prototype antenna is presented in Figure 4.10.

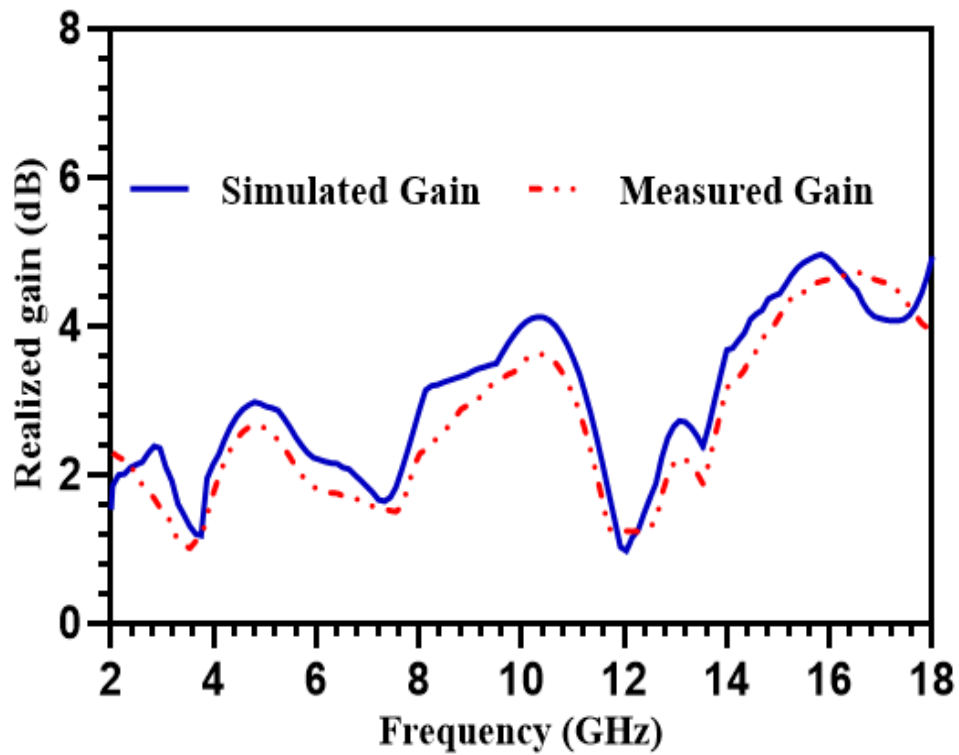


**Figure 4.9** Radiation pattern at (a) 3.07 (b) 5.37 (c) 10.66 and (d) 15.14 GHz in xz and yz plane

The gain of the antenna first decreases then increases up to resonance frequency 5.37 GHz and further decreases then increase up to another resonance frequency 10.66 GHz. The gain finally reached the maximum value at resonance frequency 15.14 GHz. The maximum measured gain of 4.8 dB and the simulated gain of 4.9 dB have been achieved. It can be seen from Figure 4.11 that the measured gain of the antenna varies from 1.2 dB to 4.8 dB.



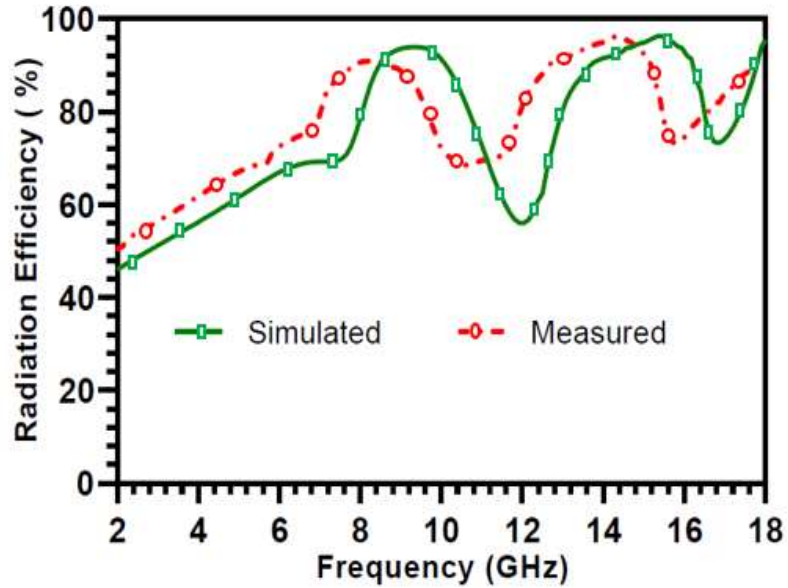
**Figure 4.10** 3-D Radiation pattern at (a) 5.37 (b) 10.66 and (c) 15.14 GHz



**Figure 4.11** Simulated and measured realized gain

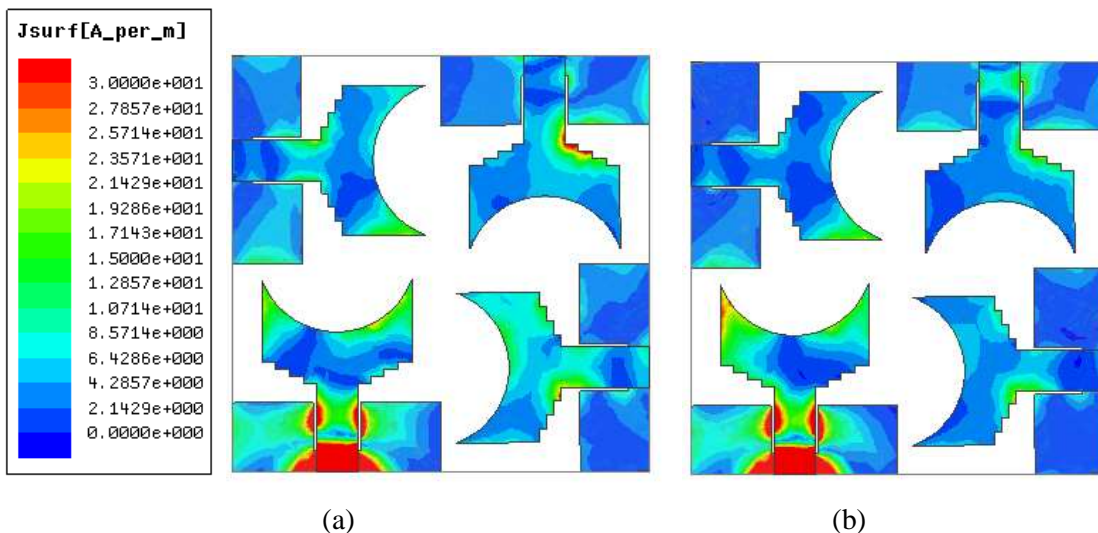
The measured and simulated radiation efficiency of the proposed antenna has more than 60 % through the entire frequency band as illustrated in Figure 4.12. The efficiency of the

antenna first increases up to 90 % then further decreases and after that increases to the peak value of 96 %.



**Figure 4.12** Simulated and measured radiation efficiency

Figure 4.13, represents the surface current distribution at 3.07, 5.37, 10.66, and 15.14 GHz respectively when port 1 is excited and other ports terminated with 50-ohm impedance. It is observed that a very small amount of current is coupled with other elements, and this is due orthogonal arrangement of the antenna element. This observation is valid for the entire frequency range.



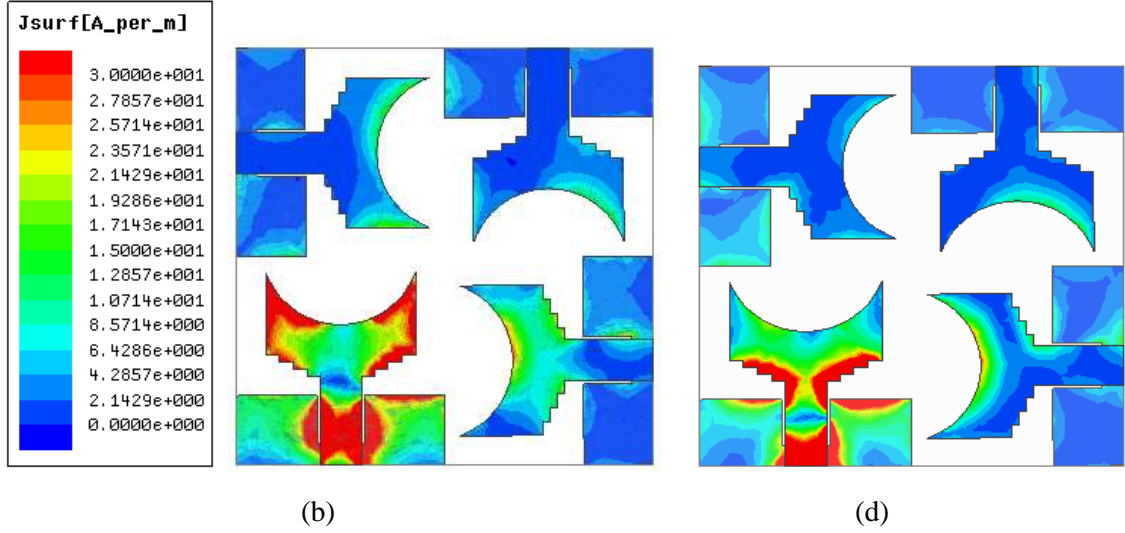


**Figure 4.13** Surface current at (a) 3.07 GHz (b) 5.37 GHz (c) 10.66 GHz (d) 15.14 GHz

## 4.7 MIMO Diversity Analysis

The performance of the MIMO antenna cannot be fully measured only by return loss and isolation parameters. Other parameters like ECC, diversity gain, TARC and mean effective gain are also used to evaluate the performance of the MIMO antenna.

### 4.7.1 Envelope Correlation Coefficient

It is very important for diversity parameters that explain the mutual coupling between antenna elements. There are two ways to evaluate ECC, using far-field radiation pattern and S-parameter [146].

$$ECC = \rho_e(i, j, N) = \frac{|\sum_{n=1}^N S_{i,n}^* S_{n,j}|^2}{|\prod_{k=i,j}(1 - \sum_{n=1}^N S_{k,n}^* S_{n,k})|} \quad (4.2)$$

Where  $i$  and  $j$  are the port number       $N$  = no of an antenna element

For quad-port MIMO antenna, ECC between antenna elements can be evaluated by putting  $N=4$  in equation (4.2).

$$ECC_{12} = \frac{|S_{11}^* S_{12} + S_{21}^* S_{22} + S_{13}^* S_{32} + S_{14}^* S_{42}|^2}{(1 - |S_{11}|^2 - |S_{21}|^2 - |S_{31}|^2 - |S_{41}|^2)(1 - |S_{12}|^2 - |S_{22}|^2 - |S_{32}|^2 - |S_{42}|^2)} \quad (4.3)$$

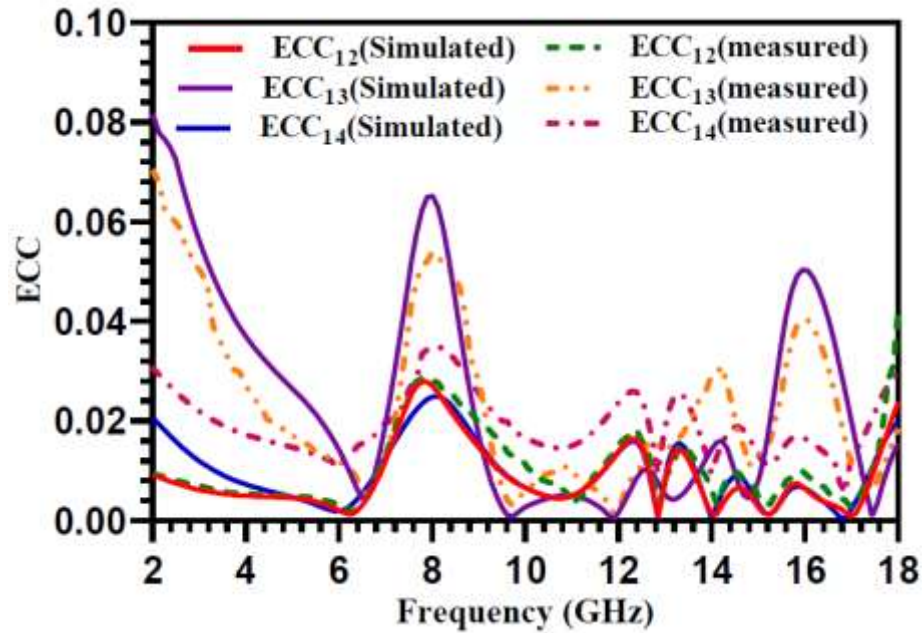


**Figure 4.14** Envelope correlation coefficient with frequency

Where  $ECC_{12}$  is the mutual coupling on port 1 due to port 2. Similarly, we can evaluate  $ECC_{13}$  and  $ECC_{14}$  from equation 4.2. It can be seen from Figure 4.14, that the ECC value is lower than 0.065 in the whole operating band. The measured value is very low as compared to the practical acceptable value of 0.5. It means that the MIMO antenna shows very good diversity performance.

#### 4.7.2 Diversity Gain

It measures how much the transmission power can be reduced after implementing various diversity schemes without any performance loss. The diversity gain should be close to 10 dB for the effective performance of the MIMO antenna as it can be directly calculated from the ECC value. The DG of the designed antenna is evaluated from equation 1.9.



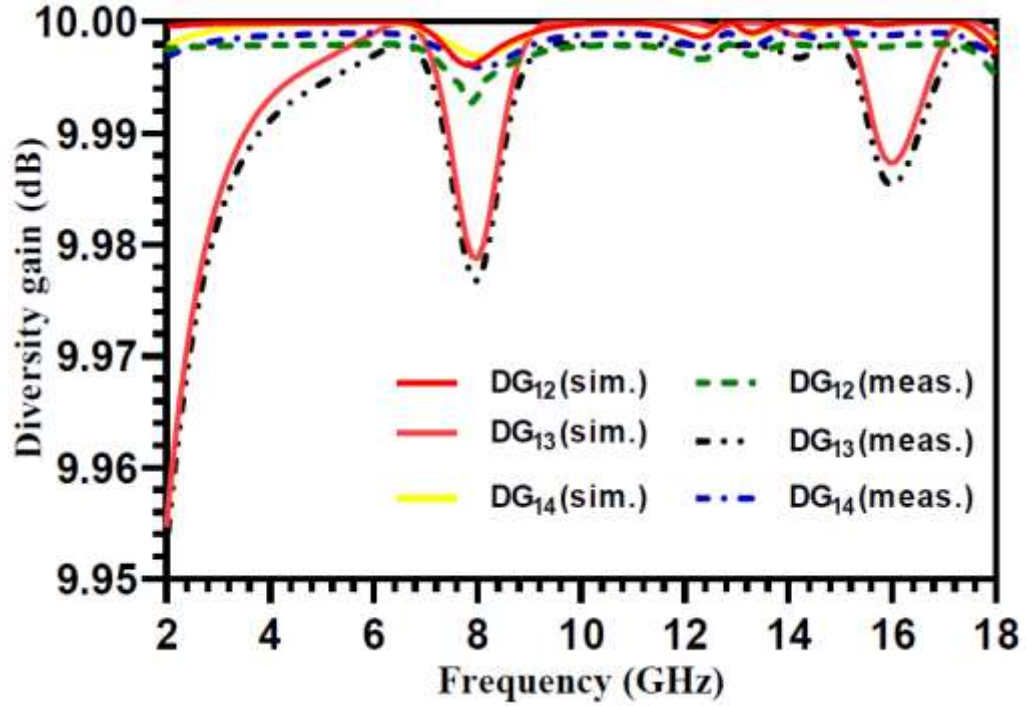


**Figure 4.15** Diversity gain with frequency

Figure 4.15 shows the diversity gain when port 1 is excited and the other port is terminated. It is noticed that the DG value in all three cases is more than 9.98 dB which is greater than the practical accepted value of 9.5

### 4.7.3 Total Active Reflection Coefficient

In the MIMO system, operating bandwidth and efficiency will be affected when all the antenna element operates simultaneously. Thus, S-parametric results are not sufficient to judge how good the antenna is, so we also used another important parameter known as TARC to evaluate the antenna performance. TARC can be evaluated from equation 1.21. In this proposed MIMO antenna, it is considered that all incoming signals at all ports have the same amplitude and phase ( $0^0$  phase difference), then the equation for TARC is given by [135].

$$TARC = \sqrt{\frac{|S_{11}+S_{12}+S_{13}+S_{14}|^2 + |S_{21}+S_{22}+S_{23}+S_{24}|^2 + |S_{31}+S_{32}+S_{33}+S_{34}|^2 + |S_{41}+S_{42}+S_{43}+S_{44}|^2}{\sqrt{4}}} \quad (4.4)$$

It can be observed that the TARC value is lower than -10 dB which is lower than the practical accepted value of 0 dB over the entire frequency band as shown in Figure 4.16.

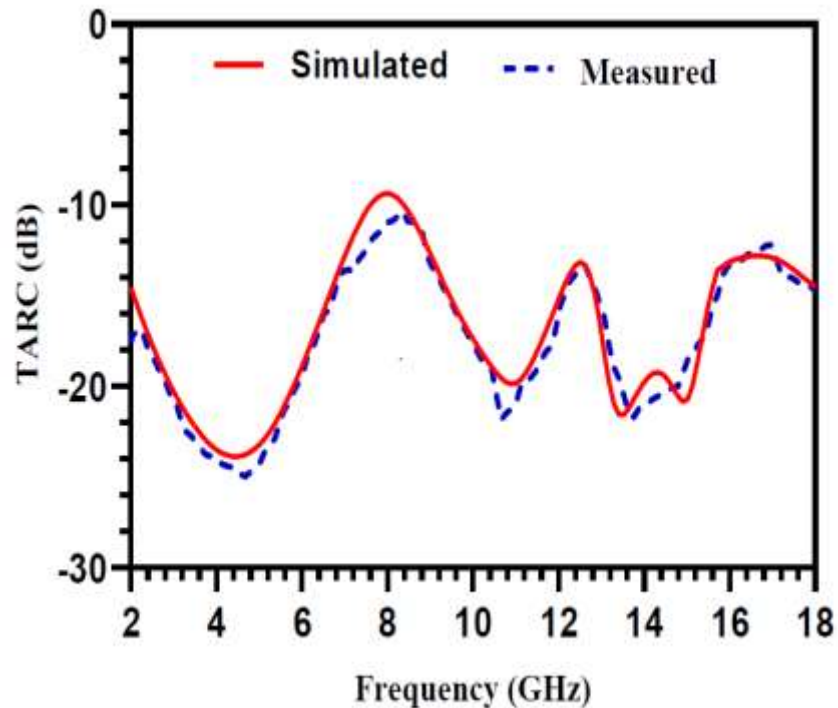


**Figure 4.16** Simulate and measured TARC with frequency

#### 4.7.4 Mean Effective Gain

For MIMO diversity performance, MEG is also a very important parameter. It is the ratio of the average power of an outgoing signal to an incoming signal. MEG at each port can be evaluated from equation 1.13. For effective performance of the MIMO antenna, the MEG should be below -3 dB at each port, and the magnitude of the difference of MEG between any ports should be below 3 dB. It is clear from Figure 4.17, that MEG at each port is less than -6 dB in the whole range of frequency band. The magnitude of the difference of MEG between any port is also within 1 dB.



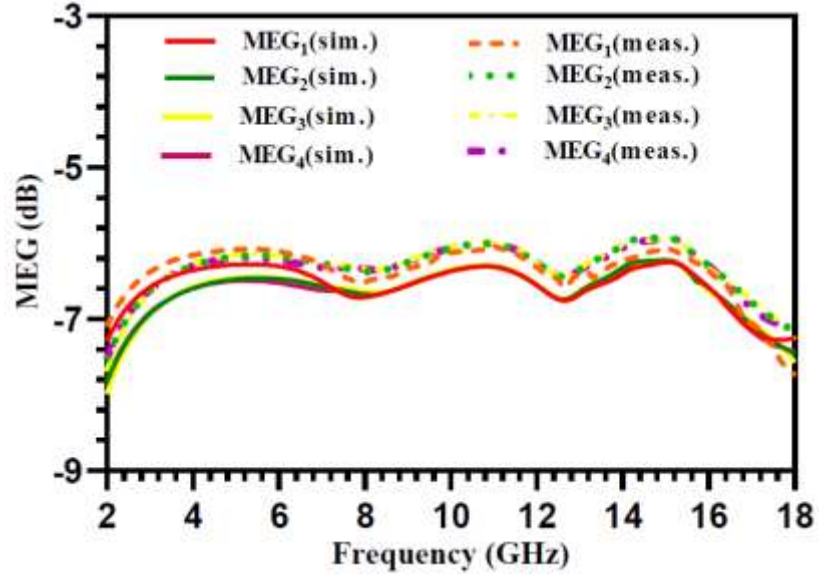
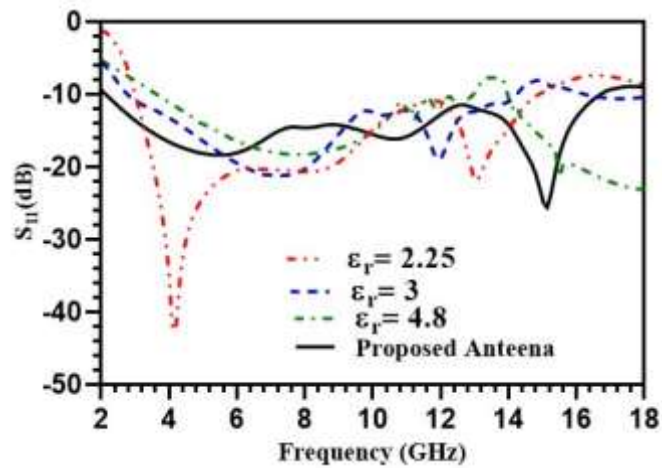


Figure 4.17 Simulated and measured MEG with frequency

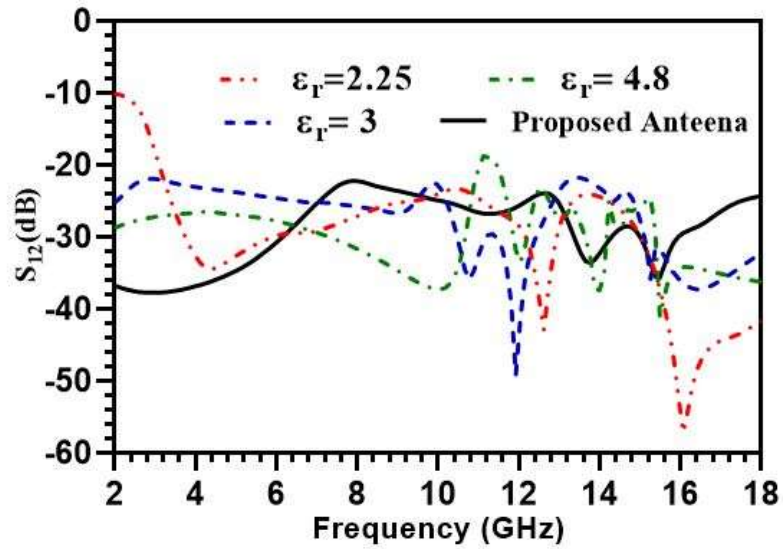
#### 4.8 Effect of Device Housing

The proposed antenna is placed inside three different plastic materials whose permittivity values are 2.25, 3, and 4.48. The size of the plastic housing has taken the same as the size of the antenna ie.  $30 \times 30 \text{ mm}^2$ . The height and thickness of the box have taken 15 mm and 1mm respectively.

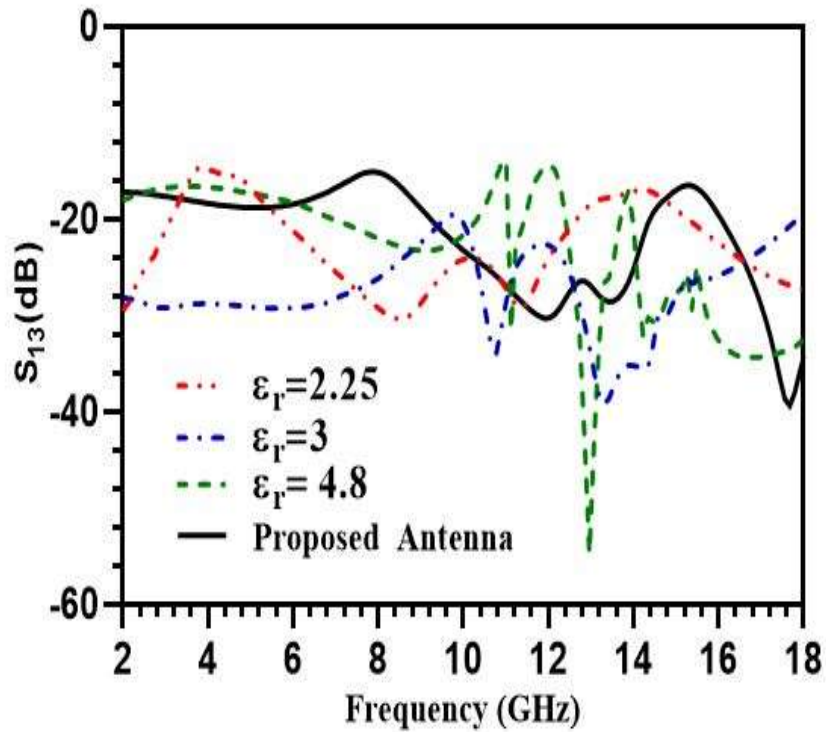


(a)

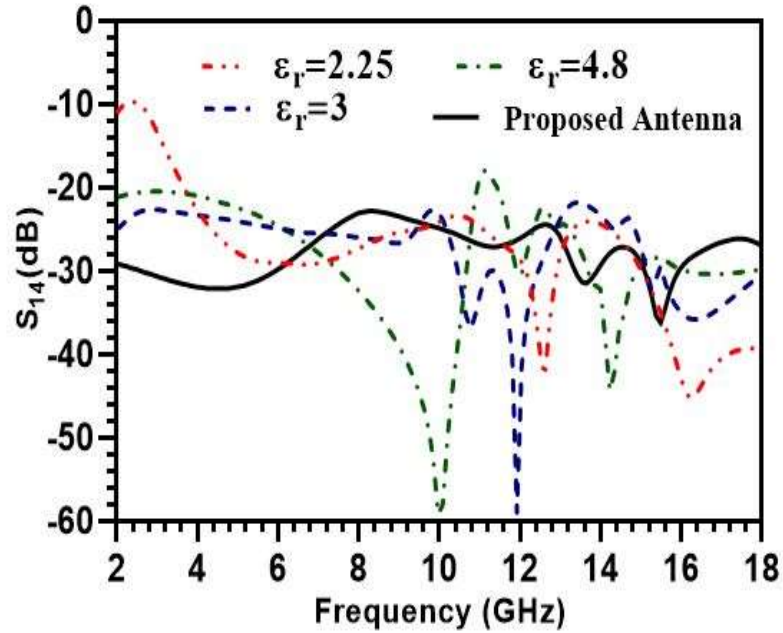
Figure 4.18 (a), shows that the lower frequency band shifts downward as the  $\epsilon_r$  value decreases from 4.48 to 2.2, and the isolation parameter  $S_{12}$ ,  $S_{13}$  and  $S_{14}$  are less than  $-20$  dB as illustrated in Figures 4.18 (b), (c), and (d). So the proposed antenna will satisfactorily work with different device housing.



(b)



(c)



(d)

**Figure 4.18** Comparison of S-parameter for different plastic materials with the proposed MIMO antenna (a) return loss (b)  $S_{12}$  (c)  $S_{13}$  (d)  $S_{14}$

## 4.9 Summary

A very compact  $30 \times 30 \text{ mm}^2$  quad-port high-performance UWB MIMO antenna has been proposed. The design provides an excellent isolation ( $S_{12} < -22 \text{ dB}$ ,  $S_{13} < -17 \text{ dB}$  and  $S_{14} < -22 \text{ dB}$ ) which is an essential ingredient as far as the MIMO antenna is concerned. This was possible just by positioning all the antennas in an orthogonal fashion. Cutting arc on the radiator and modifying the ground structure with staircase-shaped cuts at both the lower corner of the patch boosted the isolation to a greater extent which is expected in a MIMO environment. The proposed design is meant to comprehend a high-performing UWB MIMO antenna. This is due to various MIMO diversity parameters as well as high impedance bandwidth (2.15-16.75 GHz). The measured MIMO diversity parameters ECC, DG, and TARC were also within acceptable practical limits in the entire UWB range. Therefore, the designed antenna is a good candidate for various handheld portable devices. In the next chapter, the design and fabrication of CSRR loaded quad-port UWB MIMO antenna will be discussed.

# Chapter-5

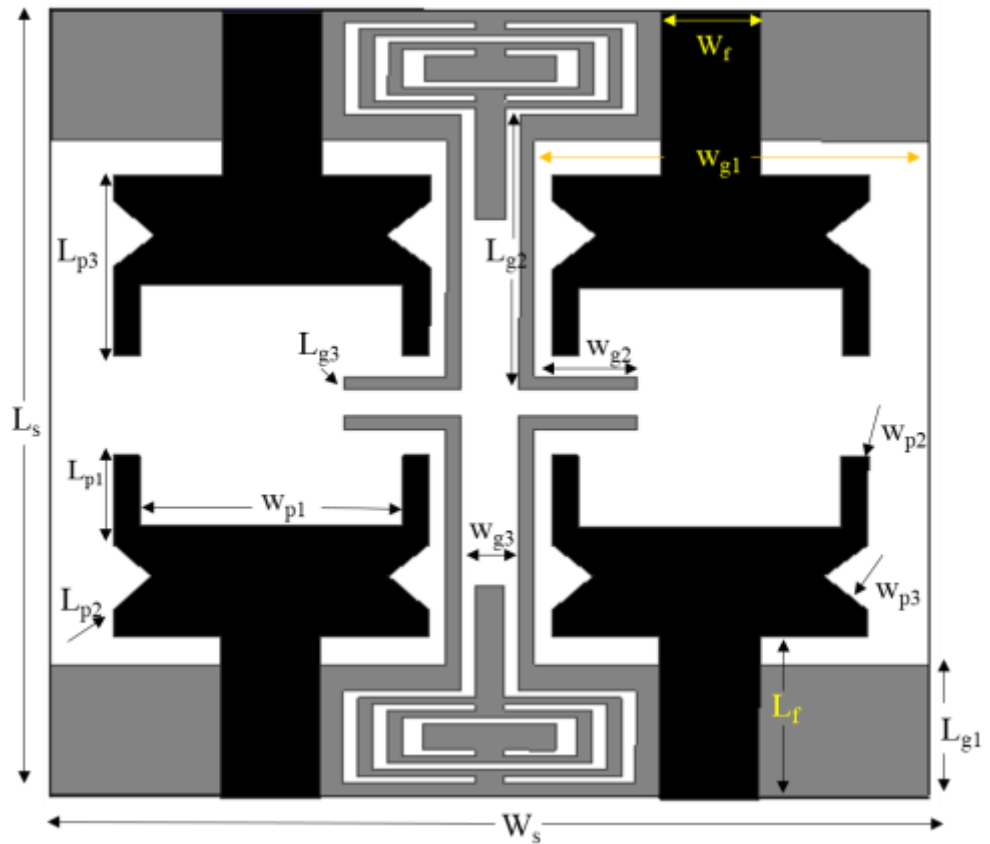
## CSRR Loaded Compact Quad Port MIMO Diversity Antenna for UWB Applications

### 5.1 Introduction

In the MIMO system, diversity and channel capacity are improved by placing multiple antennas in the transmitter and receiver. Moreover, by placing multiple antennas in a small area, more coupling occurs between antenna elements. So, in today's design, the multiple antennas in a very small space with low ECC values are challenging work for antenna designers. The compactness in the UWB MIMO system is achieved by decreasing the dimensions of the antenna element or placing the antenna element very close in an orthogonal fashion. The performance of the MIMO antenna is affected by mutual coupling between antenna elements. The MIMO diversity parameters, such as ECC, DG, TARC, and CCL, which depend on isolation parameters, are the key to having a better design. Various techniques have been proposed to enhance the bandwidth and improvise the isolation by adding slots, stubs, or defected ground structures [99], [138],[87],[45] that lead to suppressing the surface current. As a consequence of that, there will be an increment in the path of electrical current. Different types of electromagnetic bandgap (EBG) periodic structures are used between antenna elements either on the ground plane or both on the ground and topsides [136], [137],[147]. They absorb the electromagnetic signals and suppress the surface waves and improve the in-phase reflection coefficients. Furthermore, a metamaterial structure [139], [132], [148], [149], an artificial structure and magneto dielectric material, enhances the isolation by absorbing mutual interference signals and various techniques like polarization diversity in which multiple antenna elements are orthogonally [142], [143], [144]. The mutual coupling is also reduced using the

neutralization line technique in which strip lines are placed between antenna elements [135], [150]. It usually produces opposite coupling between antenna elements.

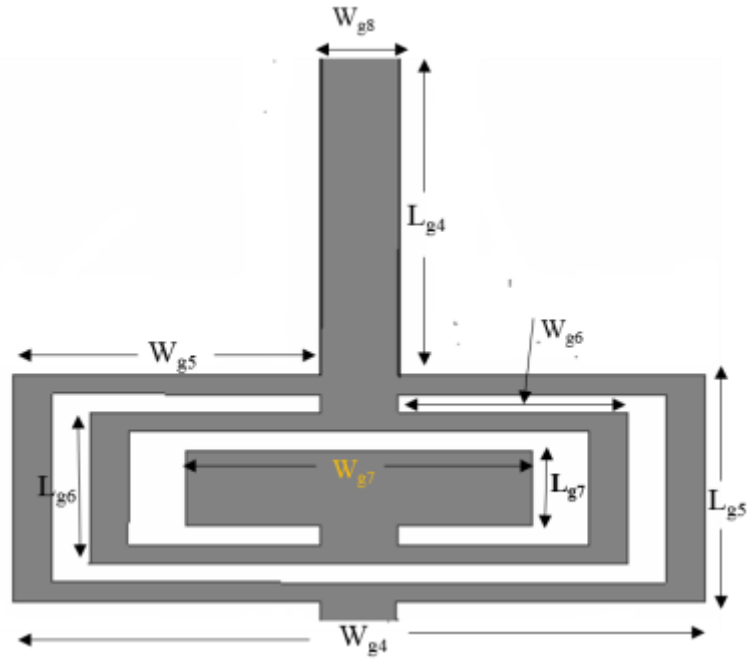
In this chapter, design and developed the MIMO antenna which is housed in a  $30 \text{ mm} \times 30 \text{ mm}$  dimension. The prototype antenna has very compact for placing four antenna elements. In addition, the isolation is significantly improved by inserting a complementary split-ring resonator (CSRR) structure along with the L-shaped strip on the ground plane between antenna elements, which restricts the strong current coupling.



(a)

The inclusion of CSRR not only prevents the current that flowing from one antenna to another antenna element but also diverts the current in another direction and acts as a filter. In actual practice, metamaterial behaves like a medium for electromagnetic signals. As CSRR or SRR is the unit cell, named a metamaterial, when the signal is excited it impinges

through this kind of structure, absorbs energy, and acts as a band stop filter due to its internal structure.



(b)

**Figure 5.1** Structure of (a) the proposed antenna and (b) CSRR unit cell

The proposed prototype antenna has been fabricated and measured and the results obtained show the antenna has got a very high fractional bandwidth of 146.15 % for a wide range of frequencies (2.8- 18 GHz). Apart from that, it has also provided good isolation of more than 18 dB in most of the band and a very low ECC value of less than 0.02 with high channel capacity. Keeping the above-mentioned results in view the proposed design becomes potential and suitable for modern communication devices, especially for the portable UWB-MIMO system. The structure of the proposed antenna is illustrated in Figure 5.1.

## 5.2 Antenna Design and Analysis

### 5.2.1 Evolution of Single UWB Antenna Element

Figure 5.2, represents the step-by-step procedure to get the final design of a single element antenna that operates in an ultra-wideband frequency range. Initially, the design starts from

the basic rectangular patch in step1, which resonates at 8.4 GHz and after that, a 9 mm x 2.7 mm size rectangular slot is cut from radiating patch in step2, and the resonance frequency is shifted to 7 GHz. Furthermore, the resonance frequency is shifted to a lower frequency by cutting two triangular slots with a dimension of  $1.8 \times 2.5 \times 1.8 \text{ mm}^3$  sizes in step3 and getting the UWB frequency range. The reflection coefficient of all the steps is presented in Figure 5.3. The approximate theoretical resonant frequency for a single element in a step1 is calculated from equation 4.1.

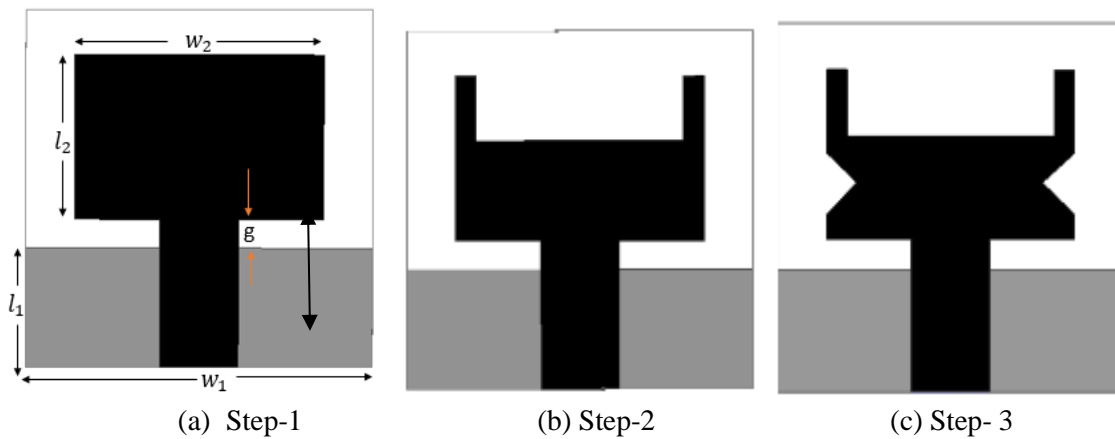


**Figure 5.2** Evolution steps of a single UWB element

The theoretical and simulated resonant frequency are presented in Table-5.1.

**TABLE 5.1:** Simulated and theoretical resonant frequency

Theoretical Resonance Frequency (GHz)	Simulated Resonance Frequency (GHz)
8.3	8.4

It can be observed that the theoretical value of resonance frequency is very close to the simulated value.

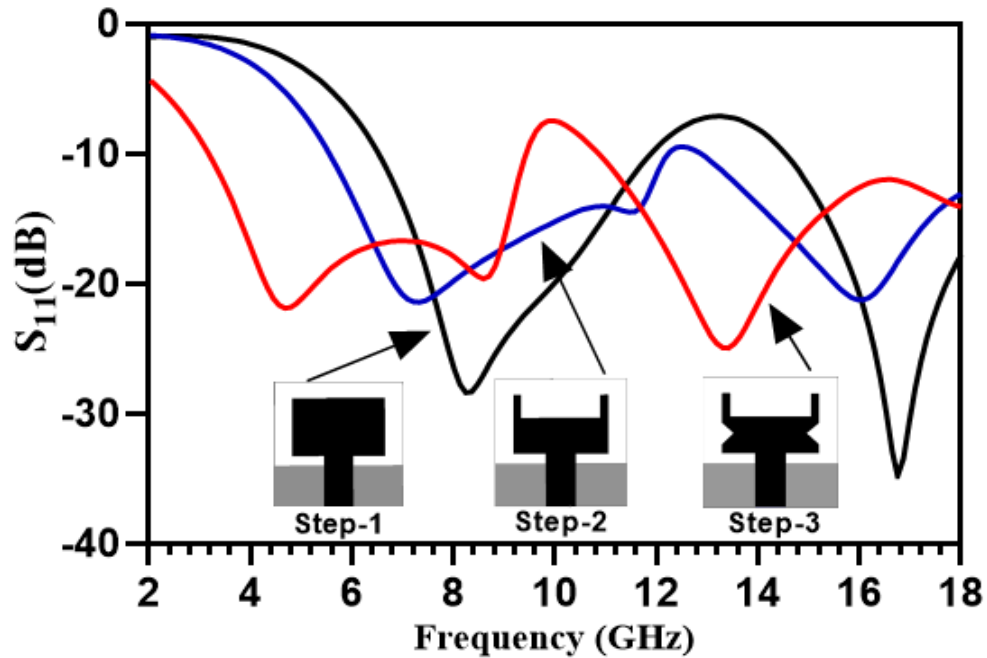


**Figure 5.3** Return loss of a single antenna element at various steps

### 5.2.2 Evolution of MIMO Antenna with Various Ground Structures

The evolution of the four-port MIMO antenna is represented in Figure 5.4. The antenna consists of four identical radiators, which are gradually modified from the basic rectangular structure, as presented in design 1, in which all the radiating elements are placed on one side and just opposite to that partial ground plane, have been developed with a dimension of  $30 \text{ mm} \times 5 \text{ mm}$  to enhance the bandwidth. In design-2, four L-shaped strips are placed on a partial ground plane for isolation improvement. Furthermore, for miniaturization and more isolation improvement, the CSRR structure has been introduced on the ground plane. After performing parametric analysis, the optimum dimension for each parameter is selected as shown in Table 5.2.



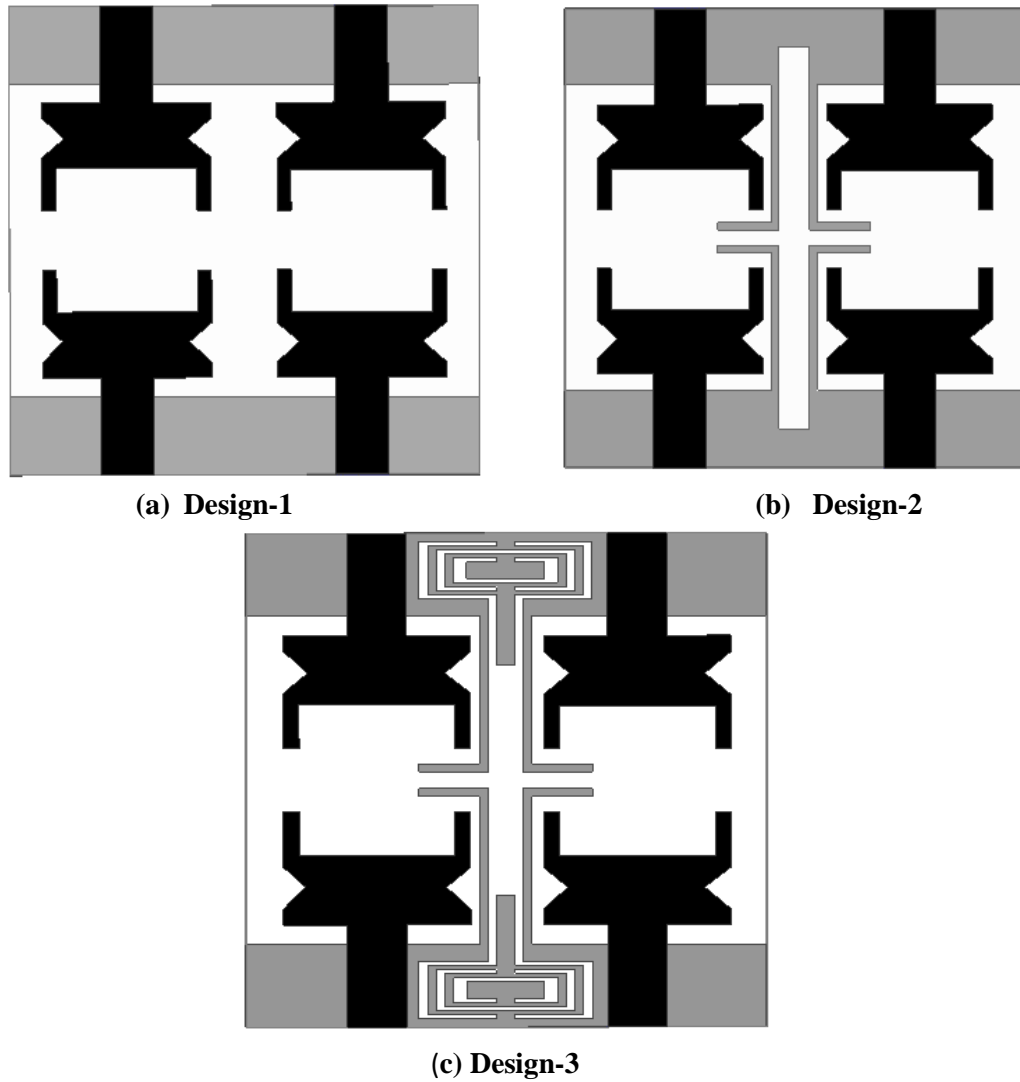


**Figure 5.4** Evolution steps with different ground structures

**TABLE 5.2** Various parameter values of the proposed model

Parameter	$W_s$	$W_f$	$W_{g1}$	$W_{g2}$	$W_{g3}$	$W_{g4}$	$W_{g5}$	$W_{g6}$	$W_{g7}$	$L_s$	$L_f$	$L_{p1}$	$L_{p2}$
Unit (mm)	30	3.4	13.5	3.5	2	9	4	3	4.5	30	6.2	3.4	1
Parameter	$L_{p3}$	$L_{g1}$	$L_{g2}$	$L_{g3}$	$L_{g4}$	$L_{g5}$	$L_{g6}$	$L_{g7}$	$W_{p1}$	$W_{p2}$	$W_{p3}$	$W_{g8}$	
Unit (mm)	6.9	5	10.5	0.5	4.25	3	2	1	9	0.9	1.8	1	

The resonance frequencies of the MIMO antenna for design 1 are 6.4, 9.2, and 12.8 GHz. After adding an L-shaped stub on the ground plane the frequencies got shifted to lower frequencies are 5.2, 9.1, and 12.4 GHz. The resonance frequency has been further shifted to the lower frequency at 4, 8, and 10.8 GHz with good impedance matching after inserting the CSRR structure in the ground plane, as illustrated in Figure 5.5.

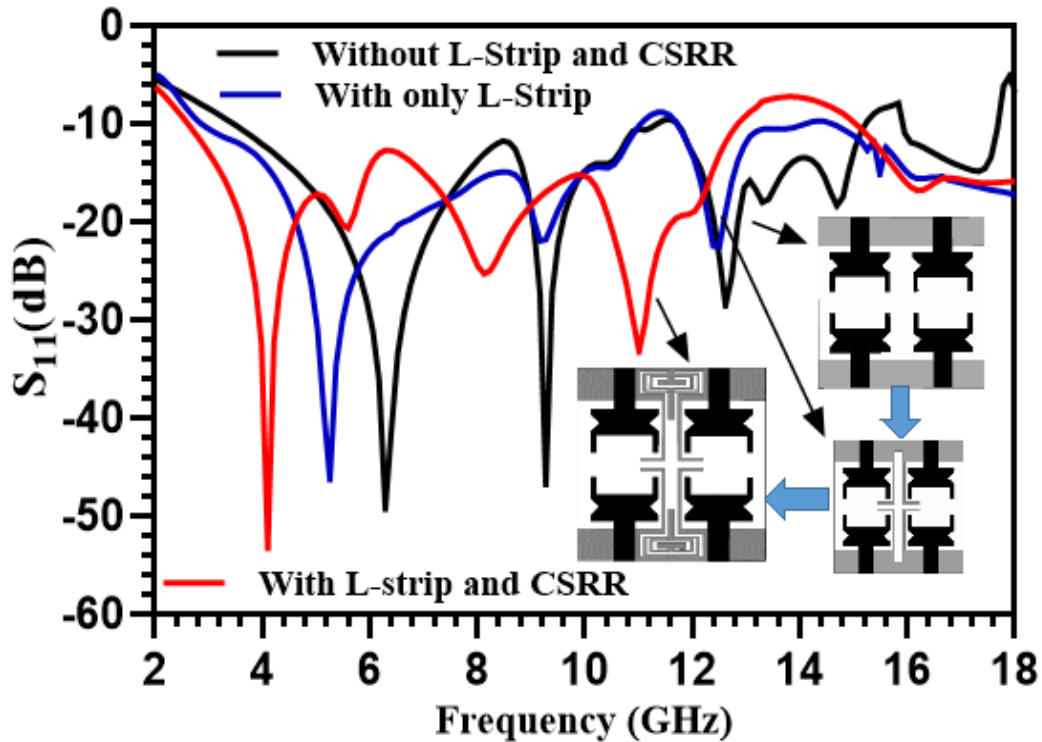


**Figure 5.5** Reflection coefficient of the MIMO antenna with different ground structure

The isolation parameter of all three MIMO antenna design is presented in Figure 5.6. It can be seen that for design-1 ( $S_{12} < -5$  dB,  $S_{13} < -10.4$  dB,  $S_{14} < -6$  dB), design-2 ( $S_{12} < -16$  dB,  $S_{13} < -20$  dB,  $S_{14} < -14$  dB) and design-3 ( $S_{12} < -17$  dB,  $S_{13} < -20$  dB,  $S_{14} < -18$  dB). The isolation has improved by inserting L-shaped strip on ground and further for more isolation CSRR structure has introduced on the ground plane between two antenna elements.

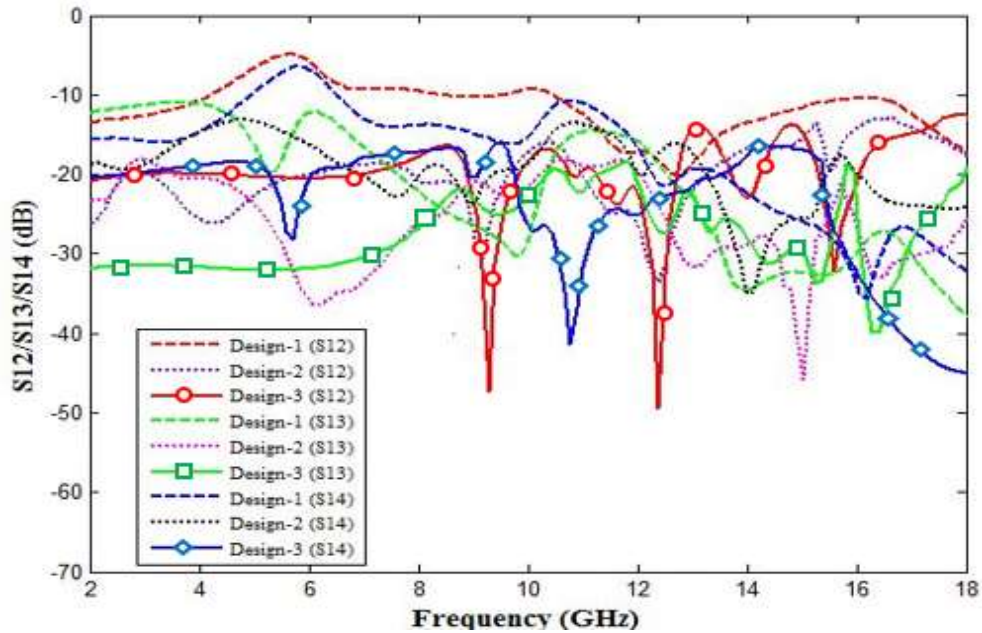


**Figure 5.6** Isolation parameter of the proposed antenna (a) only partial ground plane (b) partial ground with L-shape stub (c) partial ground and L-shape stub along with CSRR structure

### 5.3 CSRR Structure and Equivalent Model

The CSRR (unit cell) is a periodic structure that is made up of three rectangular complementary split-ring resonators. Each ring is cut from a metallic plate and a gap is introduced which connects the inner conducting area to the surrounding conducting area in Figure 5.7(a). It acts as an LC resonance circuit and functions as a filter which enhances the isolation over the required frequency band. This is because metamaterial usually restricts the current flow and behaves as a filter for the resonating frequency. The total inductance of CSRR is calculated by taking a parallel combination of three individual inductances, which connect the inner metal surface to the outer metal surface. Similarly, the capacitance value is also estimated and it is due to rings placed between two metallic plates, depicted in Figure 5.7(b) through an equivalent circuit. The resonance frequency of the CSRR structure is found using the expression given below.

$$f_{r2} = \frac{1}{2\pi\sqrt{\frac{L_0}{6}C_{eq}}} \quad (5.1)$$

Where  $L_0 = P * L_{pul}$  and P is the perimeter of the ring and  $L_{pul}$  is the inductance per unit length between the inner conductor and the outer conductor.

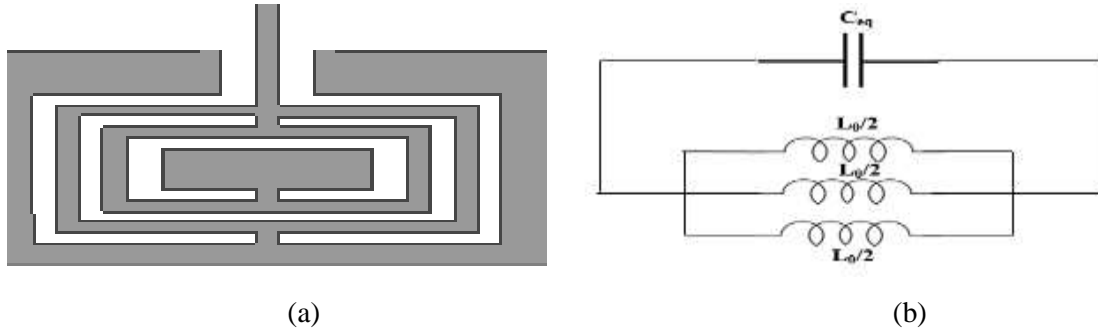


**Figure 5.7** (a) CSRR structure and (b) equivalent circuit

#### 5.4 Equivalent Circuit Model for the Proposed MIMO Antenna

The equivalent circuit model of the MIMO antenna is illustrated in Figure 5.8, in which all the four identical radiating patches are represented by a parallel combination of resistance, capacitance, and inductance.

**TABLE 5.3:** Lumped parameter values

Lumped Parameter	Value (nH)	Lumped Parameter	Value (pF)	Lumped Parameter	Value ( $\Omega$ )
L <sub>1</sub>	9.6	C <sub>1</sub>	1.51	R <sub>1</sub>	60
L <sub>6</sub>	1.05	C <sub>3</sub>	1.51	R <sub>3</sub>	60
L <sub>10</sub>	1.05	C <sub>5</sub>	12.5	R <sub>4</sub>	60
L <sub>11</sub>	1.05	C <sub>6</sub>	12.5	R <sub>9</sub>	60
L <sub>12</sub>	1.05	C <sub>7</sub>	12.5	R <sub>10</sub>	45
L <sub>13</sub>	35.5	C <sub>8</sub>	12.5	R <sub>12</sub>	45
L <sub>15</sub>	35.5	C <sub>9</sub>	0.052	R <sub>13</sub>	45
L <sub>16</sub>	9.6	C <sub>10</sub>	0.052	R <sub>16</sub>	45
L <sub>25</sub>	9.6	C <sub>19</sub>	1.51		
L <sub>27</sub>	9.6	C <sub>23</sub>	1.51		

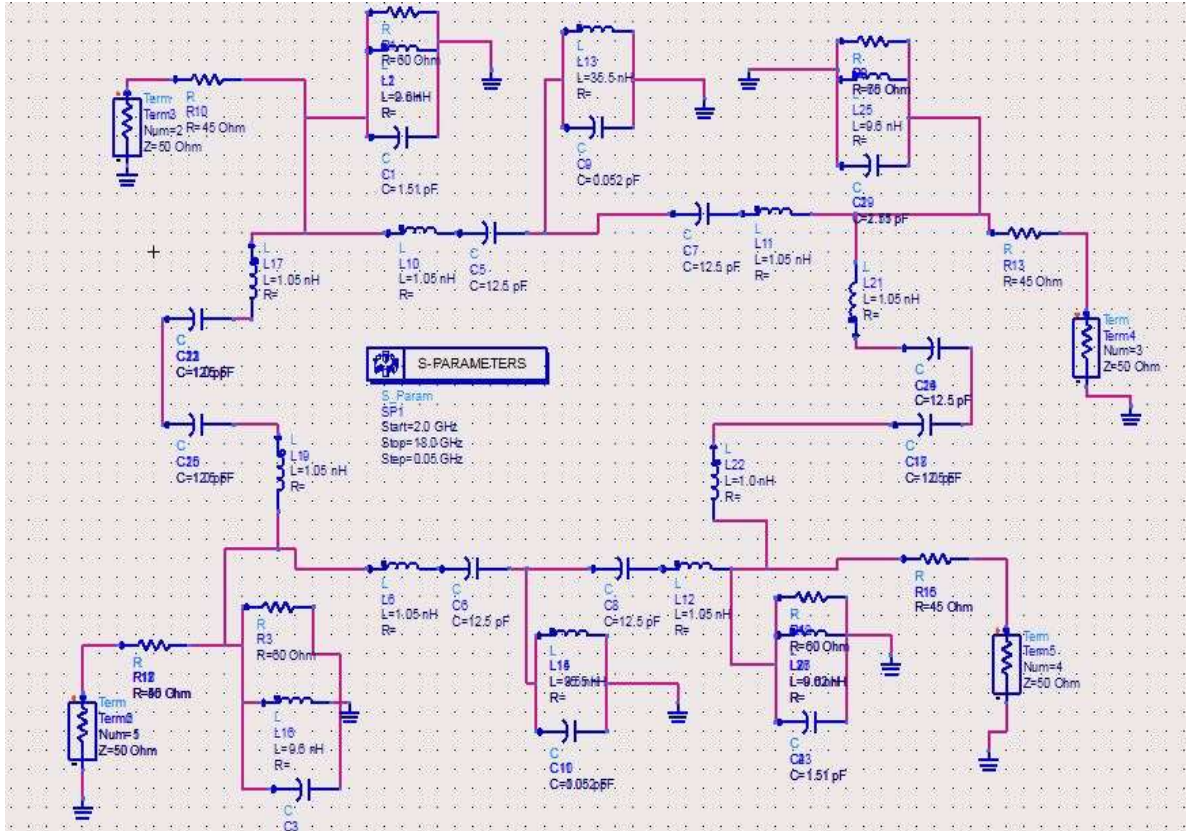


**Figure 5.8** Equivalent circuit of the proposed MIMO antenna

The effect of mutual coupling between each radiator is estimated by a combination of capacitance and inductance. Finally, the parallel combination of inductance and capacitance defines the equivalence of the CSRR structure. All these derived lumped parameters are depicted in Table 5.2. The comparison of reflection coefficient ( $S_{11}$ ) through EM and circuit simulator is presented in Figure 5.9.

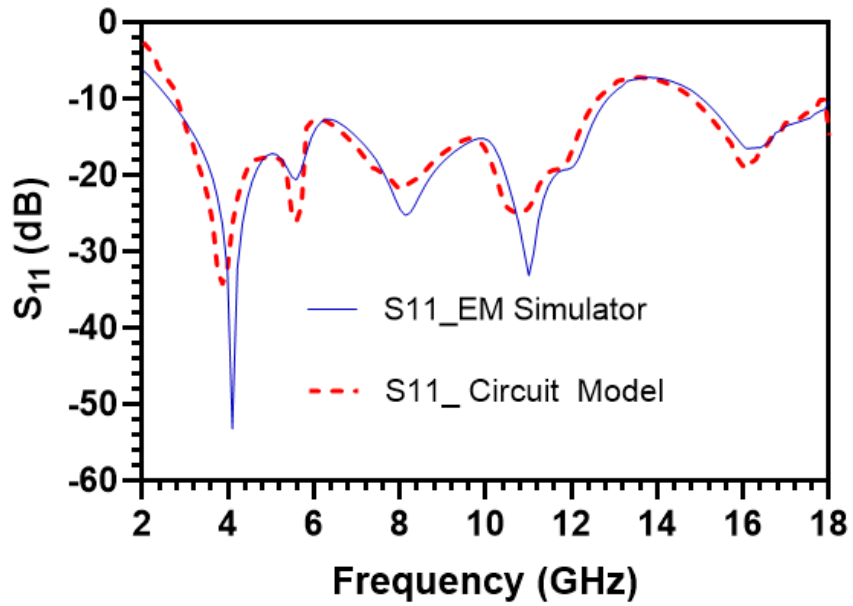


Figure 5.9: EM and circuit simulator result

### 5.5 Results and Discussion

The prototype has been developed on a high-frequency structure simulator and then fabricated with a MITS-Eleven PCB machine. The design consists of four antennas, fabricated with FR4 substrate (dielectric constant value of 4.4) on a very compact size of  $30 \times 30 \times 1.6 \text{ mm}^3$ , as shown in Figure 5.10.

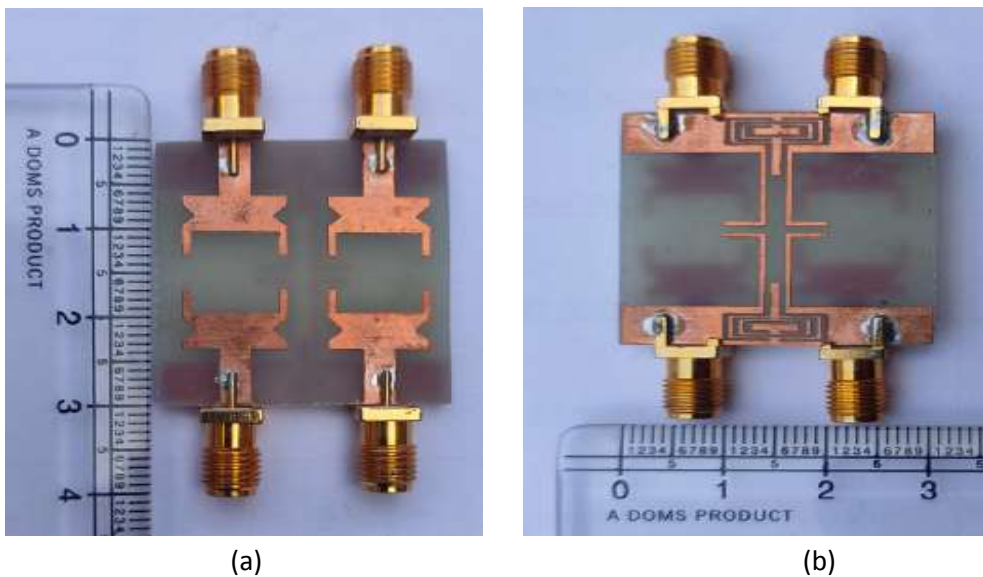
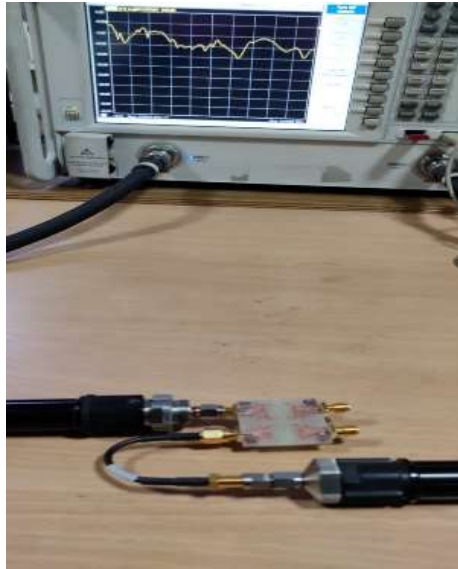


Figure 5.10 (a) Front and (b) Bottom sides of the prototype model



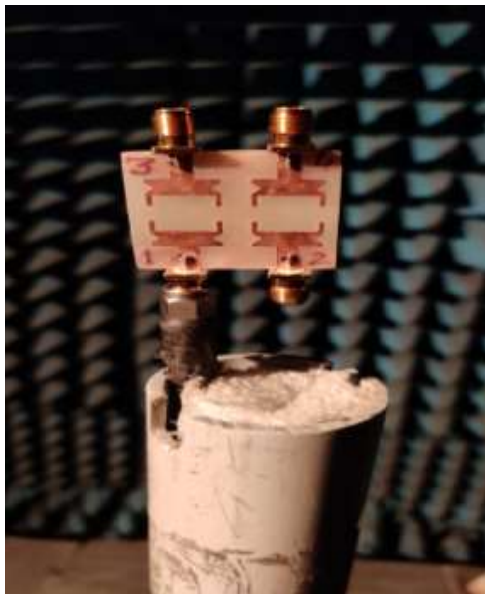
The simulated result has been verified with the measured result which was obtained through the Agilent N5230A vector network analyzer (VNA) and corresponding radiation characteristics are obtained from an anechoic chamber, presented in Figure 5.11.



(a)



(b)



(c)



(d)

**Figure 5.11** Antenna measurement setup (a), (b) with VNA and (c), (d) inside an anechoic chamber

### 5.5.1 Reflection Coefficient and Isolation Parameter

Figure 5.12 demonstrates the comparison between the measured and simulated reflection coefficients. There is a little deviation, due to the environmental effect, SMA connector soldering, cable effect, and many others. The measured impedance bandwidth ranges from 2.8 to 18 GHz. The bandwidth of the prototype antenna fulfilled the frequency range 3.1-10.6 GHz for the UWB requirement decided by FCC. Figure 5.13, represents the measured isolation parameter ( $S_{12} < -19$  dB,  $S_{13} < -24$  dB and  $S_{14} < -19$  dB) and simulated isolation parameter ( $S_{12} < -18$  dB,  $S_{13} < -20$  dB and  $S_{14} < -18$  dB) throughout the operating frequency range. It indicates the proposed prototype has very low coupling between each port.

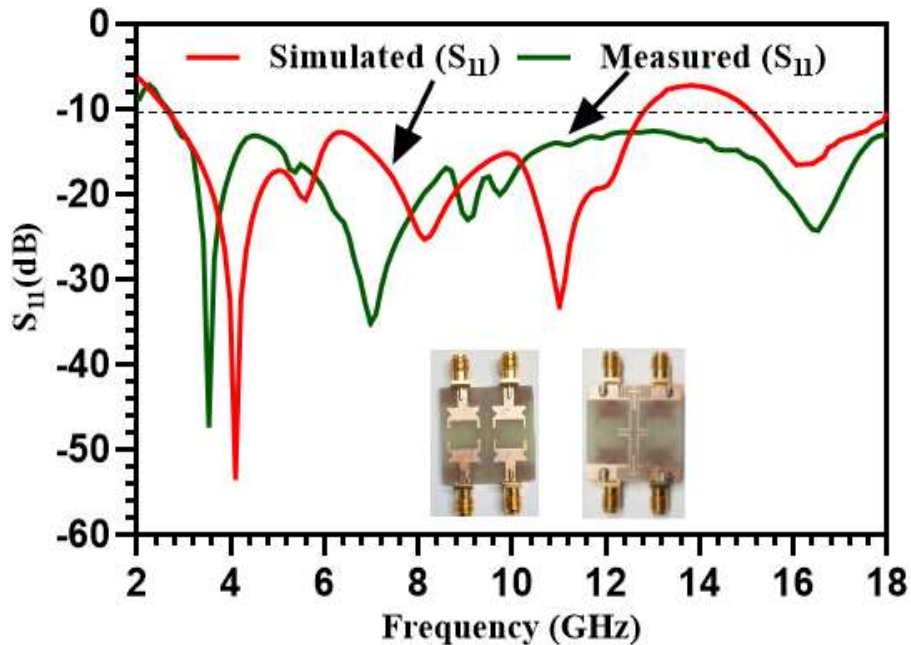
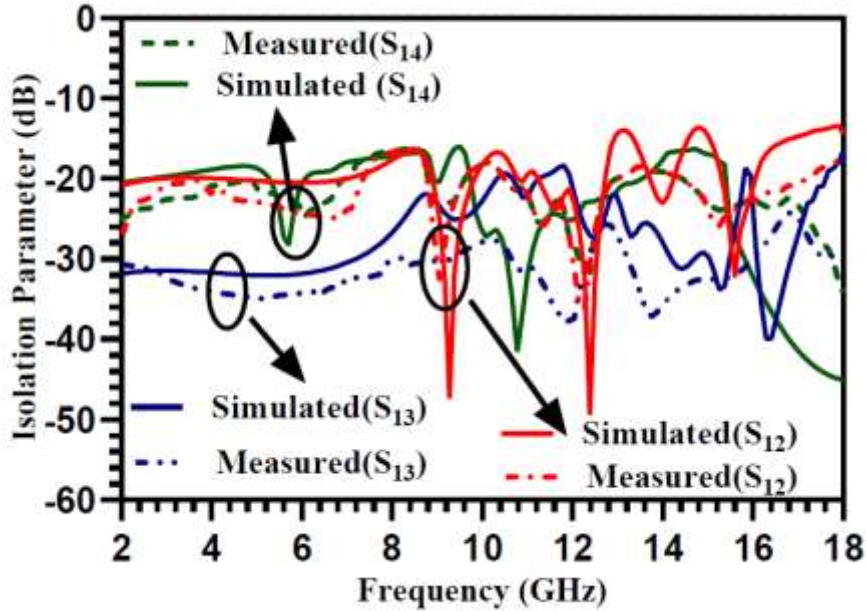


Figure 5.12 Measured and simulated return loss

Figure 5.13, represent the measured and simulated isolation parameter and it can be observed that  $S_{12}$  less than  $-17$  dB,  $S_{13}$  is less than  $-20$  dB and  $S_{14}$  is less than  $-18$  dB throughout the UWB range. It indicates proposed prototype has very low coupling between each port.





**Figure 5.13** Measured and simulated isolation parameter

### 5.5.2 Gain and Efficiency

Initially, the measured peak gain increases monotonically to a maximum of 3.6 dB at 8.8 GHz and then decreases to a minimum of 0.5 dB. It is replicated further to have a maximum of 3.6 dB at 15.4 GHz through the entire operating UWB range, as presented in Figure 5.14. The total radiation efficiency of the MIMO antenna from port n,

$$\eta_{t,n} = \eta_{r,n}\eta_{d,n} \quad (5.2)$$

Where  $\eta_{d,n}$  denotes the decoupling efficiency and is given by

$$\eta_{d,n} = 1 - \sum_{m=1}^M |S_{mn}|^2 \quad (5.3)$$

‘M’ denotes the number of ports in the MIMO antenna,  $\eta_{r,n}$  represents the radiation efficiency of the radiating mode at port n. The radiation efficiency of the antenna varied from 50 % to 84 %. It can be observed that simulated and measured results are parallel to each other.

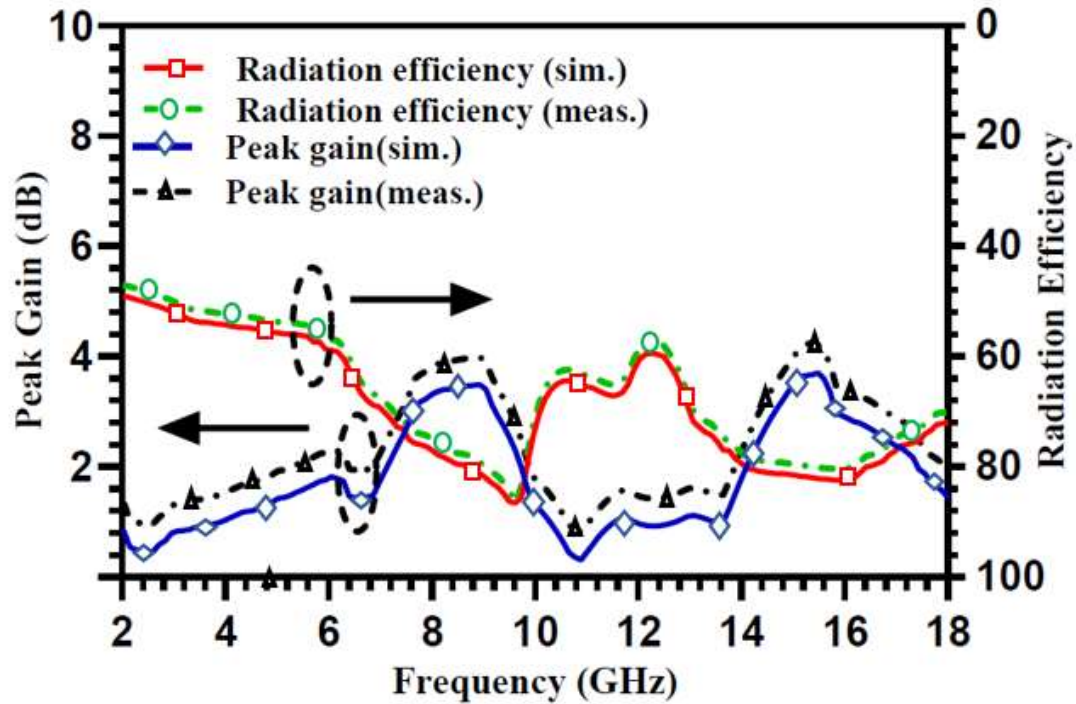
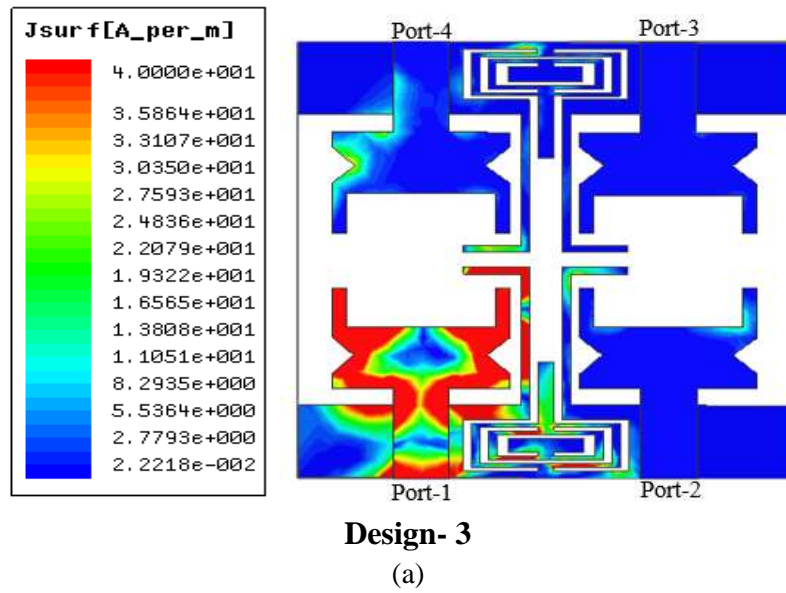
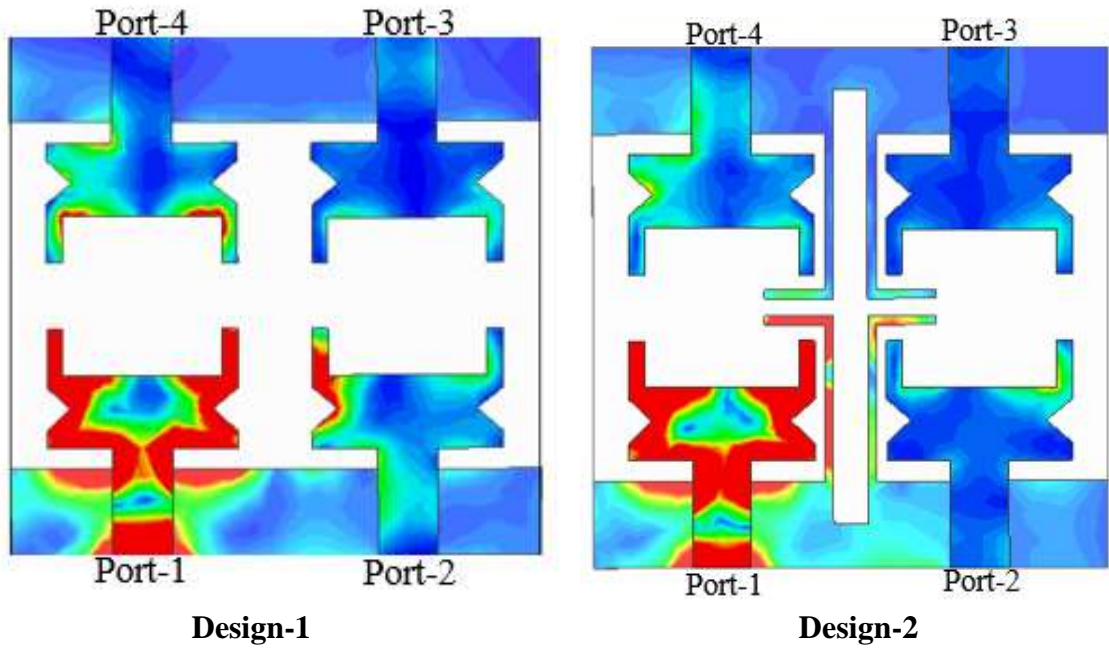
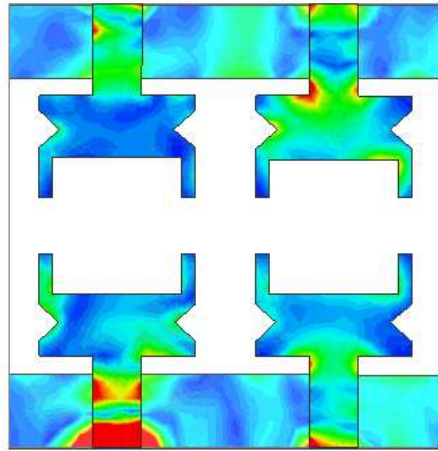


Figure 5.14 Peak gain and radiation efficiency of the proposed antenna

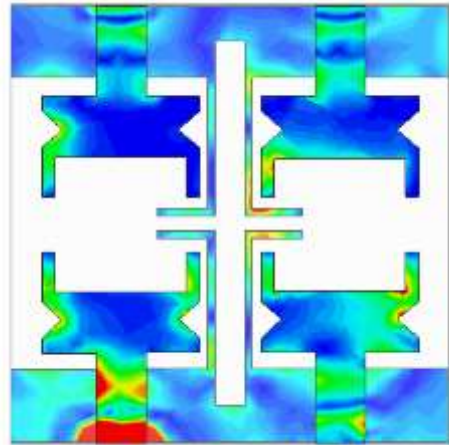
### 5.5.3 Current Distribution

The effect of the L-shaped stub and the CSRR structure on isolation improvement can be easily understood by an amount of surface current linked from one element to another, as demonstrated in Figure 5.15 at different frequencies. The first port of the MIMO antenna is excited and remaining all other ports are terminated with 50-ohm load impedance. Currents are strongly coupled to all elements in the absence of CSRR and L-shaped stub on the ground plane. The amount of coupling current has been reduced due to the addition of an L-shaped stub on the ground between antenna elements. Furthermore, a significant amount of coupling has been reduced by introducing the CSRR structure, along with an L-shaped stub at an optimum place. The function of CSRR is to prevent the maximum amount of current that flows between two antennas.

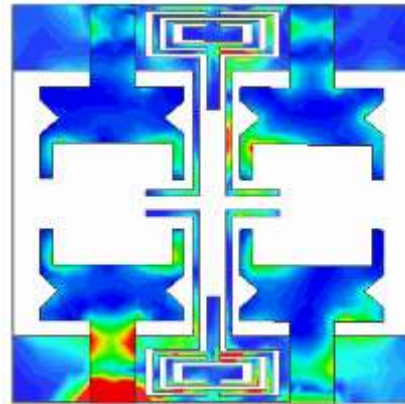
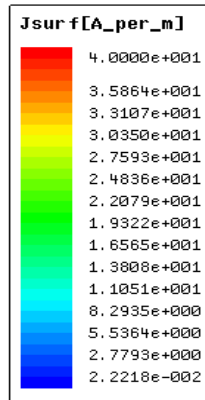




**Design-1**

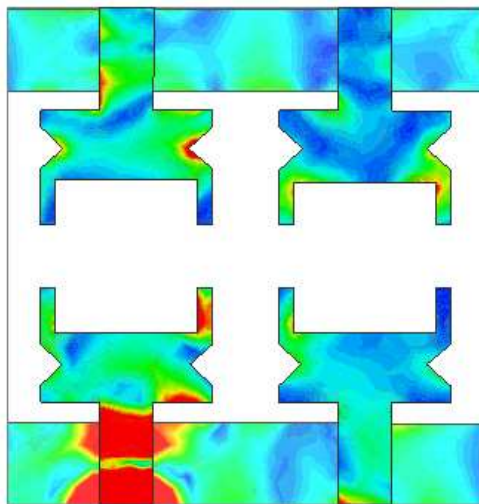


**Design-2**

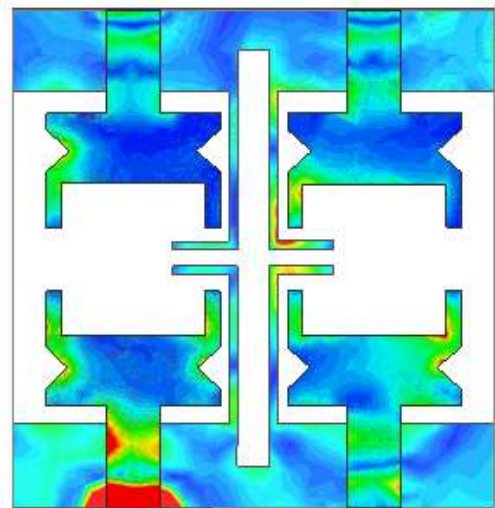


**Design- 3**

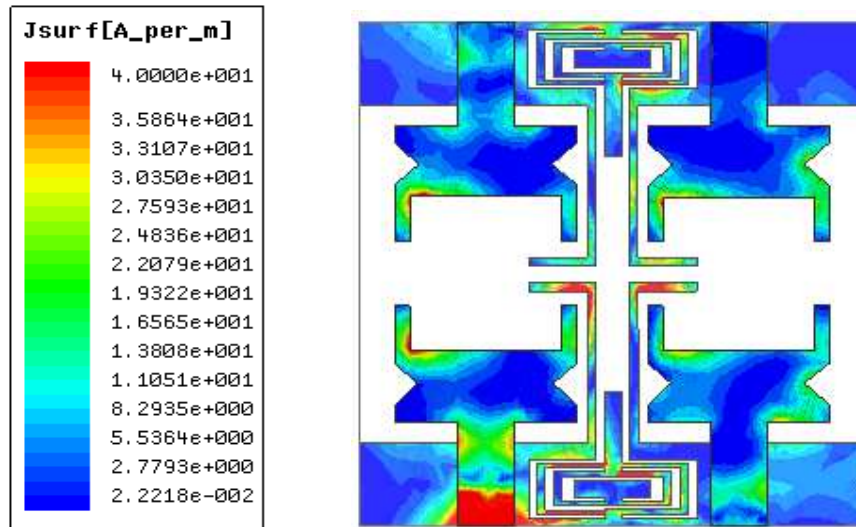
(b)



**Design- 1**



**Design-2**



**Design-3**  
(c)

**Figure 5.15** Current distribution at (a) 4 (b) 8 and (c) 10.8 GHz

#### 5.5.4 Radiation Characteristics

The two-dimensional radiation pattern in the y-z and x-z planes at 4, 8, and 10.8 GHz of the proposed four-port prototype model is illustrated in Figure 5.16. The radiation characteristic of the MIMO antenna is carried inside an anechoic chamber and during the measurement of the first port of the antenna is fed by 50-ohm impedance, and the rest of all three ports have been terminated with 50-ohm load impedance. The radiation pattern from the HFSS simulator and measured one inside the anechoic chamber agree well. The radiation pattern in the H-plane almost approaches omnidirectional, whereas the E-plane pattern follows directional behavior.



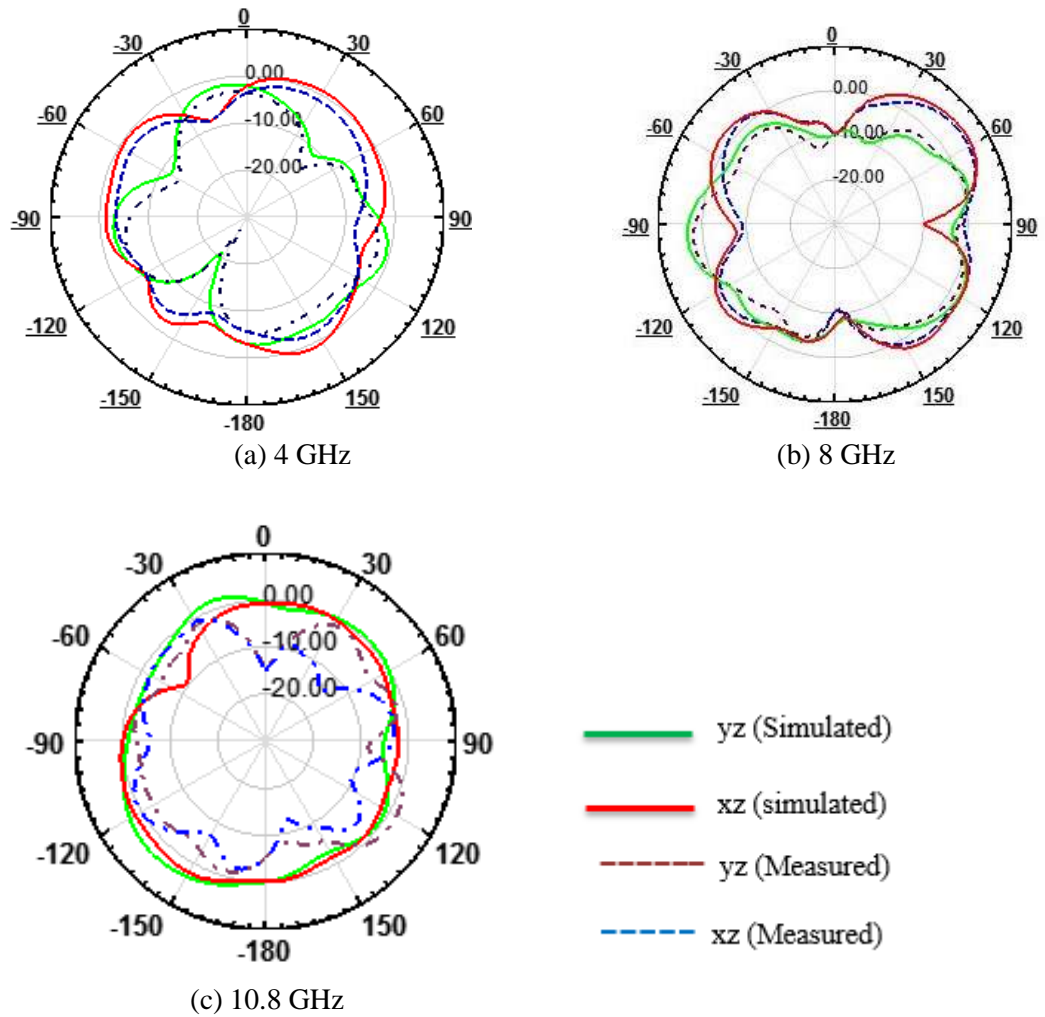


**Figure 5.16** Two dimensional radiation pattern at (a) 4 (b) 8 (c) 10.8 GHz

## 5.6 MIMO Performance Analysis

The performance of the MIMO antenna is not only decided by return loss and isolation parameters. There are a few more parameters such as ECC, diversity gain, TARC, MEG, and CCL that also decide the performance of the prototype antenna. These parameters are evaluated by creating MATLAB code and the results are compared with the measured result.

### 5.6.1 Envelope Correlation Coefficient and Diversity Gain

In the MIMO system, multiple antennas are placed in a small area, then a very high chance of correlation may happen between elements. The ECC parameter decides the amount of mutual coupling between antenna elements. The practical, acceptable value is 0.5 for effective performance and it is assumed that the lower the value of ECC the better the diversity performance of the MIMO antenna. The  $ECC_{12}$ ,  $ECC_{13}$ , and  $ECC_{14}$  are the mutual coupling on port1 due to ports 2, 3, and 4 respectively which can be evaluated from equation 1.6. It can be seen from Figure 5.17, that the ECC value is found to be  $< 0.02$  for the entire frequency band. The measured value is very low compared to the practical acceptable value of 0.5.

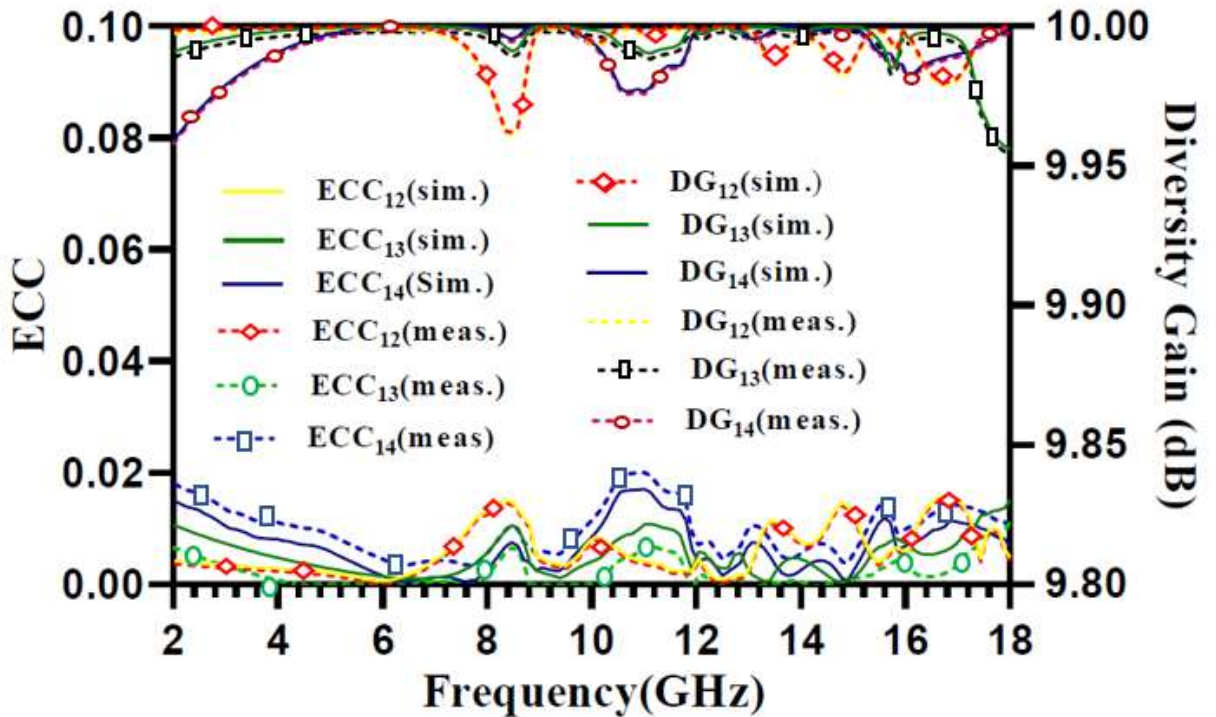


Figure 5.17: ECC and DG for the prototype antenna

The parameter diversity gain can be directly evaluated from the ECC value from equation 1.8. Figure 5.17, explains the diversity gain when the first port is excited and all three ports are terminated with 50-ohm load impedance. The DG value in all three cases is more than

9.95 dB which is greater than the practical accepted value of 9.5 and the ideal value for diversity gain of 10 dB. It means that the prototype antenna shows a very good diversity performance.

### 5.6.2 Mean Effective Gain

It is an important parameter for diversity performance and is defined as the ratio of power received from the prototype antenna to the reference antenna under the same working condition. MEG can be evaluated from S-parameter as [151],

$$MEG_i = 0.5[1 - \sum_{j=1}^N |S_{ij}|^2] \quad (5.4)$$

The mean effective gain at each port can be calculated from equation 5.4 after considering N=4.

$$MEG_1 = 0.5[1 - |S_{11}|^2 - |S_{12}|^2 - |S_{13}|^2 - |S_{14}|^2] \quad (5.5)$$

$$MEG_2 = 0.5[1 - |S_{21}|^2 - |S_{22}|^2 - |S_{23}|^2 - |S_{24}|^2] \quad (5.6)$$

$$MEG_3 = 0.5[1 - |S_{31}|^2 - |S_{32}|^2 - |S_{33}|^2 - |S_{34}|^2] \quad (5.7)$$

$$MEG_4 = 0.5[1 - |S_{41}|^2 - |S_{42}|^2 - |S_{43}|^2 - |S_{44}|^2] \quad (5.8)$$

The mean effective gain at each port should be less than  $-3$  dB and the magnitude of the difference in MEG between each port  $<-3$  dB for the effective performance of the prototype model. From Figure 5.18, it is found to be a value of MEG at all ports and the difference between the two ports is less than the practical limit for the entire frequency band.



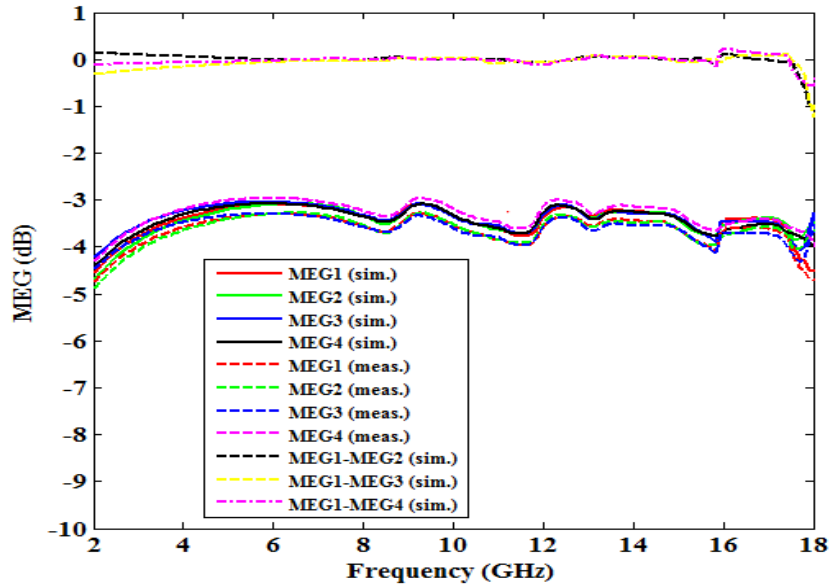


**Figure 5.18** Mean effective gain at different ports

### 5.6.3 Total Active Reflection Coefficient

In the MIMO system, operating bandwidth and efficiency will be affected when all the antenna elements operate simultaneously. S-parameter result is not sufficient to judge how good the antenna is, so we tried to introduce another important parameter known as TARC.

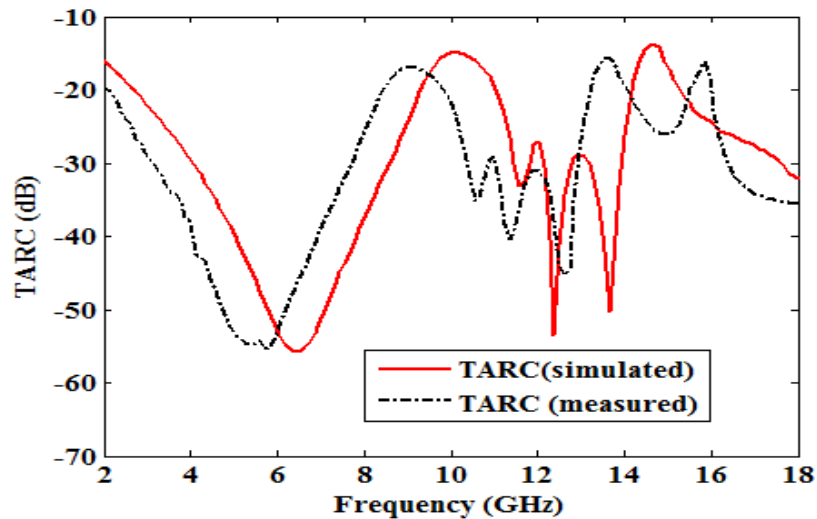


**Figure 5.19** Measured and simulated TARC

It provides complete characteristics to measure MIMO efficiency. In the proposed MIMO antenna, all incoming signals irrespective of any port are of the same amplitude and phase

( $0^\circ$  phase difference), then TARC can be evaluated from equation 1.21. As shown in Figure 5.19, the measured and simulated TARC are less than -15 dB in the entire frequency range. A slight difference was found in simulated and measured results due to the variation in the phase of all incoming signals and measurement of the S-parameter from VNA.

#### 5.6.4 Channel Capacity Loss

The channel capacity loss occurs due to uncorrelated Rayleigh fading in the MIMO system. The value of CCL is calculated from equation 1.13. The measured and simulated result of CCL is reflected in Figure 5.20, and it is found to be  $CCL < 0.35$  bits/s/Hz over the entire operating frequency range which satisfies the practical limit  $< 0.4$  bits/s/Hz.

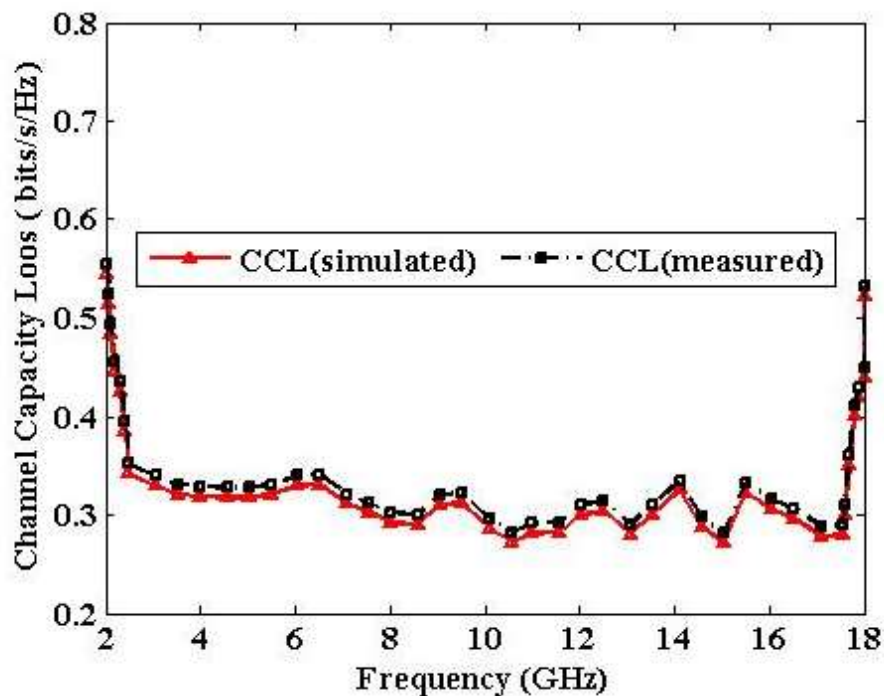


Figure 5.20 Measured and simulated CCL

### 5.7 Comparison of the Proposed Antenna with the Existing MIMO Antenna

The performance of this work is compared with that of the previously published work in Table 5.4. The proposed prototype design has a miniature size, a large frequency band, and

high isolation along with very low mutual coupling. By considering a single rectangular antenna approximately 88.5 % compactness is achieved. Furthermore, for better bandwidth and impedance matching, it is further modified step by step.

**TABLE 5.4** Performance comparison of the prototype proposed model with the existing work

Previous Work	Size (mm <sup>2</sup> )	No of port	Frequency Range (GHz)	Isolation (dB)	Maximum Gain (dB)	Efficiency (%)	ECC	Technique Used
[99]	30 × 40 = 1200	2	3.1-10.6	> 15	-----	70-77.5	< 0.10	L-shaped parasitic strip
[138]	30 × 50 = 1500	2	3-10.9	> 20	3.8	---	< 0.06	Defected ground structure
[87]	32 × 32 = 1024	2	3.1- 10.6	>20	4.2	60-80	< 0.02	Orthogonal orientation and narrow slot
[45]	35 × 40 = 1400	2	3.1-10.6	> 16	6.5	-----	< 0.01	Tree-like structure on Ground
[136]	27.2 × 46 = 1251	2	3.6-17.9	> 18	4	78-96.7	< 0.018	Electromagnetic band gap structure
[137]	60 × 60 = 3600	4	3-16.2	> 17.5	8.4	25-91.2	<0.30	Mushroom-like EBG structure
[142]	26 × 55 = 1430	2	3.1-12.3	> 20	4	-----	<0.10	Orthogonal orientation arrangement
[135]	48 × 34 = 1632	4	3.52- 10.08	> 23	2.91	70.01- 79.87	< 0.039	Neutralization line
<b>This Work</b>	<b>30×30 = 900</b>	<b>4</b>	<b>2.8-18</b>	<b>&gt; 18</b>	<b>3.6</b>	<b>50- 84</b>	<b>&lt; 0.02</b>	<b>L-shape stub and CSRR</b>

## 5.8 Summary

In this paper, a very compact  $30\text{ mm} \times 30\text{ mm}$  quad-port high isolation CSRR-loaded UWB MIMO antenna is presented. The compactness is achieved owing to closely spaced elements, and isolation is improved due to the CSRR structure. The impedance bandwidth was achieved in the range of 2.8-18 GHz with the maximum peak gain of 3.6 dB and radiation efficiency varied from 50-84%. The proposed antenna has a very low ECC value, TARC  $< -15\text{ dB}$ , MEG  $< -3\text{ dB}$  and CCL  $< 0.35\text{ bits/s/Hz}$ . Therefore, this proposed prototype antenna satisfies all the characteristics of the MIMO application and is quite suitable for various UWB portable devices, making it multi-dimensional. From the technical point of view, sometimes notch bands are invited to make necessary changes in the results. More elaborately, this band will assist to minimize the interference that is present in a narrow band system. Therefore, we have included a detailed design and its responses in the next chapter.

# Chapter-6

## High Isolation Miniature Antenna with Dual Band Notch Characteristics for UWB MIMO Applications

### 6.1 Introduction

The UWB technology has many advantages for wireless communication but it suffers from certain interference problems due to a few narrowband systems such as WLAN, WiMAX, and X-band satellite communication. It degrades the quality and the signal strength of the whole system. Furthermore, the MIMO system along with the UWB technology leads to enhance the reliability of the system, because it allows several users to access the device simultaneously. The MIMO system also reduces the multipath fading issue and increases the transmission capacity. Due to this, the channel capacity is enhanced. The MIMO antenna is designed in such a way that, the isolation should be less than  $-15$  dB. In most MIMO systems, antennas are typically positioned with a distance of half-wavelength pertaining to the lowest operating frequency to improve the isolation between them, resulting in an overall increment in the dimension. The design of the MIMO antenna generally fetches compactness in size and it enhances the isolation performance, which assists the antenna designer tremendously for further work. Including this, in many situations rejection of notch band characteristics has been developed, which reduces the interference level significantly [146-153]. In [152], A notch band at 5.5 GHz is obtained by etching a pair of L-shaped strips on the ground plane. The isolation is enhanced due to the positioning of antennas in an orthogonal fashion, along with the inclusion of a T-shaped decoupling structure. The mushroom-type electromagnetic structure (EBG) is used to reject the single and triple-band [153]-[131] and the isolation is enhanced by adjusting the length of the MMR stub on the top of the substrate. A CSRR structure is used to achieve dual-band notch characteristics. The author highlighted getting a dual-band notch due to C

– shaped and unsymmetrical H-shaped [124]. At the same time, improve the isolation due to inserting the stub in the particular corner of the antenna element. A thin stub is used on the ground plane which acts as an LC notch filter and rejects the WLAN [154]-[155], and the antenna elements are placed orthogonally to reduce the mutual coupling. A C-shaped slot is etched on the radiator to create band notch characteristics [156] and the vertical stub is introduced on the ground plane to reduce the mutual coupling between antenna elements. Furthermore, there are several other techniques for isolation improvement is also investigated by researcher like defected ground structure (DGS) [157],[96], parasitic element [26], neutralization line [25],[150] , metamaterial structure [158]-[159] and decoupling network [160]-[161].

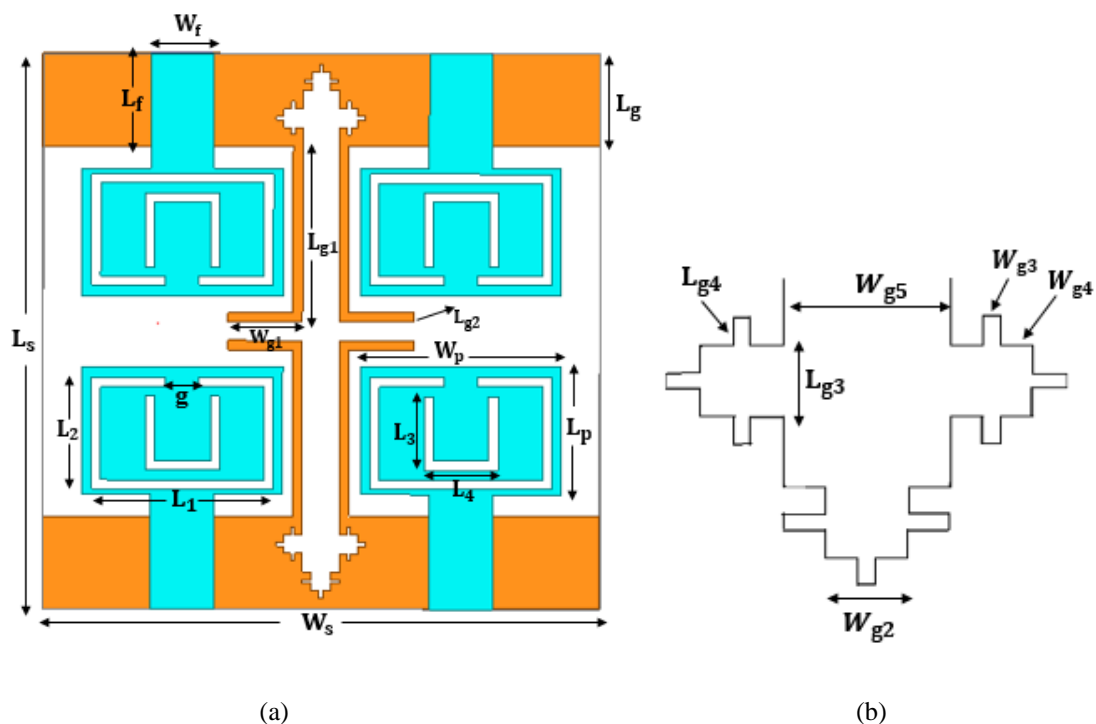


**Figure-6.1** (a) Structure of the proposed MIMO antenna (b) Modified minkowski fractal structure

In this chapter, designed and developed a high isolation miniature UWB MIMO antenna having quad ports. This designed antenna simultaneously reduces the interference that exists in the WLAN and X-band. The high isolation and miniaturization are achieved due

to the L-shape stub and modified fractal structure on the ground plane. This restricts the flow of current from one element to another. In the above statement, the kind of noise found in the WLAN and X- band system is very much reduced by involving U-shaped and C-shaped slots on the radiating element. As per our findings, this antenna is likely to work in the multipath environment without any obstruction, which brings the feasibility to the fading environment. The antenna layout is presented in Figure 6.1 and optimized parameters of the designed antenna are available in Table 6.1.

**TABLE-6.1:** Optimized design parameter of the proposed antenna with dimension

<b>Parameter</b>	$W_S$	$L_S$	$W_f$	$L_f$	$L_1$	$L_2$	$L_3$	$L_4$	$L_P$	$L_{g1}$	$L_{g2}$
<b>Unit (mm)</b>	30	30	3.4	6.2	9.8	6.4	4	4	6.9	10.5	0.5
<b>Parameter</b>	$L_{g3}$	$L_{g4}$	$W_P$	$W_{g1}$	$W_{g2}$	$W_{g3}$	$W_{g4}$	$W_{g5}$	$g$	$L_g$	
<b>Unit (mm)</b>	1	0.4	10.8	4	1	0.2	0.4	2	1.2	5	

## 6.2 Antenna Design and Analysis

This design consists of four identical radiating elements which are placed on the top layer of the substrate and modified the ground structure. The overall dimension of the proposed MIMO antenna is  $30 \times 30 \text{ mm}^2$  and it is fabricated on a 1.6 mm thick FR4 substrate whose  $\epsilon_r = 4.4$  and  $\tan\delta = 0.02$ . The feeding mechanism to each radiator is provided with a 50-ohm microstrip feed having a dimension of  $L_f \times W_f$ . The simulation and optimization of the antenna parameter are carried out on the Ansys HFSS 3-D electromagnetic simulator.

### 6.2.1 Evolution Steps of Single Antenna Element

The step-by-step procedure to get the dual-band notch characteristics UWB antenna is illustrated in Figure 6.2. In step1, the design starts with the rectangular patch radiator, excited by a 50-ohm microstrip feed line with a partial ground plane depicted in Figure 6.2 (a). The monopole antenna achieved an ultra-wideband, due to the partial ground and it resonates at 4.4 and 8.4 GHz within the UWB frequency range. Furthermore, a C-shaped

slot is etched on the radiator as shown in Figure 6.2 (b), to get a single notch band that suppresses the noise present in the WLAN band. The theoretical center frequency for the lower notch band can be calculated as:

$$f_{n1} = \frac{c}{(2L_1+2L_2-g)\sqrt{\frac{\epsilon_r+1}{2}}} \quad (6.1)$$

Where  $f_{n1}$  represents the lower notch band center frequency, C denotes the speed of light,  $\epsilon_r$  indicates the dielectric constant, g illustrates the gap,  $L_1$  and  $L_2$  represent design parameters. The calculated notch frequency is 5.7 GHz, which is very close to the simulated result of 5.5 GHz as shown in Figure 6.3. Later on, upper notch band characteristics are achieved due to the etching of a U-shaped slot on the radiator. Subsequently in Figure 6.2 (c), C-shaped and U-shaped slots combine to get a dual-band notch characteristic, which suppresses the noise that presents in the WLAN and X-band.

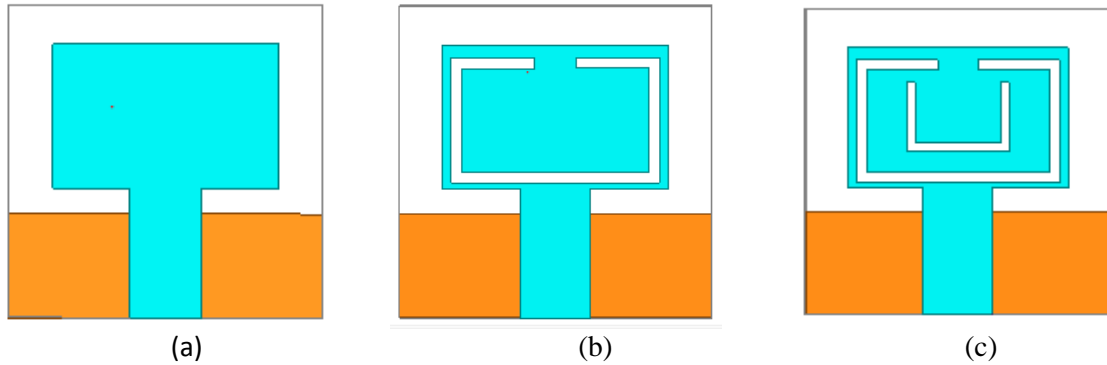
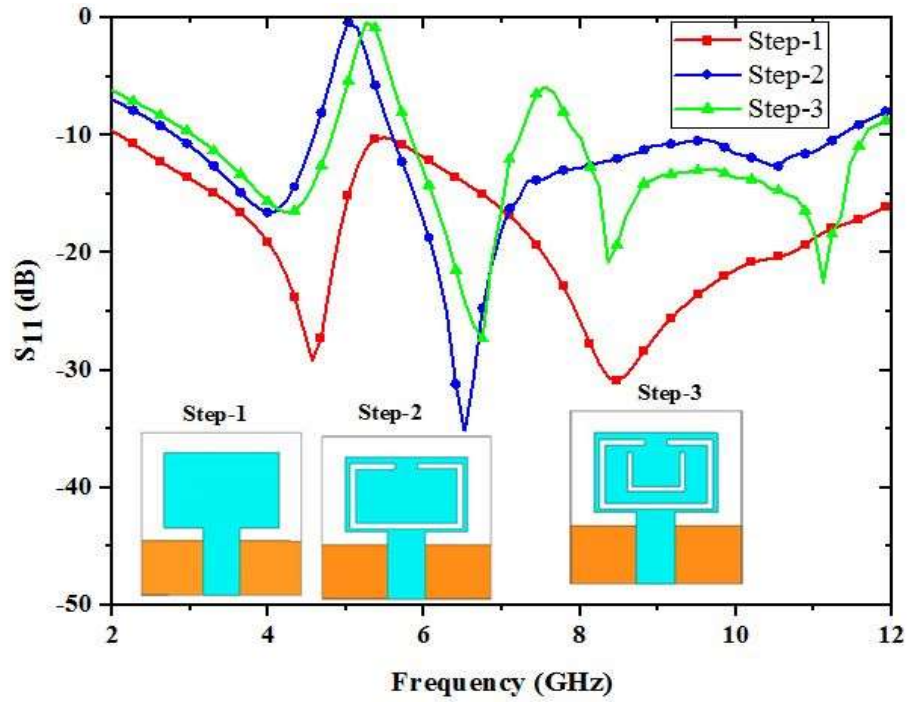


**Figure 6.2:** Evolution steps (a) Rectangular patch (b) With C-slot (c) With C-slot and U-slot

The theoretical center frequency for the upper notch band can be calculated as:

$$f_{n2} = \frac{c}{2(2L_3+L_4)\sqrt{\frac{\epsilon_r+1}{2}}} \quad (6.2)$$

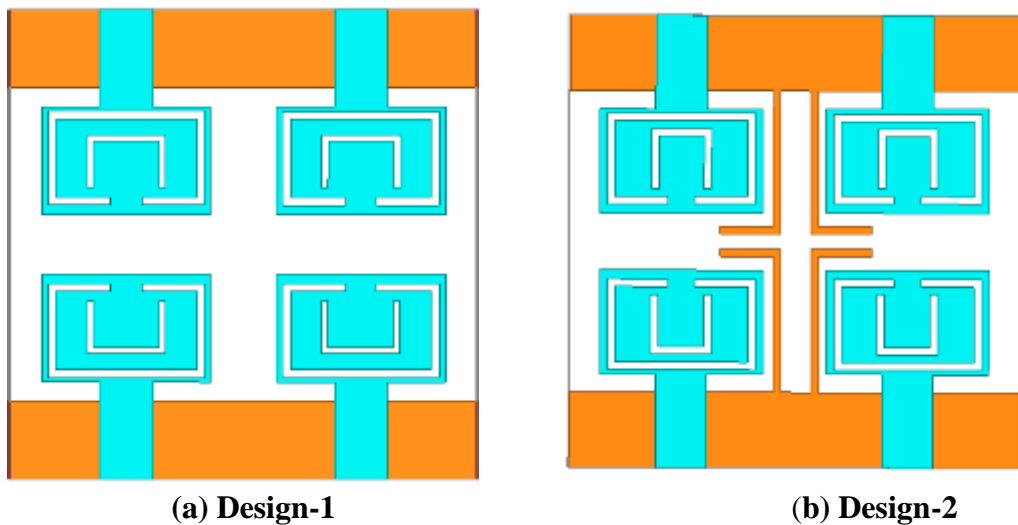


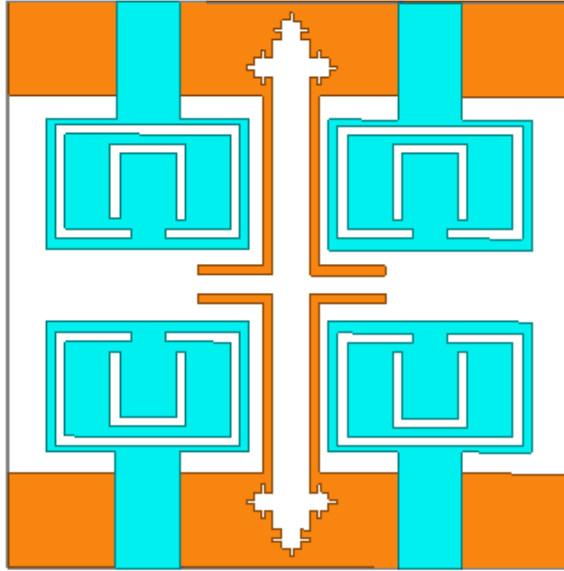


**Figure 6.3:** Reflection coefficient of single antenna element at various steps

Where  $L_3$  and  $L_4$  represent the design parameter. The calculated center frequency for the upper notch band is 7.62 GHz, which is very close to the simulated result of 7.5 GHz as illustrated in Figure 6.3.

### 6.2.2 Effect of Ground Plane on the UWB MIMO Antenna





(c) Design-3

**Figure 6.4:** (a) Only partial ground (b) partial ground with L – shaped stub (c) partial ground, L-shape stub along with modified minkowski fractal structure

The four identical radiators are placed on one side and a partial ground plane on the other side of the substrate layer as illustrated in Figure 6.4(a). The antenna is achieved wider impedance bandwidth due to the partial ground plane. But, the isolation between the antenna elements is very less ( $S_{12} < -14$  dB,  $S_{13} < -15$  dB,  $S_{14} < -12$  dB). Further, four L-shaped stubs are introduced on the ground plane between antenna elements, which improves the isolation ( $S_{12} < -20$  dB,  $S_{13} < -17$  dB,  $S_{14} < -18$  dB) as depicted in Figure 6.4 (b). The L-shaped stub restricts the flow of current from one element to another. Moreover, high isolation is achieved by etching a modified minkowski fractal structure along with an L-shaped stub on the ground plane between the radiating elements as illustrated in Figure 6.4(c). After introducing the modified minkowski structure, the isolation between the antenna elements  $S_{12} < -22$  dB,  $S_{13} < -22$  dB and  $S_{14} < -22$  dB are achieved in the entire frequency band as depicted in figure 6.5.

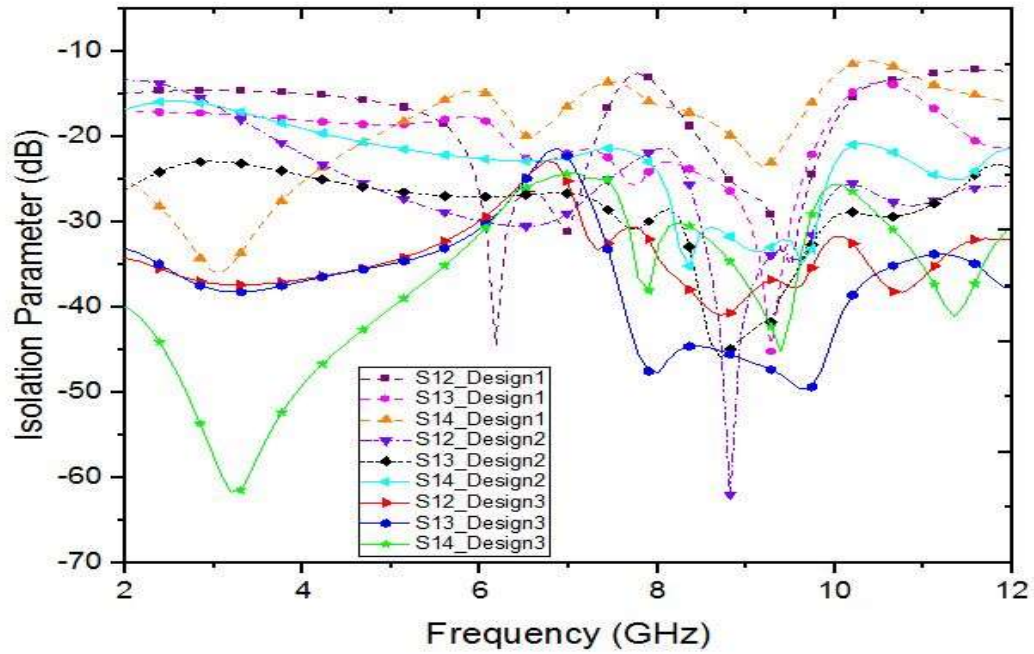


**Figure 6.5** Isolation parameter with different ground structure

### 6.3 Results and Discussion

The prototype antenna is designed and developed on the FR4 substrate, which is reflected in Figure 6.6. The various MIMO diversity parameters are measured using an Agilent N5247A vector network analyzer. The measurement setup with VNA and inside an anechoic chamber is depicted in Figure 6.7.

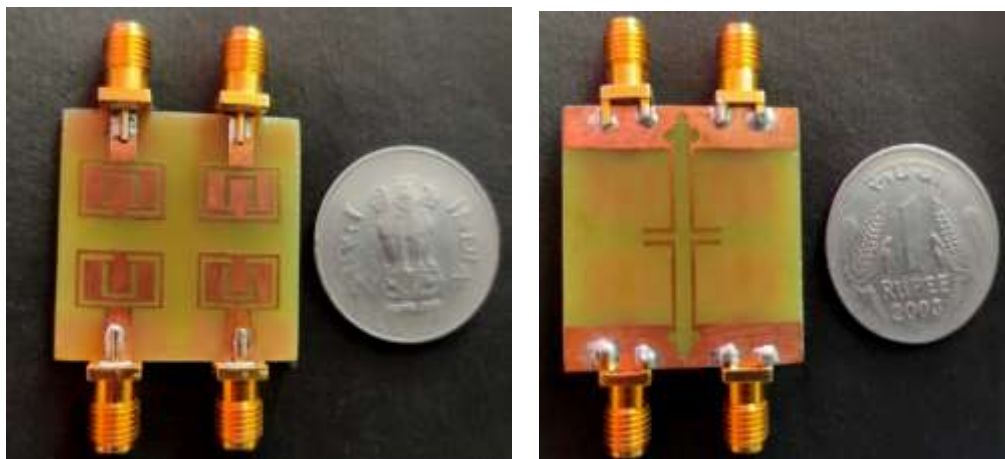


**Figure 6.6** Fabricated prototype (a) Top View (b) Bottom View



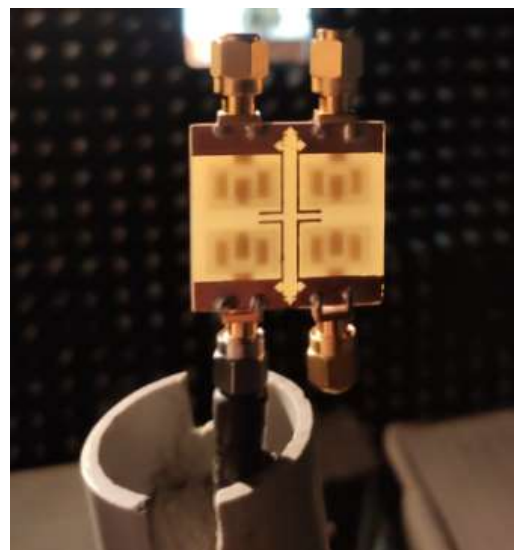
(a)



(b)



(c)



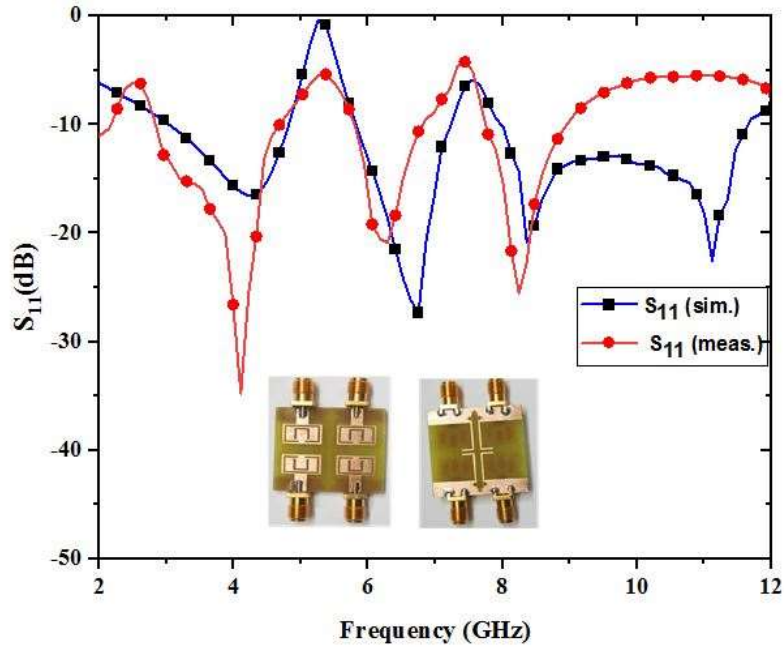
(d)

**Figure 6.7:** Measurement setup with VNA (a), (b) and inside an anechoic chamber (c) front view (d) back view

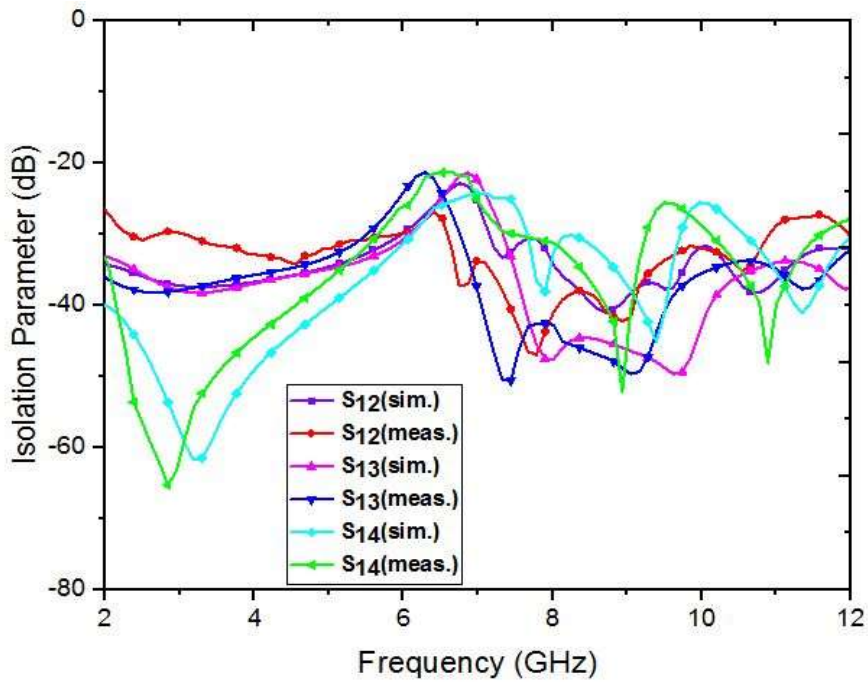
### 6.3.1 Return Loss and Isolation Parameter

It has been noticed that in Figure 6.8(a), the simulated and the measured reflection coefficient find identical results. It is less than  $-10$  dB in the entire operating band except

at the notch band. But, there is a minute deviation found, which is due to the presence of the SMA connector soldering and cabling effect.



(a)



(b)

**Figure 6.8** Simulated and measured (a) reflection coefficient and (b) isolation parameter

This is quite obvious for any design. While measuring the diversity parameters at port -1, other ports are terminated with 50-ohm load impedance. A similar process was repeated at ports 2, 3, and 4 respectively. From Figure 6.8 (b), the measured and the simulated isolation parameter at port 1 with respect to the other ports are below  $-22$  dB in the entire operating band.

### 6.3.2 Gain and Radiation Efficiency

The antenna gain is measured inside an anechoic chamber using a standard horn antenna. Figure 6.9 shows the measured and the simulated, gain and radiation efficiency for the prototype MIMO antenna. In this design, the gain is maintained from 2.2 to 6.2 dB except at the notch band, where its value drops to  $-3.6$  dB at the lower notch band and  $-3.8$  dB at the upper notch band respectively. This gain is fit enough for several short-range communication purposes such as a smartwatch, handheld wireless devices, etc.

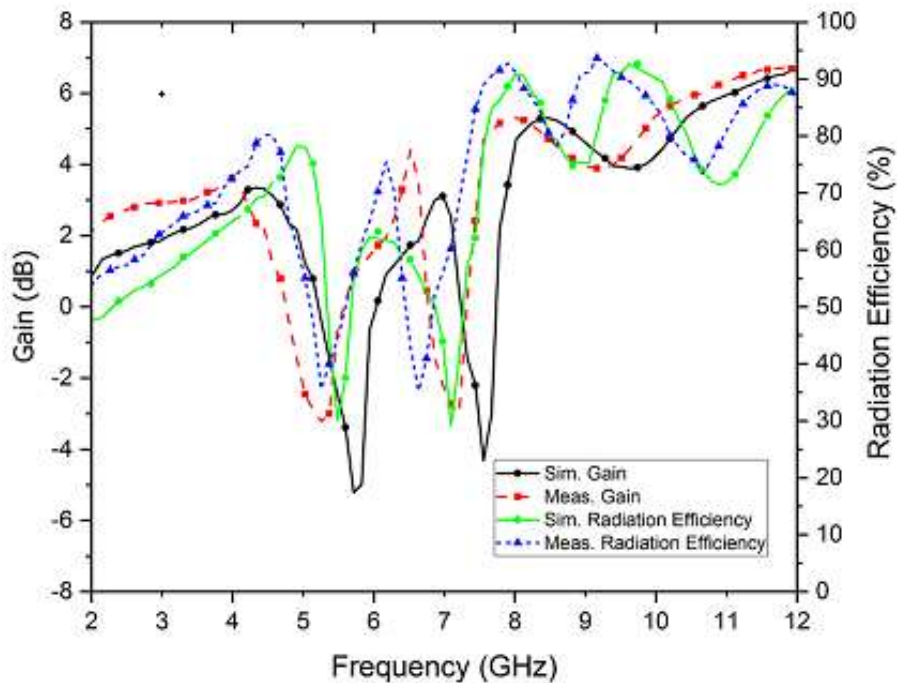


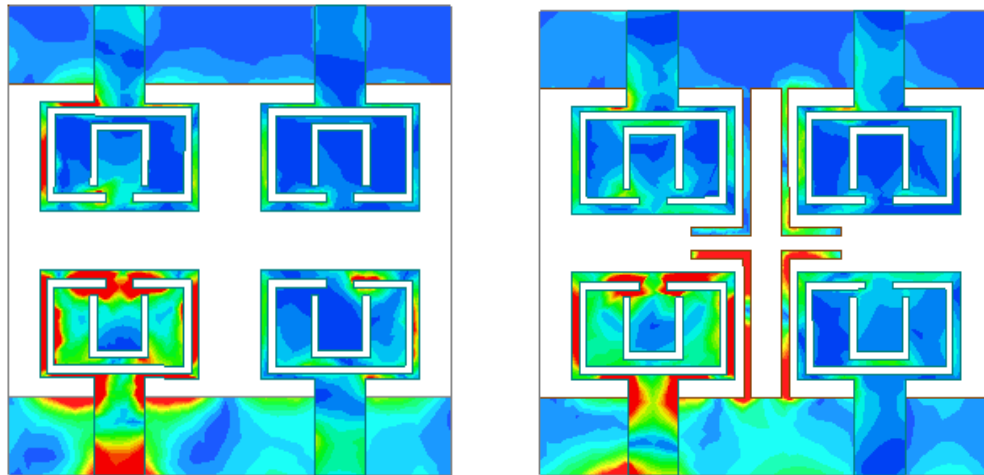
**Figure 6.9:** Gain and radiation efficiency of the proposed model

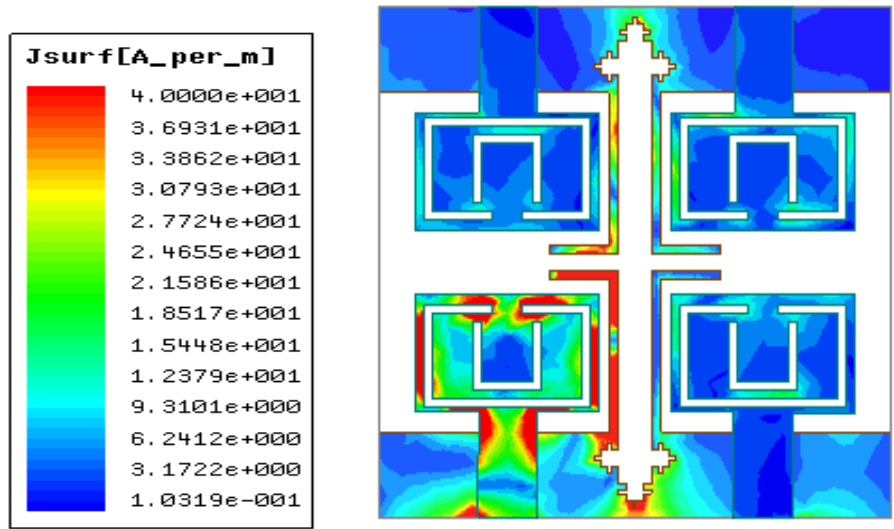


The radiation efficiency of the prototype model varies from 50 % to 92 % and is significantly reduced at notch frequency as depicted in Figure 6.9. The maximum measured radiation efficiency of 78 % at 4.2 GHz, 56 % at 6.4 GHz, and 84 % at 8.4 GHz are achieved. The radiation efficiency decreases at the notch band, this is due to the low dielectric loss tangent and frequency dependency of the dissipation factor of the substrate.

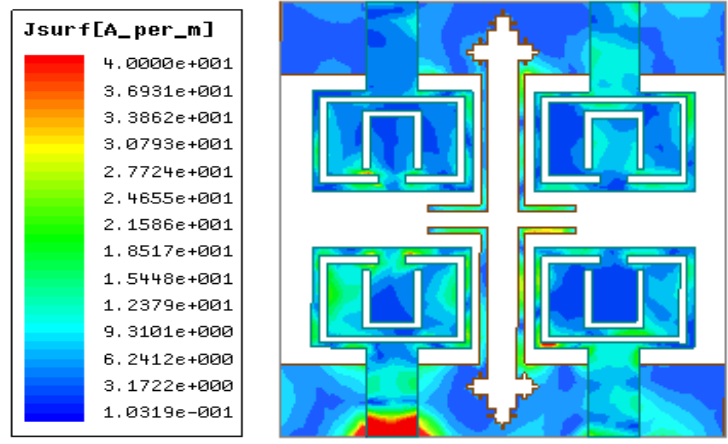
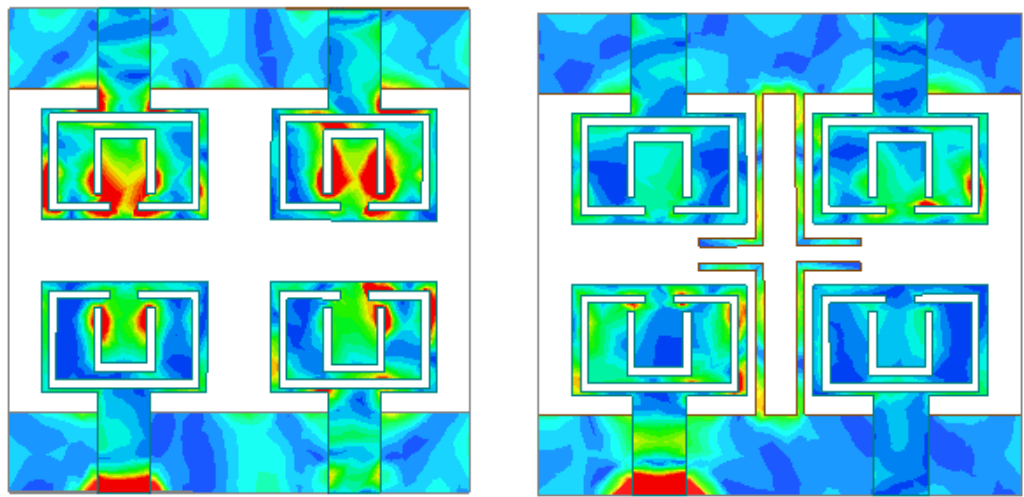
### 6.3.3 Surface Current Distribution

The simulated surface current distribution with the different ground planes at 4.2, 6.4, and 8.4 GHz are presented in Figure 6.10. The surface currents are strongly coupled to all the four antenna elements when a partial ground plane is used. The amount of surface current is reduced by introducing an L-shaped stub between antenna elements. Further, more surface current is reduced by etching a modified minkowski fractal structure on the center of the partial ground plane. This reduction in coupling current enhanced the isolation between antenna elements. As a consequence of the gain and radiation efficiency of the antenna which depends on the isolation, the parameter has improved.





(a)



(b)



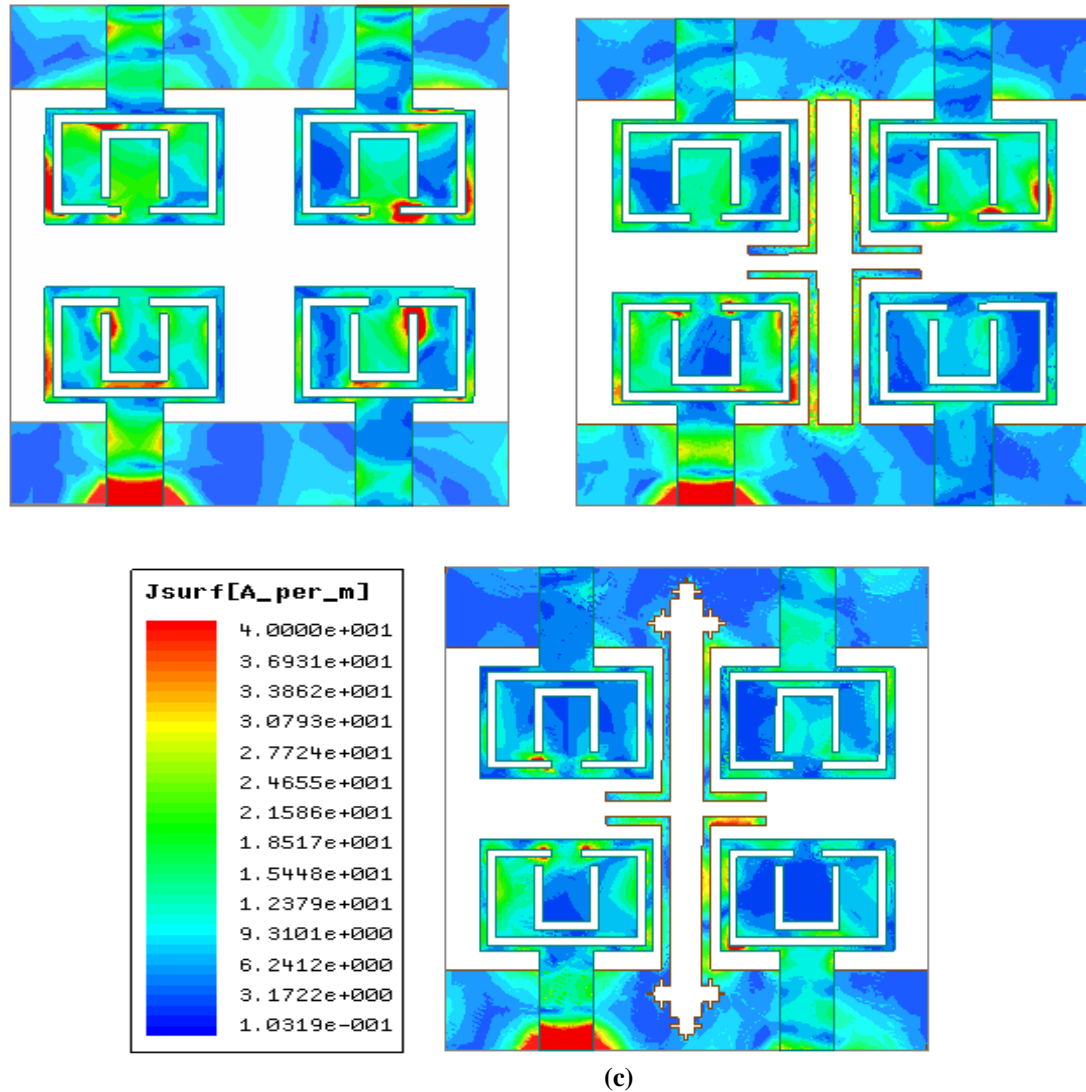
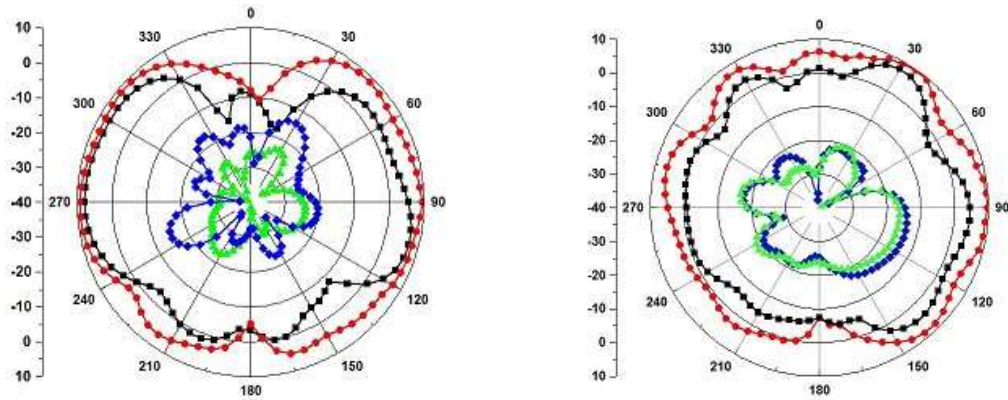


**Figure 6.10** Surface current distribution with various ground structures at (a) 4.2 GHz (b) 6.4 GHz (c) 8.4 GHz

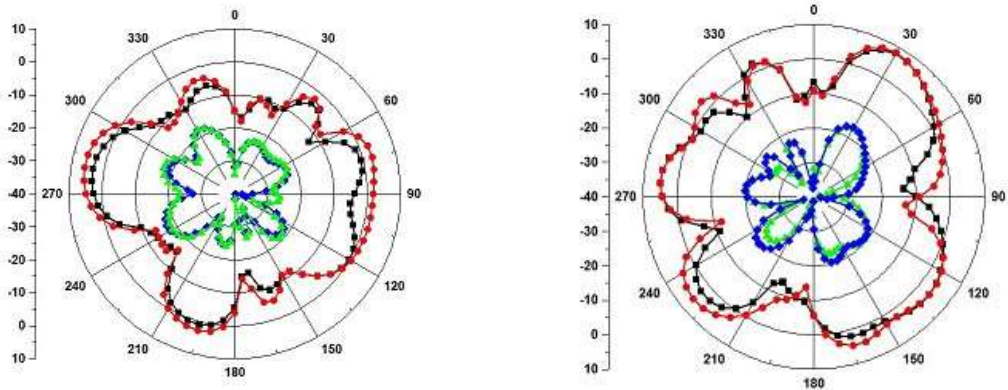
### 6.3.4 Radiation Characteristics

The two-dimensional co-pol and cross-pol radiation pattern in  $xz$ - plane (E-plane,  $\phi=0^\circ$ ) and  $yz$  - (H-plane,  $\phi=90^\circ$ ) at 4.2, 6.4, and 8.4 GHz are depicted in Figure 6.11. The cross-pol level in E-plane and H-plane are approximately less than  $-20$  dB for all the above-said frequencies. While measuring the radiation pattern one particular antenna is excited at a time keeping others terminated with a matched load of 50 ohms to avoid reflection. There is a good amount of agreement noticed between the simulated and measured ones. The

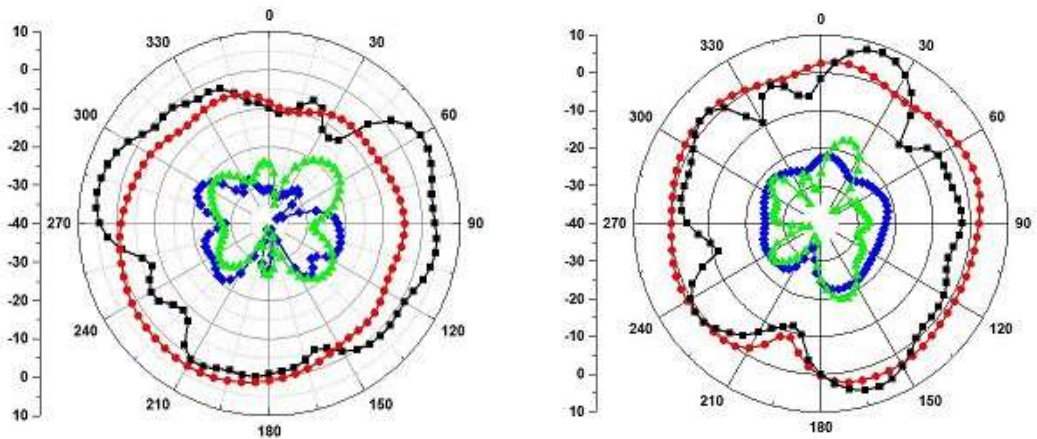
radiation pattern is quasi omnidirectional at a lower frequency and slight distortion occurs at a higher frequency due to the higher-order mode.



(a) E-Plane and H-Plane at 4.2 GHz



(b) E-Plane and 6.4 GHz H-Plane



(c) E-Plane and H-Plane at 8.4 GHz



**Figure 6.11** E-plane and H-plane radiation characteristic at (a) 4.2 (b) 6.4 and (C) 8.4 GHz

## 6.4 Diversity Performance

The ECC, DG, TARC, and CCL are the few important consequences, which are simply termed as diversity parameters. It decides the effective performance of the MIMO system. More elaborately, the practical accepted limit for above said parameters are  $ECC < 0.5$ ,  $DG > 9.5$  dB,  $TARC < -10$  dB and  $CCL < 0.4$  bits/s/Hz respectively.

### 6.4.1 ECC and DG

Though all the above parameter results are equally important, still ECC has got the highest priority in decision making as the MIMO system is a concern in general. Because it measures the amount of coupling between antenna elements, which should be as minimum as possible. In other words, the lesser the value better would be the performance of the MIMO system. The ECC can be computed either from the scattering parameter or using a far-field radiation pattern [162].

$$\rho_e(i, j) = \frac{|\iint_{4\pi}^0 [E_i(\theta, \phi, f) E_j(\theta, \phi, f)] d\Omega|^2}{\left[ \iint_{4\pi}^0 |E_i(\theta, \phi, f)|^2 d\Omega \right] \left[ \iint_{4\pi}^0 |E_j(\theta, \phi, f)|^2 d\Omega \right]} \quad (6.3)$$

Where  $E_i$  and  $E_j$  denote the magnitude of the electric radiated field of  $i^{th}$  and  $j^{th}$  antenna,  $\Omega$  represents the solid angle,  $\phi$  and  $\theta$  illustrate the azimuthal and the elevation angle for the spherical coordinate respectively. The ECC value at each port is lower than 0.02 throughout the frequency band except at the notch band illustrated in Figure 6.12, which confirms the prototype antenna has excellent diversity performance. The diversity gain at port 1 with respect to other ports is more than 9.9 dB as depicted in Figure 6.12. This diversity gain is very close to the ideal value of 10 dB in the entire operating band except at the notch band, where diversity gain is a very low value.

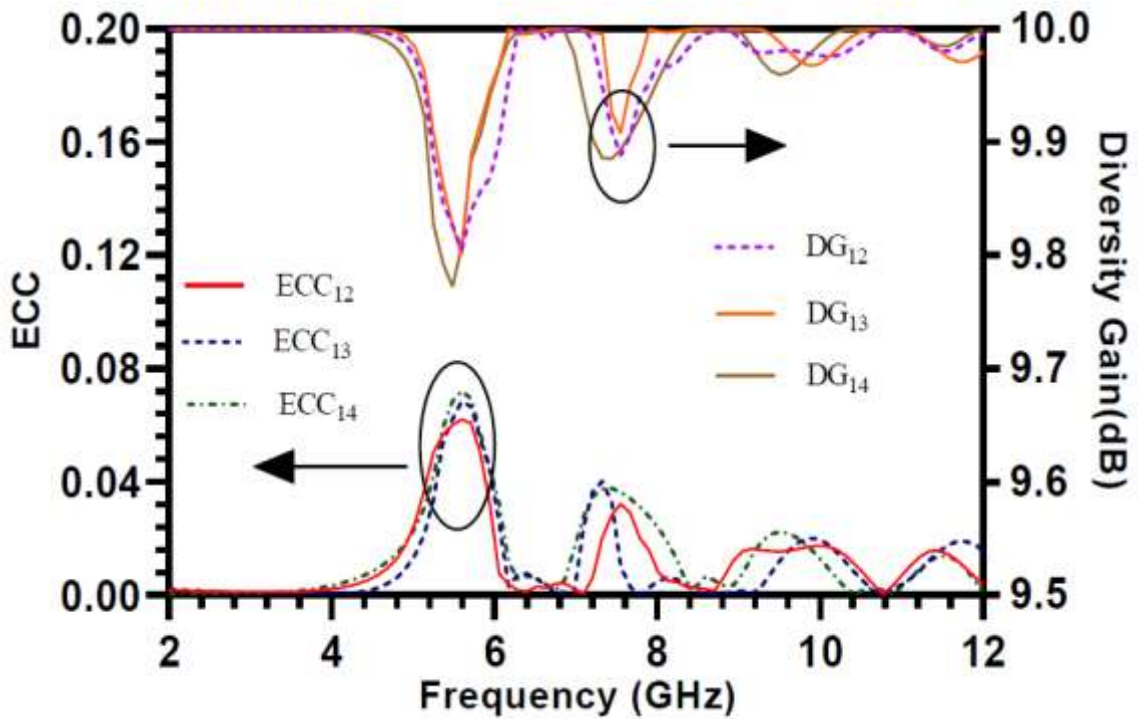
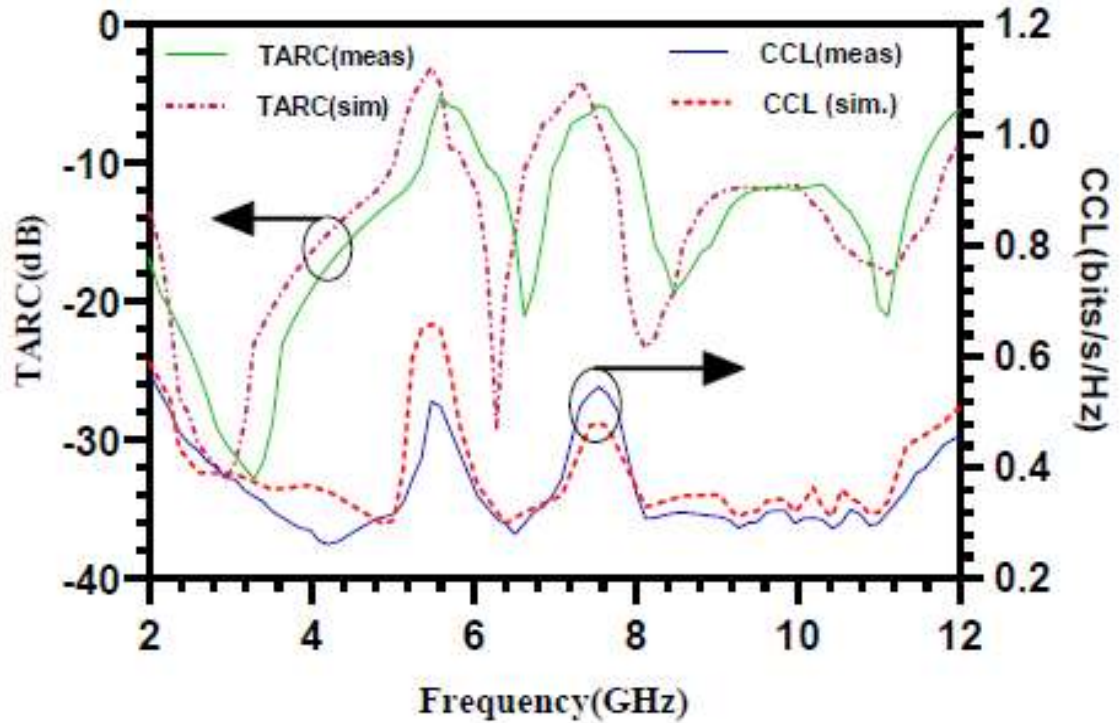


Figure 6.12 ECC and DG of the proposed design

#### 6.4.2 TARC and CCL

In the multiport system, the only reflection coefficient is not enough to evaluate the effective radiation performance and correct frequency bandwidth. Because of the self-impedance and the mutual impedance alter, due to random phase excitation and reflection from other ports. A new parameter TARC has been introduced to give the complete characteristics of the MIMO antenna. TARC for the four ports MIMO antenna system can be computed from equation 1.21. It can be seen that the value of TARC is less than  $-10$  dB in the entire operating band except at the notch band as shown in Figure 6.13.



**Figure 6.13:** TARC and CCL of the proposed design

The channel capacity loss is due to the uncorrelated fading in the MIMO system. The CCL can be calculated from equation 1.13. The measured and simulated CCL is depicted in Figure 6.13, which is lower than the practical acceptable value in the whole frequency band except at the notch band.

### **6.5 Comparison of the Proposed Model with the Previous Work**

To justify the differences with respect to other existing work, we made a comparative analysis which is available in Table 6.2. From the outcome of the comparison, it is easy to estimate the size, isolation, number of antenna elements, and number of notch bands along with gain. The most interesting part is the size is very much reduced and isolation improves significantly.

**TABLE 6.2:** Comparison of various existing UWB MIMO antennas with the prototype antenna

Ref	Antenna Size (mm <sup>2</sup> )	No of Antenna Element	Band width (GHz)	Notch Band (GHz)	Isolation (dB)	ECC	Gain (dB)	No. of Notch Bands
[95]	38.5 × 38.5	2	3.08-11.8	5.03-5.97	< -15	< 0.02	1.4-3.6	1
[153]	60 × 60	4	2.73-10.6	5.36-6.34	< -15	---	2-6	1
[131]	64 × 45	2	3-11	3.3-3.6 , 5-6 and 7.1-7.9	< -15	<0.02	--	3
[163]	35 × 68	2	3.1-10.6	3.35-3.55, 5.65-5.95	< -20	<0.002	1.7-4.2	3
[164]	50 × 50	4	3.1-10.4	3.1-4.2, 5.1-5.9	< -14	< 0.30	1-7	2
[165]	72 × 72	4	2.8-13.3	3.25-3.75, 5.3-5.7	< -18	< 0.06	2-6.7	2
[124]	45 × 45	4	2-16.8	4.8-5.9, 7-7.9	< -22	< 0.10	2-4	2
[154]	50 × 25	4	2-12	4.9-6.4	< -17	< 0.45	3.15	1
[155]	40 × 40	4	2.4-10.6	5-6	< -20	< 0.02	--	1
[156]	29 × 40	2	3.1-11	5.72-5.82	< -20	< 0.0005	2-4.9	1
<b>This Work</b>	<b>30 × 30</b>	<b>4</b>	<b>3.1-12</b>	<b>5-5.9 , 7.1-7.9</b>	<b>&lt; -22</b>	<b>&lt; 0.02</b>	<b>2.2-6.2</b>	<b>2</b>

## 6.6 Summary

This chapter exploits a quad-port high isolation miniature antenna. It identifies with the dual notch band characteristics which reject the structure to use for X-band downlink satellite communication and WLAN application with the frequency band of 5-5.9 GHz and 7.1-7.9 GHz. This is due to the inclusion of loading C-shaped and U-shaped slots on the

radiator. In addition to this, the design also included an L-shaped stub along with a modified Minkowski fractal structure to achieve high isolation which is an essential parameter in the MIMO system. The proposed antenna is fabricated and tested to measure the various MIMO diversity parameters. It has been observed that the prototype antenna has many advantages over other reported antennas in terms of size, low mutual coupling (less than 0.02), number of antenna elements, and high isolation (less than  $-22$  dB). Moreover, the MIMO diversity antenna is quite suitable to work in the UWB system. The Conclusion and future scopes are presented in the next chapter.

# **Chapter-7**

## **Conclusion and Future Scope**

### **7.1 Summary**

In this research work, systematically we have investigated the design and the analysis of the UWB MIMO diversity antenna. There are four different types of antenna structures that were designed and simulated through HFSS software. In this process, we obtained various parameters such as return loss, isolation parameter, gain, radiation efficiency, surface current distribution, ECC, DG, TARC, MEG, and CCL. Finally, the antenna is fabricated and the results are measured through VNA as well as inside an anechoic chamber. The obtained results are then compared with the simulated one to find the amount of resemblance. It is found that both the results are matched perfectly with slight deviation and this is due to the effect of cable, SMA connector soldering, and environmental effect. In this chapter, I am trying to put all the final outputs which briefly justify my work.

In chapter 1, a brief introduction to UWB and MIMO technology, MIMO performance parameter, various techniques for isolation improvement and antenna miniaturization techniques has been presented. Further, the detailed literature survey on the UWB monopole and the MIMO antenna for various applications has been extensively discussed in the next chapter.

In chapter three, Four-port multiple input multiple output antenna with the microstrip fed for the UWB applications is proposed. The antenna consists of four fork-shaped radiators, out of the four two are placed on the top and the rest are on the bottom part of the substrate. The isolation has been improved by placing the two antennas in an orthogonal position at the top and bottom, which provides dual polarization.

Four symmetrical radiating elements which are orthogonally placed on the top surface of the substrate with the partial slotted ground plane is presented in the next



chapter. The isolation among the antenna elements is improved by placing the antenna element orthogonally without any additional decoupling structure.

In chapter five, a four-port miniature MIMO antenna along with a complementary split-ring resonator (CSRR) structure embedded in the ground plane is presented. The isolation of the prototype antenna has been improved by taking 4 L-shape strips and two rectangular CSRR structures on the ground plane between antenna elements. A dual notch band characteristics UWB MIMO antenna is designed and developed, which is reflected in chapter six. The specialty of this design finds the compactness and high isolation, which is achieved by the etching of modified minkowski fractal structure and inverted L-shaped stubs on the ground plane.

Finally, the results that we have obtained can claim the efficacy towards the design of the 5 G system, short-distance communication, and many other power full applications on various wireless devices.

## **7.2 Future Scope**

It is customary to say that, for any technology, there will a saturation point due to the demand or maybe the evolution of some other technology that is more efficient than the existing one. Keeping view of that, we can suggest some of the clues which may be implemented in this existing work to fulfill future demand. The following could be the possible solution which is listed below.

- Design and development of UWB MIMO antenna for high channel capacity. So a new technique massive MIMO can be implemented.
- Design and development of miniature antenna. It could be achieved by adding metamaterial, metasurface, or a combination of both or by adopting any other suitable method.
- The performance of the designed antenna can be evaluated after being embedded into a device such as a mobile, laptop, or other wireless portable devices.
- One can further extend this work to estimate the radiation effect on environment.

# List of Publications

## Journal

- [1] Pankaj Kumar Keshri, Sanjay Sahu and Richa Chandel, “CSRR Loaded Compact Quad Port MIMO Diversity Antenna for UWB Applications” IETE Journal of Research, Nov 2021. (Taylor and Francis)- SCI
- [2] Pankaj Kumar keshri, Richa Chandel, Sanjay Sahu, AK Gautam “Compact Quad Port High-Performance UWB MIMO Diversity Antenna with Slotted Ground Structure” Progress In Electromagnetics Research C, Vol. 112, 193–205, 2021.- Scopus
- [3] Pankaj Kumar Keshri, Sanjay Sahu and Richa Chandel, “High Isolation Miniature Antenna With Dual Band Notch Characteristics for UWB MIMO Applications” International Journal of electronics- Taylor and Francis (SCI)

## International Conference

- [1] Pankaj Kumar Keshri, Richa Chandel “Wideband MIMO Antenna with Improved Isolation” 3rd International Conference on Intelligent Circuits and Systems, June-2020.
- [2] Pankaj Kumar Keshri, Sanjay Sahu and Richa Chandel “Compact Multiple Input Multiple Output Antenna with High Isolation for UWB Applications” International Conference on VLSI and microwave and wireless technology” March 2021

## Bibliography

- [1] C. A. Balanis, *Antenna Theory: Analysis and Design*. 2012.
- [2] F. C. Commission, “First report and order in the matter of revision of part 15 of the commission’s rules regarding ultrawideband transmission systems,” *Washington, DC, USA*, no. 190211614895, 2002.
- [3] J. G. Proakis, “Digital communications,” 2001.
- [4] J. Sharony, “Introduction to Wireless MIMO–Theory and Applications,” *Center Excell. Wirel.*, p. 1 to 63, 2006, [Online]. Available: [http://www.applications.www.mobiusconsulting.com/papers/IEEE-Wireless MIMO-Sharony.pdf](http://www.applications.www.mobiusconsulting.com/papers/IEEE-Wireless-MIMO-Sharony.pdf).
- [5] L. Thomas, G. Erik, H. Yang, and H. Q. Ngo, *Fundamentals of Massive MIMO*. .
- [6] Engel, “Wireless Communication,” *Pap. Knowl. . Towar. a Media Hist. Doc.*, 2014.
- [7] N. and Costa and S. Haykin, *MULTIPLE-INPUT, MULTIPLE-OUTPUT CHANNEL MODELS Theory and Practice*. .
- [8] J. Thaysen and K. B. Jakobsen, “ENVELOPE CORRELATION IN (N, N) MIMO ANTENNA ARRAY FROM SCATTERING PARAMETERS,” *Microw. Opt. Technol. Lett.*, vol. 48, no. 5, pp. 832–834, 2006, doi: 10.1002/mop.
- [9] R. Mathur and S. Dwari, “A compact UWB-MIMO with dual grounded CRR for isolation improvement,” *Int. J. RF Microw. Comput. Eng.*, vol. 29, no. 1, pp. 1–9, 2019, doi: 10.1002/mmce.21500.
- [10] M. Sharma, V. Dhasarathan, S. K. Patel, and T. K. Nguyen, “An ultra-compact four-port  $4 \times 4$  superwideband MIMO antenna including mitigation of dual notched bands characteristics designed for wireless network applications,” *AEU - Int. J. Electron. Commun.*, vol. 123, p. 153332, 2020, doi: 10.1016/j.aeue.2020.153332.

- [11] I. Nadeem and D. Y. Choi, "Study on Mutual Coupling Reduction Technique for MIMO Antennas," *IEEE Access*, vol. 7, pp. 563–586, 2019, doi: 10.1109/ACCESS.2018.2885558.
- [12] R. Chandel, A. K. Gautam, and K. Rambabu, "Tapered Fed Compact UWB MIMO-Diversity Antenna with Dual Band-Notched Characteristics," *IEEE Trans. Antennas Propag.*, vol. 66, no. 4, pp. 1677–1684, 2018, doi: 10.1109/TAP.2018.2803134.
- [13] A. Alayón Glazunov, A. F. Molisch, and F. Tufvesson, "Mean effective gain of antennas in a wireless channel," *IET Microwaves, Antennas Propag.*, vol. 3, no. 2, pp. 214–227, 2009, doi: 10.1049/iet-map:20080041.
- [14] T. TAGA, "Analysis for Mean Effective Gain of Mobile Antennas in Land Mobile Radio Environments," *IEEE Trans. Veh. Technol.*, vol. 39, no. 2, 1990.
- [15] E. Thakur, N. Jaglan, and S. D. Gupta, "Design of compact uwb mimo antenna with enhanced bandwidth," *Prog. Electromagn. Res. C*, vol. 97, no. November, pp. 83–94, 2019, doi: 10.2528/pierc19083004.
- [16] H. Shin and J. H. Lee, "Capacity of multiple-antenna fading channels: Spatial fading correlation, double scattering, and keyhole," *IEEE Trans. Inf. Theory*, vol. 49, no. 10, pp. 2636–2647, 2003, doi: 10.1109/TIT.2003.817439.
- [17] M. Manteghi and Y. Rahmat-Samii, "Multiport characteristics of a wide-band cavity backed annular patch antenna for multipolarization operations," *IEEE Trans. Antennas Propag.*, vol. 53, no. 1 II, pp. 466–474, 2005, doi: 10.1109/TAP.2004.838794.
- [18] S. H. Chae, S. K. Oh, and S. O. Park, "Analysis of mutual coupling, correlations, and TARC in WiBro MIMO array antenna," *IEEE Antennas Wirel. Propag. Lett.*, vol. 6, no. 6, pp. 122–125, 2007, doi: 10.1109/LAWP.2007.893109.
- [19] J. Y. Lee, S. H. Kim, and J. H. Jang, "Reduction of Mutual Coupling in Planar Multiple Antenna by Using 1-D EBG and SRR Structures," *IEEE Trans. Antennas*

- Propag.*, vol. 63, no. 9, pp. 4194–4198, 2015, doi: 10.1109/TAP.2015.2447052.
- [20] M. S. Alam, N. Misran, B. Yatim, and M. T. Islam, “Development of electromagnetic band gap structures in the perspective of microstrip antenna design,” *Int. J. Antennas Propag.*, vol. 2013, 2013, doi: 10.1155/2013/507158.
- [21] A. Veeramani, A. S. Arezomand, J. Vijayakrishnan, and F. B. Zarrabi, “Compact S-shaped EBG structures for reduction of mutual coupling,” *Int. Conf. Adv. Comput. Commun. Technol. ACCT*, vol. 2015-April, pp. 21–25, 2015, doi: 10.1109/ACCT.2015.112.
- [22] L. Yang, M. Fan, F. Chen, J. She, and Z. Feng, “A novel compact electromagnetic-bandgap (EBG) structure and its applications for microwave circuits,” *IEEE Trans. Microw. Theory Tech.*, vol. 53, no. 1, pp. 183–189, 2005, doi: 10.1109/TMTT.2004.839322.
- [23] M. S. Alam, M. T. Islam, and N. Misran, “A novel compact split ring slotted electromagnetic bandgap structure for microstrip patch antenna performance enhancement,” *Prog. Electromagn. Res.*, vol. 130, no. August, pp. 389–409, 2012, doi: 10.2528/PIER12060702.
- [24] S. W. Su, C. T. Lee, and F. S. Chang, “Printed MIMO-antenna system using neutralization-line technique for wireless USB-dongle applications,” *IEEE Trans. Antennas Propag.*, vol. 60, no. 2 PART 1, pp. 456–463, 2012, doi: 10.1109/TAP.2011.2173450.
- [25] S. Zhang and G. F. Pedersen, “Mutual Coupling Reduction for UWB MIMO Antennas with a Wideband Neutralization Line,” *IEEE Antennas Wirel. Propag. Lett.*, vol. 15, no. c, pp. 166–169, 2016, doi: 10.1109/LAWP.2015.2435992.
- [26] Z. Li, Z. Du, M. Takahashi, K. Saito, and K. Ito, “Reducing mutual coupling of MIMO antennas with parasitic elements for mobile terminals,” *IEEE Trans. Antennas Propag.*, vol. 60, no. 2 PART 1, pp. 473–481, 2012, doi:

10.1109/TAP.2011.2173432.

- [27] H. Makimura, Y. Watanabe, K. Watanabe, and H. Igarashi, "Evolutional design of small antennas for passive UHF-band RFID," *IEEE Trans. Magn.*, vol. 47, no. 5, pp. 1510–1513, 2011, doi: 10.1109/TMAG.2010.2089607.
- [28] M. Fallahpour and R. Zoughi, "Antenna Miniaturization Techniques," no. February, 2018.
- [29] A. A. Rakholiya and N. V Langhnoja, "A review on miniaturization techniques for microstrip patch antenna," no. 2, pp. 4281–4287, 2017.
- [30] A. M. Abbosh and M. E. Bialkowski, "Design of ultrawideband planar monopole antennas of circular and elliptical shape," *IEEE Trans. Antennas Propag.*, vol. 56, no. 1, pp. 17–23, 2008, doi: 10.1109/TAP.2007.912946.
- [31] Q. Wu, R. Jin, J. Geng, and M. Ding, "Printed Omni-Directional UWB Monopole Antenna," vol. 56, no. 3, pp. 896–899, 2008.
- [32] S. Cheng, P. Hallbjörner, and A. Rydberg, "Printed slot planar inverted cone antenna for ultrawideband applications," *IEEE Antennas Wirel. Propag. Lett.*, vol. 7, pp. 18–21, 2008, doi: 10.1109/LAWP.2007.914115.
- [33] I. Kim, C. won Jung, Y. Kim, and Y. eil Kim, "Low Profile Wideband MIMO Antenna with Suppressing Mutual Coupling between Two Antennas," *Microw. Opt. Technol. Lett.*, vol. 50, no. 5, pp. 1336–1339, 2008, doi: 10.1002/mop.
- [34] H. T. Chattha, F. Latif, F. A. Tahir, M. U. Khan, and X. Yang, "Small-Sized UWB MIMO Antenna with Band Rejection Capability," *IEEE Access*, vol. 7, pp. 121816–121824, 2019, doi: 10.1109/ACCESS.2019.2937322.
- [35] A. Dastranj, A. Imani, and M. Naser-Moghaddasi, "Printed wide-slot antenna for wideband applications," *IEEE Trans. Antennas Propag.*, vol. 56, no. 10, pp. 3097–3102, 2008, doi: 10.1109/TAP.2008.929459.

- [36] O. Ahmed and A. R. Sebak, "A printed monopole antenna with two steps and a circular slot for UWB applications," *IEEE Antennas Wirel. Propag. Lett.*, vol. 7, pp. 411–413, 2008, doi: 10.1109/LAWP.2008.2001026.
- [37] J. Y. Sze and C. C. Chang, "Circularly polarized square slot antenna with a pair of inverted-L grounded strips," *IEEE Antennas Wirel. Propag. Lett.*, vol. 7, pp. 149–151, 2008, doi: 10.1109/LAWP.2008.921341.
- [38] G. M. Yang, R. H. Jin, G. B. Xiao, C. Vittoria, V. G. Harris, and N. X. Sun, "Ultrawideband (UWB) antennas with multiresonant split-ring loops," *IEEE Trans. Antennas Propag.*, vol. 57, no. 1, pp. 256–260, 2009, doi: 10.1109/TAP.2008.2009744.
- [39] S. K. Rajgopal and S. K. Sharma, "Investigations on ultrawideband pentagon shape microstrip slot antenna for wireless communications," *IEEE Trans. Antennas Propag.*, vol. 57, no. 5, pp. 1353–1359, 2009, doi: 10.1109/TAP.2009.2016694.
- [40] W. P. Lin and C. H. Huang, "Coplanar waveguide-fed rectangular antenna with an inverted-L stub for ultrawideband communications," *IEEE Antennas Wirel. Propag. Lett.*, vol. 8, pp. 228–231, 2009, doi: 10.1109/LAWP.2009.2014573.
- [41] L. Guo, S. Wang, X. Chen, and C. Parini, "A small printed quasi-self-complementary antenna for ultrawideband systems," *IEEE Antennas Wirel. Propag. Lett.*, vol. 8, pp. 554–557, 2009, doi: 10.1109/LAWP.2009.2018711.
- [42] T. S. P. See and Z. N. Chen, "An ultrawideband diversity antenna," *IEEE Trans. Antennas Propag.*, vol. 57, no. 6, pp. 1597–1605, 2009, doi: 10.1109/TAP.2009.2019908.
- [43] A. M. Abbosh, "Miniaturized microstrip-fed tapered-slot antenna with ultrawideband performance," *IEEE Antennas Wirel. Propag. Lett.*, vol. 8, pp. 690–692, 2009, doi: 10.1109/LAWP.2009.2025613.
- [44] W. K. Toh, Z. N. Chen, X. Qing, and T. S. P. See, "A planar UWB diversity

- antenna,” *IEEE Trans. Antennas Propag.*, vol. 57, no. 11, pp. 3467–3473, 2009, doi: 10.1109/TAP.2009.2024131.
- [45] S. Zhang, Z. Ying, J. Xiong, and S. He, “Ultrawideband MIMO/diversity antennas with a tree-like structure to enhance wideband isolation,” *IEEE Antennas Wirel. Propag. Lett.*, vol. 8, pp. 1279–1282, 2009, doi: 10.1109/LAWP.2009.2037027.
- [46] H. W. Liu and C. F. Yang, “Miniature hook-shaped monopole antenna for UWB applications,” *Electron. Lett.*, vol. 46, no. 4, pp. 265–266, 2010, doi: 10.1049/el.2010.3080.
- [47] and C.-H. L. Chow-Yen-Desmond Sim, Wen-Tsan Chung, “Compact MIMO Slot Antenna for UWB Applications,” *IEEE Antennas Wirel. Propag. Lett.*, vol. 9, pp. 63–66, 2010, doi: 10.1109/LAWP.2010.2491968.
- [48] M. Sonkki and E. Salonen, “Low mutual coupling between monopole antennas by using two  $\lambda/2$  slots,” *IEEE Antennas Wirel. Propag. Lett.*, vol. 9, pp. 138–141, 2010, doi: 10.1109/LAWP.2010.2044476.
- [49] R. Zaker and A. Abdipour, “A very compact ultrawideband printed omnidirectional monopole antenna,” *IEEE Antennas Wirel. Propag. Lett.*, vol. 9, pp. 471–473, 2010, doi: 10.1109/LAWP.2010.2050852.
- [50] M. Koohestani and M. Golpour, “U-shaped microstrip patch antenna with novel parasitic tuning stubs for ultra wideband applications,” *IET Microwaves, Antennas Propag.*, vol. 4, no. 7, pp. 938–946, 2010, doi: 10.1049/iet-map.2009.0049.
- [51] R. A. Sadeghzadeh-Sheikhan, M. Naser-Moghadasi, E. Ebadifallah, H. Rousta, M. Katouli, and B. S. Virdee, “Planar monopole antenna employing back-plane ladder-shaped resonant structure for ultra-wideband performance,” *IET Microwaves, Antennas Propag.*, vol. 4, no. 9, pp. 1327–1335, 2010, doi: 10.1049/iet-map.2009.0067.
- [52] S. Baek and S. Lim, “Compact planar MIMO antenna array with polarisation



- diversity on single layer,” *Electron. Lett.*, vol. 46, no. 13, pp. 880–882, 2010, doi: 10.1049/el.2010.0626.
- [53] R. Azim, M. T. Islam, and N. Misran, “Ground modified double-sided printed compact UWB antenna,” *Electron. Lett.*, vol. 47, no. 1, pp. 9–11, 2011, doi: 10.1049/el.2010.3160.
- [54] A. Najam, Y. Duroc, and S. Tedjni, “UWB-MIMO antenna with novel stub structure,” *Prog. Electromagn. Res. C*, vol. 19, no. December 2010, pp. 245–257, 2011, doi: 10.2528/PIERC10121101.
- [55] S. Ghosh, “Design of planar crossed monopole antenna for ultrawideband communication,” *IEEE Antennas Wirel. Propag. Lett.*, vol. 10, no. 11, pp. 548–551, 2011, doi: 10.1109/LAWP.2011.2157888.
- [56] M. Koohestani, M. N. Moghadasi, and B. S. Virdee, “Miniature microstrip-fed ultrawideband printed monopole antenna with a partial ground plane structure,” *IET Microwaves, Antennas Propag.*, vol. 5, no. 14, pp. 1683–1689, 2011, doi: 10.1049/iet-map.2010.0450.
- [57] M. R. Ghaderi and F. Mohajeri, “A compact hexagonal wide-slot antenna with microstrip-fed monopole for UWB application,” *IEEE Antennas Wirel. Propag. Lett.*, vol. 10, pp. 682–685, 2011, doi: 10.1109/LAWP.2011.2158629.
- [58] S. K. Mishra, R. K. Gupta, A. Vaidya, and J. Mukherjee, “A compact dual-band fork-shaped monopole antenna for bluetooth and UWB applications,” *IEEE Antennas Wirel. Propag. Lett.*, vol. 10, no. 1, pp. 627–630, 2011, doi: 10.1109/LAWP.2011.2159572.
- [59] K. R. Chen, C. Y. D. Sim, and J. S. Row, “A compact monopole antenna for super wideband applications,” *IEEE Antennas Wirel. Propag. Lett.*, vol. 10, pp. 488–491, 2011, doi: 10.1109/LAWP.2011.2157071.
- [60] M. Sonkki, E. Antonino-Daviu, M. Ferrando-Bataller, and E. T. Salonen, “Planar

- wideband polarization diversity antenna for mobile terminals,” *IEEE Antennas Wirel. Propag. Lett.*, vol. 10, no. c, pp. 939–942, 2011, doi: 10.1109/LAWP.2011.2167589.
- [61] J. Li, Q. Chu, and T. Huang, “A Compact Wideband MIMO Antenna With Two Novel Bent Slits,” *IEEE Trans. Antennas Propag.*, vol. 60, no. 2, pp. 482–489, 2012.
- [62] C. L. Tsai and C. L. Yang, “Novel compact eye-shaped UWB antennas,” *IEEE Antennas Wirel. Propag. Lett.*, vol. 11, pp. 184–187, 2012, doi: 10.1109/LAWP.2012.2186276.
- [63] M. Gallo, E. Antonino-daviu, M. Ferrando-bataller, M. Bozzetti, and J. M. Molinagarcia-pardo, “A Broadband Pattern Diversity Annular Slot Antenna,” *IEEE Trans. Antennas Propag.*, vol. 60, no. 3, pp. 1596–1600, 2012.
- [64] R. Kumar, D. Magar, and K. Kailas Sawant, “On the design of inscribed triangle circular fractal antenna for UWB applications,” *AEU - Int. J. Electron. Commun.*, vol. 66, no. 1, pp. 68–75, 2012, doi: 10.1016/j.aeue.2011.05.003.
- [65] C. M. Wu, Y. L. Chen, and W. C. Liu, “A compact ultrawideband slotted patch antenna for wireless USB dongle application,” *IEEE Antennas Wirel. Propag. Lett.*, vol. 11, pp. 596–599, 2012, doi: 10.1109/LAWP.2012.2202366.
- [66] Z. J. Tang, J. Zhan, and H. L. Liu, “Compact CPW-fed antenna with two asymmetric U-shaped strips for UWB communications,” *Electron. Lett.*, vol. 48, no. 14, pp. 810–812, 2012, doi: 10.1049/el.2012.0445.
- [67] J. H. Lu and C. H. Yeh, “Planar broadband arc-shaped monopole antenna for UWB system,” *IEEE Trans. Antennas Propag.*, vol. 60, no. 7, pp. 3091–3095, 2012, doi: 10.1109/TAP.2012.2196954.
- [68] F. Fereidoony, S. Chamaani, and S. A. Mirtaheeri, “Systematic design of UWB monopole antennas with stable omnidirectional radiation pattern,” *IEEE Antennas Wirel. Propag. Lett.*, vol. 11, pp. 752–755, 2012, doi:

10.1109/LAWP.2012.2205658.

- [69] C. Lin, "Compact Bow-Tie Quasi-Self-Complementary Antenna for UWB Applications," *IEEE Antennas Wirel. Propag. Lett.*, vol. 11, pp. 987–989, 2012.
- [70] Y. Li, W. X. Li, C. Liu, and T. Jiang, "Two UWB-MIMO antennas with high isolation using sleeve coupled stepped impedance resonators," *IEEE Asia-Pacific Conf. Antennas Propagation, APCAP 2012 - Proc.*, pp. 21–22, 2012, doi: 10.1109/APCAP.2012.6333128.
- [71] S. Wang, Q. Wu, and D. Su, "A novel reversed t-match antenna with compact size and low profile for ultrawideband applications," *IEEE Trans. Antennas Propag.*, vol. 60, no. 10, pp. 4933–4937, 2012, doi: 10.1109/TAP.2012.2207360.
- [72] W. L. Lei Chang, Cheng Liao, Ling-lu Chen and and X. Zheng, "Design of a printed compact antenna with enhanced impedance bandwidth," *Microw. Opt. Technol. Lett.*, vol. 55, no. 1, pp. 86–89, 2013, doi: 10.1002/mop.
- [73] and H. K. M.Bitchikh, R.Aksas, A.Azrar, "A 2.3–14 GHz UWB planar octagonal antenna with modified ground plane," *Microw. Opt. Technol. Lett.*, vol. 55, no. 3, pp. 479–482, 2013, doi: 10.1002/mop.
- [74] and A. F. Sajad Mohammad, ali nezhad, Hamid Reza Hassani, "A dual band WLAN/UWB printed wide slot antenna for MIMO / diversity applications," *Microw. Opt. Technol. Lett.*, vol. 55, no. 3, pp. 461–465, 2013, doi: 10.1002/mop.
- [75] B. P. Chacko, G. Augustin, and T. A. Denidni, "Uniplanar slot antenna for ultrawideband polarization-diversity applications," *IEEE Antennas Wirel. Propag. Lett.*, vol. 12, pp. 88–91, 2013, doi: 10.1109/LAWP.2013.2242841.
- [76] and S. M. M. Sefidi, Y. Zehforoosh, "A novel monopole antenna for wireless communication systems and UWB application," *Microw. Opt. Technol. Lett.*, vol. 55, no. 8, pp. 1856–1860, 2013, doi: 10.1002/mop.

- [77] G. H. Kim and T. Y. Yun, "Compact ultrawideband monopole antenna with an inverted-I-shaped coupled strip," *IEEE Antennas Wirel. Propag. Lett.*, vol. 12, pp. 1291–1294, 2013, doi: 10.1109/LAWP.2013.2283863.
- [78] L. Liu, S. W. Cheung, and T. I. Yuk, "Compact MIMO Antenna for Portable Devices in UWB Applications," *IEEE Trans. Antennas Propag.*, vol. 61, no. 8, pp. 4257–4264, 2013, doi: 10.1109/TAP.2013.2263277.
- [79] M. S. Sharawi, M. U. Khan, A. B. Numan, and D. N. Aloï, "A CSRR loaded MIMO antenna system for ISM band operation," *IEEE Trans. Antennas Propag.*, vol. 61, no. 8, pp. 4265–4274, 2013, doi: 10.1109/TAP.2013.2263214.
- [80] R. S. Nayab Gogosh, M. Farhan Shafique and A. M. F. Imran Usman, "An UWB diversity antenna array with a novel H-type decoupling structure," *Microw. Opt. Technol. Lett.*, vol. 55, no. 11, pp. 2715–2721, 2013, doi: 10.1002/mop.
- [81] J. F. Li, Q. X. Chu, Z. H. Li, and X. X. Xia, "Compact dual band-notched UWB MIMO antenna with high isolation," *IEEE Trans. Antennas Propag.*, vol. 61, no. 9, pp. 4759–4766, 2013, doi: 10.1109/TAP.2013.2267653.
- [82] and B. K. K. Manoj K. Shrivastava, A. K. Gautam, "An M-shaped monopole - like SLOT UWB antenna," *Microw. Opt. Technol. Lett.*, vol. 56, no. 1, pp. 127–131, 2014, doi: 10.1002/mop.
- [83] L. Liu, S. W. Cheung, and T. I. Yuk, "Compact multiple-input-multiple-output antenna using quasi-self-complementary antenna structures for ultrawideband applications," *IET Microwaves, Antennas Propag.*, vol. 8, no. 13, pp. 1021–1029, 2014, doi: 10.1049/iet-map.2013.0503.
- [84] M. S. Khan, A. D. Capobianco, A. I. Najam, I. Shoaib, E. Autizi, and M. F. Shafique, "Compact ultra-wideband diversity antenna with a floating parasitic digitated decoupling structure," *IET Microwaves, Antennas Propag.*, vol. 8, no. 10, pp. 747–753, 2014, doi: 10.1049/iet-map.2013.0672.

- [85] A. Al-Rawi, A. Hussain, J. Yang, M. Franzen, C. Orlenius, and A. A. Kishk, "A new compact wideband MIMO antenna - The double-sided tapered self-grounded monopole array," *IEEE Trans. Antennas Propag.*, vol. 62, no. 6, pp. 3365–3369, 2014, doi: 10.1109/TAP.2014.2309985.
- [86] X. L. Liu, Z. D. Wang, Y. Z. Yin, J. Ren, and J. J. Wu, "A compact ultrawideband MIMO antenna using QSCA for high isolation," *IEEE Antennas Wirel. Propag. Lett.*, vol. 13, pp. 1497–1500, 2014, doi: 10.1109/LAWP.2014.2340395.
- [87] J. Ren, W. Hu, Y. Yin, and R. Fan, "Compact printed MIMO antenna for UWB applications," *IEEE Antennas Wirel. Propag. Lett.*, vol. 13, pp. 1517–1520, 2014, doi: 10.1109/LAWP.2014.2343454.
- [88] C. X. Mao and Q. X. Chu, "Compact coradiator UWB-MIMO antenna with dual polarization," *IEEE Trans. Antennas Propag.*, vol. 62, no. 9, pp. 4474–4480, 2014, doi: 10.1109/TAP.2014.2333066.
- [89] T. C. Tang and K. H. Lin, "An ultrawideband MIMO antenna with dual band-notched function," *IEEE Antennas Wirel. Propag. Lett.*, vol. 13, no. c, pp. 1076–1079, 2014, doi: 10.1109/LAWP.2014.2329496.
- [90] T. K. Roshna, U. Deepak, V. R. Sajitha, K. Vasudevan, and P. Mohanan, "A compact UWB MIMO antenna with reflector to enhance isolation," *IEEE Trans. Antennas Propag.*, vol. 63, no. 4, pp. 1873–1877, 2015, doi: 10.1109/TAP.2015.2398455.
- [91] L. Liu, S. W. Cheung, and T. I. Yuk, "Compact MIMO Antenna for Portable UWB Applications With Band-Notched Characteristic," *IEEE Trans. Antennas Propag.*, vol. 63, no. 5, pp. 1917–1924, 2015, doi: 10.1109/TAP.2015.2406892.
- [92] J. Y. Zhang, F. Zhang, W. P. Tian, and Y. L. Luo, "ACS-fed UWB-MIMO antenna with shared radiator," *Electron. Lett.*, vol. 51, no. 17, pp. 1301–1302, 2015, doi: 10.1049/el.2015.1327.

- [93] G. Srivastava and A. Mohan, "Compact dual polarized UWB diversity antenna," *Microw. Opt. Technol. Lett.*, vol. 57, no. 12, pp. 2951–2955, 2015, doi: 10.1002/mop.
- [94] M. G. N. Alsath and M. Kanagasabai, "Compact UWB Monopole Antenna for Automotive Communications," *IEEE Trans. Antennas Propag.*, vol. 63, no. 9, pp. 4204–4208, 2015, doi: 10.1109/TAP.2015.2447006.
- [95] L. Kang, H. Li, X. Wang, and X. Shi, "Compact Offset Microstrip-Fed MIMO Antenna for Band-Notched UWB Applications," *IEEE Antennas Wirel. Propag. Lett.*, vol. 14, no. c, pp. 1754–1757, 2015, doi: 10.1109/LAWP.2015.2422571.
- [96] C. M. Luo, J. S. Hong, and L. L. Zhong, "Isolation Enhancement of a Very Compact UWB-MIMO Slot Antenna with Two Defected Ground Structures," *IEEE Antennas Wirel. Propag. Lett.*, vol. 14, no. c, pp. 1766–1769, 2015, doi: 10.1109/LAWP.2015.2423318.
- [97] M. Sonkki, D. Sanchez-Escuderos, V. Hovinen, E. T. Salonen, and M. Ferrando-Bataller, "Wideband dual-polarized cross-shaped vivaldi antenna," *IEEE Trans. Antennas Propag.*, vol. 63, no. 6, pp. 2813–2819, 2015, doi: 10.1109/TAP.2015.2415521.
- [98] S. Tripathi, A. Mohan, and S. Yadav, "A Compact Koch Fractal UWB MIMO Antenna with WLAN Band-Rejection," *IEEE Antennas Wirel. Propag. Lett.*, vol. 14, no. c, pp. 1565–1568, 2015, doi: 10.1109/LAWP.2015.2412659.
- [99] J. Y. Deng, L. X. Guo, and X. L. Liu, "An Ultrawideband MIMO Antenna with a High Isolation," *IEEE Antennas Wirel. Propag. Lett.*, vol. 15, no. c, pp. 182–185, 2016, doi: 10.1109/LAWP.2015.2437713.
- [100] H.-F. Huang and Shu-Guang Xiao, "Compact MIMO antenna for BLUETOOTH, WiMAX, WLAN, AND UWB applications," *Microw. Opt. Technol. Lett.*, vol. 58, no. 4, pp. 783–787, 2016, doi: 10.1002/mop.

- [101] S. Hakimi, S. K. A. R. M. I. Sabran, A. N. O. And, and M. Hafizal, "Compact MIMO Antenna for Indoor UWB Applications," *Microw. Opt. Technol. Lett.*, vol. 58, no. 10, pp. 2387–2393, 2016, doi: 10.1002/mop.
- [102] G. Srivastava and A. Mohan, "Compact MIMO Slot Antenna for UWB Applications," *IEEE Antennas Wirel. Propag. Lett.*, vol. 15, no. c, pp. 1057–1060, 2016, doi: 10.1109/LAWP.2015.2491968.
- [103] J. Zhu, S. Li, B. Feng, L. Deng, and S. Yin, "Compact Dual-Polarized UWB Quasi-Self-Complementary MIMO/Diversity Antenna with Band-Rejection Capability," *IEEE Antennas Wirel. Propag. Lett.*, vol. 15, no. 61139001, pp. 905–908, 2016, doi: 10.1109/LAWP.2015.2479622.
- [104] G. S. Lin, C. H. Sung, J. L. Chen, L. S. Chen, and M. P. Houng, "Isolation Improvement in UWB MIMO Antenna System Using Carbon Black Film," *IEEE Antennas Wirel. Propag. Lett.*, vol. 16, pp. 222–225, 2017, doi: 10.1109/LAWP.2016.2570301.
- [105] A. Toktas, "G-shaped band-notched ultra-wideband MIMO antenna system for mobile terminals," *IET Microwaves, Antennas Propag.*, vol. 11, no. 5, pp. 718–725, 2017, doi: 10.1049/iet-map.2016.0820.
- [106] Y.-Y. Liu and Z.-H. Tu, "Compact Differential Band-Notched Stepped-Slot," *IEEE Antennas Wirel. Propag. Lett.*, vol. 16, pp. 593–596, 2017.
- [107] M. S. Khan, A. D. Capobianco, S. M. Asif, D. E. Anagnostou, R. M. Shubair, and B. D. Braaten, "A Compact CSRR-Enabled UWB Diversity Antenna," *IEEE Antennas Wirel. Propag. Lett.*, vol. 16, pp. 808–812, 2017, doi: 10.1109/LAWP.2016.2604843.
- [108] J. Tao and Q. Feng, "Compact Ultrawideband MIMO Antenna with Half-Slot Structure," *IEEE Antennas Wirel. Propag. Lett.*, vol. 16, pp. 792–795, 2017, doi: 10.1109/LAWP.2016.2604344.

- [109] M. Bilal, R. Saleem, H. H. Abbasi, and A. K. Shafique, Muhammad Farhan Brown, "An FSS-Based Nonplanar Quad-Element UWB-MIMO Antenna System," *IEEE Antennas Wirel. Propag. Lett.*, vol. 16, pp. 987–990, 2017.
- [110] M. S. Khan, A. D. Capobianco, A. Iftikhar, R. M. Shubair, D. E. Anagnostou, and B. D. Braaten, "Ultra-compact dual-polarised UWB MIMO antenna with meandered feeding lines," *IET Microwaves, Antennas Propag.*, vol. 11, no. 7, pp. 997–1002, 2017, doi: 10.1049/iet-map.2016.1074.
- [111] S. Rajkumar, N. Vivek Sivaraman, S. Murali, and K. T. Selvan, "Heptaband swastik arm antenna for MIMO applications," *IET Microwaves, Antennas Propag.*, vol. 11, no. 9, pp. 1255–1261, 2017, doi: 10.1049/iet-map.2016.1098.
- [112] S. S. Jehangir and M. S. Sharawi, "A Miniaturized UWB Bi-Planar Yagi-Like Antenna," *2017 IEEE Antennas Propag. Soc. Int. Symp. Proc.*, vol. 2017-Janua, pp. 501–502, 2017, doi: 10.1109/APUSNCURSINRSM.2017.8072293.
- [113] D. Sipal, M. P. Abegaonkar, and S. K. Koul, "Easily Extendable Compact Planar UWB MIMO Antenna Array," *IEEE Antennas Wirel. Propag. Lett.*, vol. 16, pp. 2328–2331, 2017.
- [114] T. K. Roshna, U. Deepak, and P. Mohanan, "Compact UWB MIMO antenna for tridirectional pattern diversity characteristics," *IET Microwaves, Antennas Propag.*, vol. 11, no. 14, pp. 2059–2065, 2017, doi: 10.1049/iet-map.2016.0921.
- [115] W. A. E. Ali and A. A. Ibrahim, "A compact double-sided MIMO antenna with an improved isolation for UWB applications," *AEU - Int. J. Electron. Commun.*, vol. 82, pp. 7–13, 2017, doi: 10.1016/j.aeue.2017.07.031.
- [116] X. Zhao, S. P. Yeo, and L. C. Ong, "Planar UWB MIMO Antenna with Pattern Diversity and Isolation Improvement for Mobile Platform Based on the Theory of Characteristic Modes," *IEEE Trans. Antennas Propag.*, vol. 66, no. 1, pp. 420–425, 2018, doi: 10.1109/TAP.2017.2768083.



- [117] M. M. Morsy and A. M. Morsy, "Dual-band meander-line MIMO antenna with high diversity for LTE/UMTS router," *IET Microwaves, Antennas Propag.*, vol. 12, no. 3, pp. 395–399, 2018, doi: 10.1049/iet-map.2017.0802.
- [118] R. Chandel, A. K. Gautam, and K. Rambabu, "Design and Packaging of an Eye-Shaped Multiple-Input-Multiple-Output Antenna with High Isolation for Wireless UWB Applications," *IEEE Trans. Components, Packag. Manuf. Technol.*, vol. 8, no. 4, pp. 635–642, 2018, doi: 10.1109/TCPMT.2018.2806562.
- [119] S. S. Jehangir, M. S. Sharawi, and A. Shamim, "Highly miniaturised semi-loop meandered dual-band MIMO antenna system," *IET Microwaves, Antennas Propag.*, vol. 12, no. 6, pp. 864–871, 2018, doi: 10.1049/iet-map.2017.0701.
- [120] P. Prabhu and S. Malarvizhi, "Novel double-side EBG based mutual coupling reduction for compact quad port UWB MIMO antenna," *AEU - Int. J. Electron. Commun.*, vol. 109, pp. 146–156, 2019, doi: 10.1016/j.aeue.2019.06.010.
- [121] I. Suriya and R. Anbazhagan, "Inverted-A based UWB MIMO antenna with triple-band notch and improved isolation for WBAN applications," *AEU - Int. J. Electron. Commun.*, vol. 99, pp. 25–33, 2019, doi: 10.1016/j.aeue.2018.11.030.
- [122] K. V. Babu and B. Anuradha, "Design of MIMO antenna to interference inherent for ultra wide band systems using defected ground structure," *Microw. Opt. Technol. Lett.*, vol. 61, no. 12, pp. 2698–2708, 2019, doi: 10.1002/mop.31958.
- [123] S. Chouhan, D. K. Panda, V. S. Kushwah, and S. Singhal, "Spider-shaped fractal MIMO antenna for WLAN/WiMAX/Wi-Fi/Bluetooth/C-band applications," *AEU - Int. J. Electron. Commun.*, vol. 110, p. 152871, 2019, doi: 10.1016/j.aeue.2019.152871.
- [124] P. Pannu and D. K. Sharma, "A low-profile quad-port UWB MIMO antenna using defected ground structure with dual notch-band behavior," *Int. J. RF Microw. Comput. Eng.*, vol. 30, no. 9, pp. 1–13, 2020, doi: 10.1002/mmce.22288.

- [125] X. Tang, Z. Yao, Y. Li, W. Zong, G. Liu, and F. Shan, "A high performance UWB MIMO antenna with defected ground structure and U-shape branches," *Int. J. RF Microw. Comput. Eng.*, vol. 31, no. 2, pp. 1–14, 2021, doi: 10.1002/mmce.22270.
- [126] S. Roy, S. Ghosh, S. S. Pattanayak, and U. Chakarborty, "Dual-polarized textile-based two/four element MIMO antenna with improved isolation for dual wideband application," *Int. J. RF Microw. Comput. Eng.*, vol. 30, no. 9, pp. 1–20, 2020, doi: 10.1002/mmce.22292.
- [127] F. G. Zhu, J. D. Xu, and Q. Xu, "Reduction of mutual coupling between closely-packed antenna elements using defected ground structure," *Electron. Lett.*, vol. 45, no. 12, pp. 601–602, 2009, doi: 10.1049/el.2009.0985.
- [128] M. K. Khandelwal, B. K. Kanaujia, and S. Kumar, "Defected ground structure: Fundamentals, analysis, and applications in modern wireless trends," *Int. J. Antennas Propag.*, vol. 2017, pp. 1–22, 2017, doi: 10.1155/2017/2018527.
- [129] J. Zhu, B. Feng, B. Peng, L. Deng, and S. Li, "A dual notched band MIMO slot Antenna system with Y-Shaped defected Ground structure for UWB applications," *Microw. Opt. Technol. Lett.*, vol. 58, no. 3, pp. 626–630, 2016, doi: 10.1002/mop.
- [130] S. Ghosh, T. N. Tran, and T. Le-Ngoc, "Dual-layer EBG-based miniaturized multi-element antenna for MIMO systems," *IEEE Trans. Antennas Propag.*, vol. 62, no. 8, pp. 3985–3997, 2014, doi: 10.1109/TAP.2014.2323410.
- [131] N. Jaglan, S. D. Gupta, E. Thakur, D. Kumar, B. K. Kanaujia, and S. Srivastava, "Triple band notched mushroom and uniplanar EBG structures based UWB MIMO/Diversity antenna with enhanced wide band isolation," *AEU - Int. J. Electron. Commun.*, vol. 90, pp. 36–44, 2018, doi: 10.1016/j.aeue.2018.04.009.
- [132] D. A. Ketzaki and T. V. Yioultis, "Metamaterial-based design of planar compact MIMO monopoles," *IEEE Trans. Antennas Propag.*, vol. 61, no. 5, pp. 2758–2766, 2013, doi: 10.1109/TAP.2013.2243813.

- [133] A. Iqbal, O. A. Saraereh, A. W. Ahmad, and S. Bashir, "Mutual Coupling Reduction Using F-Shaped Stubs in UWB-MIMO Antenna," *IEEE Access*, vol. 6, pp. 2755–2759, 2017, doi: 10.1109/ACCESS.2017.2785232.
- [134] A. Kayabasi, A. Toktas, E. Yigit, and K. Sabanci, "Triangular quad-port multi-polarized UWB MIMO antenna with enhanced isolation using neutralization ring," *AEU - Int. J. Electron. Commun.*, vol. 85, pp. 47–53, 2018, doi: 10.1016/j.aeue.2017.12.027.
- [135] R. N. Tiwari, P. Singh, B. K. Kanaujia, and K. Srivastava, "Neutralization technique based two and four port high isolation MIMO antennas for UWB communication," *AEU - Int. J. Electron. Commun.*, vol. 110, 2019, doi: 10.1016/j.aeue.2019.152828.
- [136] T. Dabas, D. Gangwar, B. K. Kanaujia, and A. K. Gautam, "Mutual coupling reduction between elements of UWB MIMO antenna using small size uniplanar EBG exhibiting multiple stop bands," *AEU - Int. J. Electron. Commun.*, vol. 93, pp. 32–38, 2018, doi: 10.1016/j.aeue.2018.05.033.
- [137] W. Wu, B. Yuan, and A. Wu, "A quad-element UWB-MIMO antenna with band-notch and reduced mutual coupling based on EBG structures," *Int. J. Antennas Propag.*, vol. 2018, 2018, doi: 10.1155/2018/8490740.
- [138] E. Wang, W. Wang, X. Tan, Y. Wu, J. Gao, and Y. Liu, "A UWB MIMO slot antenna using defected ground structures for high isolation," *Int. J. RF Microw. Comput. Eng.*, vol. 30, no. 5, pp. 1–10, 2020, doi: 10.1002/mmce.22155.
- [139] J. Zhao and J. Wang, "Correlation reduction in antennas with metamaterial based on newly designed SRRs," *2010 Asia-Pacific Symp. Electromagn. Compat. APEMC 2010*, no. 2008, pp. 981–984, 2010, doi: 10.1109/APEMC.2010.5475609.
- [140] M. N. Hasan, S. Chu, and S. Bashir, "A DGS monopole antenna loaded with U-shape stub for UWB MIMO applications," *Microw. Opt. Technol. Lett.*, vol. 61, no. 9, pp. 2141–2149, 2019, doi: 10.1002/mop.31877.

- [141] J. Zhang, F. Zhang, and W. Tian, "Compact 4-Port ACS-Fed UWB-MIMO Antenna with Shared Radiators," *Prog. Electromagn. Res. Lett.*, vol. 55, no. August, pp. 81–88, 2015.
- [142] A. Toktas and A. Akdagli, "Compact multiple-input multiple-output antenna with low correlation for ultra-wideband applications," *IET Microwaves, Antennas Propag.*, vol. 9, no. 8, pp. 822–829, 2015, doi: 10.1049/iet-map.2014.0086.
- [143] S. M. Khan, A. Iftikhar, S. M. Asif, and B. D. B. Antonio-Daniele Capobianco, "A Compact four elements UWB MIMO antenna with on-demand WLAN rejection," *Microw. Opt. Technol. Lett.*, vol. 58, no. 2, pp. 270–276, 2016, doi: 10.1002/mop.
- [144] Z. Tang, X. Wu, J. Zhan, S. Hu, Z. Xi, and Y. Liu, "Compact UWB-MIMO Antenna with High Isolation and Triple Band-Notched Characteristics," *IEEE Access*, vol. 7, no. c, pp. 19856–19865, 2019, doi: 10.1109/ACCESS.2019.2897170.
- [145] K. G. Thomas and M. Sreenivasan, "A Simple Ultrawideband Planar Rectangular Printed Antenna With Band Dispensation," *IEEE Trans. Antennas Propag.*, vol. 58, no. 1, pp. 27–34, 2010.
- [146] A. A. Yussuf and S. Paker, "Design of a compact quad-radiating element MIMO antenna for LTE/Wi-Fi application," *AEU - Int. J. Electron. Commun.*, vol. 111, p. 152893, 2019, doi: 10.1016/j.aeue.2019.152893.
- [147] N. Jaglan, S. D. Gupta, B. K. Kanaujia, and S. Srivastava, "Band notched UWB circular monopole antenna with inductance enhanced modified mushroom EBG structures," *Wirel. Networks*, vol. 24, no. 2, pp. 383–393, 2018, doi: 10.1007/s11276-016-1343-7.
- [148] K. Fertas, F. Ghanem, A. Azrar, and R. Aksas, "UWB antenna with sweeping dual notch based on metamaterial SRR fictive rotation," *Microw. Opt. Technol. Lett.*, vol. 62, no. 2, pp. 956–963, 2020, doi: 10.1002/mop.32111.
- [149] B. Yan, D. Jiang, R. Xu, and Y. Xu, "A UWB band-pass antenna with triple-notched

- band using common direction rectangular complementary split-ring resonators,” *Int. J. Antennas Propag.*, vol. 2013, 2013, doi: 10.1155/2013/934802.
- [150] S. Luo, Y. Li, Y. Xia, and L. Zhang, “A low mutual coupling antenna array with gain enhancement using metamaterial loading and neutralization line structure,” *Appl. Comput. Electromagn. Soc. J.*, vol. 34, no. 3, pp. 411–418, 2019.
- [151] T. Kumari, G. Das, A. Sharma, and R. K. Gangwar, “Design approach for dual element hybrid MIMO antenna arrangement for wideband applications,” *Int. J. RF Microw. Comput. Eng.*, vol. 29, no. 1, pp. 1–10, 2019, doi: 10.1002/mmce.21486.
- [152] L. Kang, H. Li, X. Wang, and X. Shi, “Compact Offset Microstrip-Fed MIMO Antenna for Band-Notched UWB Applications,” *IEEE Antennas Wirel. Propag. Lett.*, vol. 14, pp. 1754–1757, 2015, doi: 10.1109/LAWP.2015.2422571.
- [153] N. K. Kiem, H. N. B. Phuong, and D. N. Chien, “Design of compact  $4 \times 4$  UWB-MIMO antenna with WLAN band rejection,” *Int. J. Antennas Propag.*, vol. 2014, 2014, doi: 10.1155/2014/539094.
- [154] M. S. Khan, S. A. Naqvi, A. Iftikhar, S. M. Asif, A. Fida, and R. M. Shubair, “A WLAN band-notched compact four element UWB MIMO antenna,” *Int. J. RF Microw. Comput. Eng.*, vol. 30, no. 9, pp. 1–10, 2020, doi: 10.1002/mmce.22282.
- [155] S. Rajkumar, A. Anto Amala, and K. T. Selvan, “Isolation improvement of UWB MIMO antenna utilising molecule fractal structure,” *Electron. Lett.*, vol. 55, no. 10, pp. 576–579, 2019, doi: 10.1049/el.2019.0592.
- [156] I. S. Masoodi, I. Ishteyaq, K. Muzaffar, and M. I. Magray, “A compact band-notched antenna with high isolation for UWB MIMO applications,” *Int. J. Microw. Wirel. Technol.*, vol. 13, no. 6, pp. 634–640, 2021, doi: 10.1017/S1759078720001427.
- [157] J. Acharjee, K. Mandal, and S. K. Mandal, “Reduction of Mutual Coupling and Cross-Polarization of a MIMO / Diversity Antenna using a String of H-Shaped DGS,” *AEUE - Int. J. Electron. Commun.*, 2018, doi: 10.1016/j.aeue.2018.09.037.

- [158] M. A. Abdalla and A. A. Ibrahim, "Compact and Closely Spaced Metamaterial MIMO Antenna With High Isolation for Wireless Applications," vol. 12, pp. 1452–1455, 2013.
- [159] G. Zhai, Z. N. Chen, X. Qing, and S. Member, "Enhanced Isolation of a Closely-spaced Four-element MIMO Antenna System Using Metamaterial Mushroom," no. c, 2015, doi: 10.1109/TAP.2015.2434403.
- [160] L. Wang *et al.*, "Compact UWB MIMO Antenna with High Isolation Using Fence-Type Decoupling Structure," *IEEE Antennas Wirel. Propag. Lett.*, vol. 18, no. 8, pp. 1641–1645, 2019, doi: 10.1109/LAWP.2019.2925857.
- [161] F. Amin, R. Saleem, T. Shabbir, S. ur Rehman, M. Bilal, and M. F. Shafique, "A compact quad-element UWB-MIMO antenna system with parasitic decoupling mechanism," *Appl. Sci.*, vol. 9, no. 11, 2019, doi: 10.3390/app9112371.
- [162] M. Shehata, M. S. Said, and H. Mostafa, "Dual notched band quad-element MIMO antenna with multitone interference suppression for IR-UWB wireless applications," *IEEE Trans. Antennas Propag.*, vol. 66, no. 11, pp. 5737–5746, 2018, doi: 10.1109/TAP.2018.2868725.
- [163] W. T. Li, Y. Q. Hei, H. Subbaraman, X. W. Shi, and R. T. Chen, "Novel Printed Filtenna with Dual Notches and Good Out-of-Band Characteristics for UWB-MIMO Applications," *IEEE Microw. Wirel. Components Lett.*, vol. 26, no. 10, pp. 765–767, 2016, doi: 10.1109/LMWC.2016.2601298.
- [164] H. Liu, G. Kang, and S. Jiang, "Compact dual band-notched UWB multiple-input multiple-output antenna for portable applications," *Microw. Opt. Technol. Lett.*, vol. 62, no. 3, pp. 1215–1221, 2020, doi: 10.1002/mop.31960.
- [165] S. Kumar, "diversity antenna with dual band-notched characteristics for ultra-wideband applications," *Microw. Opt. Technol. Lett.*, vol. 62, no. 1, pp. 1–10, 2019, doi: 10.1002/mop.32012.

